

2010

Development of a Coaxial Electron-Laser Beam Collision Experiment

Justin Teeuwen
University of Windsor

Follow this and additional works at: <http://scholar.uwindsor.ca/etd>

Recommended Citation

Teeuwen, Justin, "Development of a Coaxial Electron-Laser Beam Collision Experiment" (2010). *Electronic Theses and Dissertations*. Paper 376.

This online database contains the full-text of PhD dissertations and Masters' theses of University of Windsor students from 1954 forward. These documents are made available for personal study and research purposes only, in accordance with the Canadian Copyright Act and the Creative Commons license—CC BY-NC-ND (Attribution, Non-Commercial, No Derivative Works). Under this license, works must always be attributed to the copyright holder (original author), cannot be used for any commercial purposes, and may not be altered. Any other use would require the permission of the copyright holder. Students may inquire about withdrawing their dissertation and/or thesis from this database. For additional inquiries, please contact the repository administrator via email (scholarship@uwindsor.ca) or by telephone at 519-253-3000ext. 3208.

Development of a
Coaxial Electron-Laser Beam
Collision Experiment

by

Justin Teeuwen

A Dissertation
submitted to the Faculty of Graduate Studies
through the Department of Physics
in Partial Fulfillment of the requirements
for the Degree of Masters of Science
at the University of Windsor

Windsor, Ontario, Canada
© 2010 Justin Teeuwen

Development of a
Coaxial Electron-Laser Beam
Collision Experiment

by

Justin Teeuwen

APPROVED BY:

Dr. Robert Schurko
Chemistry and Biochemistry

Dr. Wladyslaw Kedzierski
Physics Department

Dr. J. W. McConkey, Advisor
Physics Department

Dr. William Baylis, Chair of Defense
Physics Department

May 20, 2010

Author's Declaration of Originality

I hereby certify that I am the sole author of this thesis and that no part of this thesis has been published or submitted for publication.

I certify that, to the best of my knowledge, my thesis does not infringe upon anyone's copyright nor violate any proprietary rights and that any ideas, techniques, quotations, or any other material from the work of other people included in my thesis, published or otherwise, are fully acknowledged in accordance with the standard referencing practices. Furthermore, to the extent that I have included copyrighted material that surpasses the bounds of fair dealing within the meaning of the Canada Copyright Act, I certify that I have obtained a written permission from the copyright owner(s) to include such material(s) in my thesis and have included copies of such copyright clearances to my appendix.

I declare that this is a true copy of my thesis, including any final revisions, as approved by my thesis committee and the Graduate Studies office, and that this thesis has not been submitted for a higher degree to any other University or Institution.

Abstract

An electron optical system which propagates an electron beam coaxially with a laser was designed, developed and tested. Greatly improved signal rates were obtained when excitation of various target species under electron impact was studied. Measurements of excitation in nitrogen, specifically the (0,0) second positive band of N_2 and (0,1) first negative band of N_2^+ are made and compared with well-known previous results to calibrate the system. The direct excitation cross section of the $3p^54p [1 \frac{1}{2}] (J=1) \rightarrow 3p^54s [\frac{1}{2}] (J=0)$ transition of argon was measured and compared with previous results. Further emission cross section measurements were made of a number of argon transitions throughout the visible and near infrared spectral regions. Comparison with previous results showed remarkable agreement in both shape and threshold values. A first attempt to study excitation of an optically allowed level in argon using Laser Induced Fluorescence (LIF) was made using the $3p^54p [1 \frac{1}{2}] (J=1) \rightarrow 3p^54s [\frac{1}{2}] (J=1)$ transition. Suggestions for future modifications and developments to the present system are made.

Dedication

This work is dedicated to God, creator of the Universe, and ultimate guide in my life. Had it not been for the gifts, signs and omens left for me, I would not have reached where I am today, have the friends and family with whom I am intimately acquainted, nor have the many blessings which made this work possible.

“For truly I tell you, if you have faith the size of a mustard seed, you will say to this mountain, ‘Move from here to there,’ and it will move; and nothing will be impossible for you.” Matthew 17:20

Acknowledgements

I would like to acknowledge many people who have helped make this work possible, though I cannot possibly name them all. First, I would like to acknowledge Dr. McConkey, my mentor and one of the best supervisors I have known, without whom I can honestly say I would not have even attempted the daunting task of completing a Masters in Physics. His patient wisdom, understanding, and experience have all played a crucial role into my development as a young adult. I will always remember the lessons I have learned down in that basement of Essex Hall under his guidance.

I would also like to acknowledge Dr. Kedzierski who was a great help throughout my work, serving as a second mentor. Many thanks are owed to the long hours given by Eric Clausen and Lou Beaudry from the workshop as well as Sinisa Jezdic, the department's electronics technologist. The timely completion of this Masters is greatly due to them. I also thank Qin Tu for her continued help.

Thanks would not be complete without acknowledging my friends and family. I owe a great deal of gratitude to my parents who encouraged me to be patient and determined. My roommates I thank for being with me on the worst days and celebrating with me on the best. I greatly thank my best friends who listened to me and encouraged me to work harder than I ever knew: Beau Helbert, Jesse Breslin, Sozan Akel, Paul Emmanuel Deacon, and my girlfriend, Irene Mroz. Your words and guidance over the years have been very important among my many blessings for my continued happiness and success.

Most importantly, I wish to thank God, creator of the Universe, for guiding me through this process. I never know where I'll end up, but it's always an amazing ride.

Table of Contents

Abstract

Dedication

Acknowledgements

Chapter	Page #
1. Introduction	-1-
2. Description of the Apparatus	-5-
A. Introduction	-5-
B. The Electron Optics	-7-
1. The Electron Gun	-10-
2. The Electrostatic Analyzer	-10-
3. The Collector	-10-
C. The Electronics	-13-
1. Electron Gun Circuit	-13-
D. The Magnetic Field and Shielding	-15-
1. Magnetic Octopole	-15-
2. Magnetic Shielding	-15-
E. Optimized System Operation	-15-
1. SIMION Model	-18-
2. Configuration Potentials	-18-
F. The Gas Injection	-23-
1. Using a Pulsed Valve	-23-
2. Static Gas Setup	-24-
G. The Light Collection	-25-
H. The Data Collection	-26-
I. The Laser	-29-
3. Measurement of Excitation of Nitrogen (N_2) by Electron Impact	-31-
A. Theory of Measurement and Error Budget	-31-
B. Introduction and Review of Previous Work	-32-
C. Experimental Details	-34-
D. Results and Discussion	-34-
1. Excitation of the (0,0) Second Positive Band of N_2 (C \rightarrow B)	-35-
2. Excitation of the (0,1) First Negative Band of N_2^+ (B \rightarrow X)	-39-
E. Summary and Conclusions	-43-

4.	Measurement of Excitation of Argon (Ar) by Laser Induced Fluorescence	-44-
	A. Introduction and Review of Previous Work	-44-
	B. LIF for Argon	-45-
	C. Experimental Details	-46-
	D. Results and Discussion	-47-
	1. The $3p^5 4p [1 \frac{1}{2}] (J=1) \rightarrow 3p^5 4s [\frac{1}{2}] (J=0)$ (“794.8 nm”) Transition	-47-
	2. 340 nm Emissions	-52-
	3. 423 nm Emissions	-56-
	4. 470 nm Emissions	-60-
	5. 620 nm Emissions	-63-
	6. 710 nm Emissions	-66-
	7. Excitation by LIF	-70-
	E. Summary and Conclusions	-79-
5.	Overall Summary and Conclusions	-80-
6.	Suggested Future Modifications and Developments	-81-
	A. Present State	-81-
	B. Electron Optics Developments	-81-
	C. Laser Developments	-82-
	D. Vacuum Developments	-83-
	E. Data Collection Developments	-84-
7.	References	-85-
	Appendix	-88-
	Vita Auctoris	-95-

Chapter 1

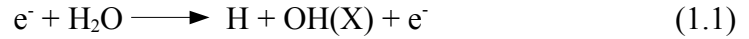
Introduction

Laser Induced Fluorescence (LIF) is important in the study of electrons impacting on atoms and simple molecules, particularly H₂O, the third-most abundant molecule in the universe [Itikawa, et al., (2005)]. Research on electron impacts involving water plays an important role in many areas including atmospheric processes of many celestial bodies, low and high temperature plasmas and radiation chemistry. The dissociation of water in particular is crucial in plasma-waste and radioactive waste disposal, and is very important in the terrestrial atmosphere and environment. Fossil fuels produce pollutants which can be reduced through plasma techniques involving water [Itikawa, et al., Becker, et al., (2000)]; radiation damage of biological cells can be better understood through knowledge of electron interactions with water [Itikawa]; lastly, electron collisions with water play a role in understanding the future effects of global warming as water is the most abundant greenhouse gas [Taylor, (2002)].

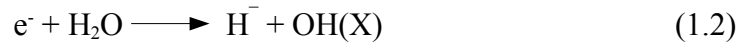
Electron collisions with argon plays a crucial role in the study of many common laboratory and industrial plasmas which utilize argon. These applications include gas-discharge lasers, such as an argon-ion or Ar-Kr-F₂ laser [Tsurubuchi et al., 1996], plasma displays, semiconductor processing, plasma physics, fluorescent lighting and even astrophysical observations [Boffard et al., (2007)]. LIF of argon is of particular importance in the study of plasma physics [Severn et al., (1998)]. The most common cause of excited atoms in plasmas is from energetic electron collisions. argon plasmas display a characteristic glow, resulting from the decay of such excited atoms and ions. Therefore, an understanding of the electron impact cross sections of argon is particularly

important in understanding these characteristic fluorescences [Boffard]. The cross sections of the resonance lines of argon, measured by electron impact, provide wavelength standards in addition to their practical uses [Tsurubuchi].

LIF experiments involving water have been previously conducted in our laboratory by Harb [Harb et al., (2001)] for the following process:



The system was calibrated using the resonance process:



which peaked at an electron energy of 6.5eV just below the onset for process (1.1). Its cross section had been measured previously [Melton, (1972)]. These experiments suffered from poor signal to noise ratios particularly near the threshold of process (1.1).

The current work provides the modifications necessary for future studies of this process by obtaining significantly increased signal rates. Well established excitation processes in nitrogen and argon are exploited for this purpose. Nitrogen is utilized as a benchmark for performance before exploring direct and LIF excitation of argon. Chapters 3 and 4 contain a review of previous work done regarding excitation by electron impact of nitrogen and argon and LIF of argon.

LIF experiments to measure the electron-impact cross sections of water, nitrogen and neon have been attempted using several different designs for the electron optical system [Harb, (2002), Zetner (1985)]. Zetner used a 180° analyzer to allow the electron beam to pass coaxially with the laser [Zetner]. It was found that space charge effects in the electrostatically-focused electron beam limited the usefulness of the system to higher

electron energies, above about 15 eV. Harb used an unselected electron beam at a 30.0° angle to the path of the laser, and also incorporated a magnetic field to collimate the electron beam at low energies [Harb, (2002)]. We note that all previous attempts to use LIF to probe electron impact excitation were limited to ground or metastable target species. To our knowledge, the present work is the first experiment to attempt LIF probing of short-lived excited states.

In the present experiment, we use a 127.0° analyzer to allow us to fire the electron beam coaxially with the laser using a magnetic field, similar to that used by Harb [Harb, (2002)] to constrain the electrons within the laser beam. Although the 127.0° monochromator limited the total current of the electron beam, the increase in the interaction volume created by the coaxial overlap of the electron and laser beams provided the necessary improvement in output signals.

To calibrate the system, the excitation functions of the (0,0) second positive band of N_2 and the (0,1) first negative band of N_2^+ were studied. These electron excitation functions are very well known and as such serve as an excellent medium for calibration. These are explored in Chapter 3. Following this, the excitation functions of various argon emissions, in particular the $3p^54p [1 \frac{1}{2}] (J=1) \rightarrow 3p^54s [\frac{1}{2}] (J=0)$ transition, were measured. The complete emission cross section for this transition had not been measured previously [Boffard, (2007)]. Excitation of the $3p^54s [\frac{1}{2}] (J=1)$ state of argon was measured using the method of LIF. It was not possible to directly study the excitation of this state because its normal decay route was in the vacuum ultra-violet (VUV) at 104.8 nm. We made use of the fact that the Ar transition was in near resonance with the diode

laser being used elsewhere in the laboratory to study Cs atom trapping. It is of particular significance that this experiment marks the first time this state of argon will be measured by LIF, and not by direct excitation. These studies of argon are explored further in Chapter 4.

Chapter 2 describes in detail the implementation and design process involved in the creation of the electron optical system. Several optimized configurations were studied, the best of which were then employed in the experiment. Improvements were made over the design as the process was explored and these resulted in an effective electron optical system, one that provided a slowly varying electron current from 3-200eV. Applications of the present system are described in Chapter 6 along with suggested improvements which should be made in order to further optimize results. Specific focus is placed on the electron optical system as it plays a crucial role in the experiment. Chapter 5 provides a summary and conclusions.

Chapter 2

Description of the Apparatus

2.A. Introduction

The system consists of co-axial electron and laser beams housed in a high-vacuum chamber into which a target, low pressure gas, normally Ar or N₂, is introduced. A schematic diagram is shown in Figure 2.1. Photons arising from the interaction of these beams with the target gas are detected orthogonally to the laser-electron beam axis. The electron source was contained within a mu metal box, to prevent the magnetic field from adversely affecting the behaviour of the electron optical system. The electron beam was produced by an electron monochromator with a 127° analyzer. One lens was used to focus the electrons from the source into the analyzer and a second lens was used to refocus the electrons from the analyzer at the exit of the electron optical system where they were injected into a 150 gauss longitudinal magnetic field. The magnetic field minimized the repulsive space charge effects which occurred at low energies [Harb, (2002)]. The magnetic field was produced by four parallel bar magnets symmetrically positioned within an aluminum yoke, at the end of which was a cross-field collector. The cross field collector permitted the path of the laser while allowing a measure of the current. The electron source (filament) was biased negatively with respect to the grounded interaction region, thus defining the electron energy. Typical gun performance resulted in collector currents of 0.6 μA at 3 eV, 2 μA at 200 eV with a total emission from the filament of 6 μA. After operation for some time, gun elements tended to become contaminated leading to a reduction in performance. Consequently the gun was able to transmit between 10% and 33.3% of the total emission through to the collector.

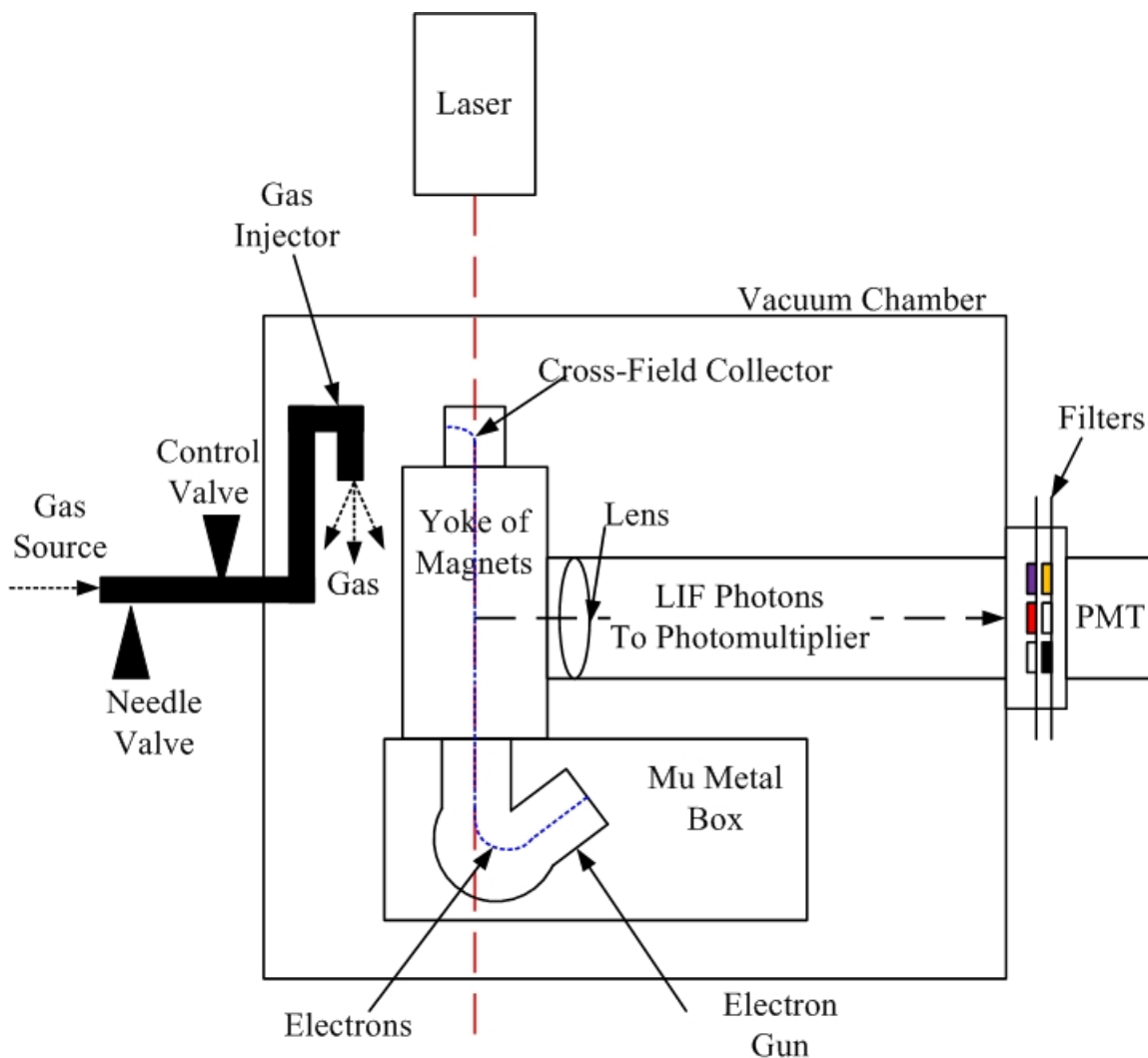


Figure 2.1 - Overall schematic of the experimental apparatus used. The interaction region is focused by the lens onto the photomultiplier cathode.

A vacuum was created by the use of a Edwards ED 660 rotary pump as a backing to a 6" Diffstak diffusion pump. Ultimate background pressure in the chamber was typically 10^{-6} torr as measured with an IG2200 ionization guage controller from Kurt J. Lesker.

The gas injection system was controlled primarily by a needle valve which determined the driving pressure. During experiments the target gas in the chamber was maintained at a pressure no higher than 8.8×10^{-4} torr to ensure optimum gun performance and freedom from secondary collision effects (see later discussion). During data taking

the butterfly valve separating the diffusion pump from the main vacuum chamber was almost totally closed to ensure a uniform pressure throughout the interaction region.

A XP2233B photomultiplier was used for photon detection preceded by an appropriate filter for wavelength selection (see Figure 2.1).

2.B. The Electron Optics

A schematic, exploded view, and photo of the electron optical system are shown in Figures 2.2, 2.3 and 2.4. The labels given to each plate were the labels used for describing the various lens elements. The potentials will be described in a subsequent section. Each piece of the gun is described individually in the following subsections. 6mm apertures had to be used in the output section of the electron optical system to allow “clean” passage of the counter-propagating laser beam.

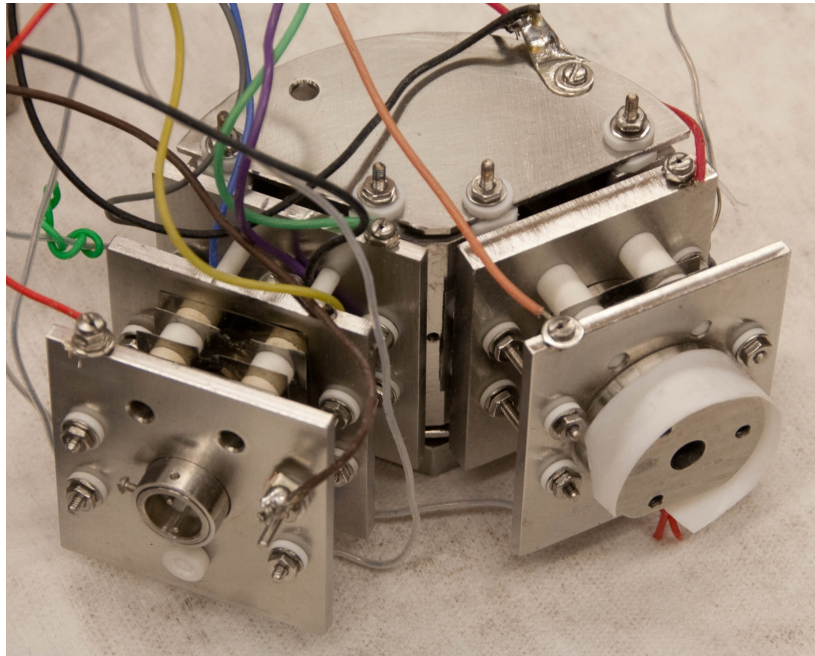


Figure 2.2 - A photo of the electron gun.

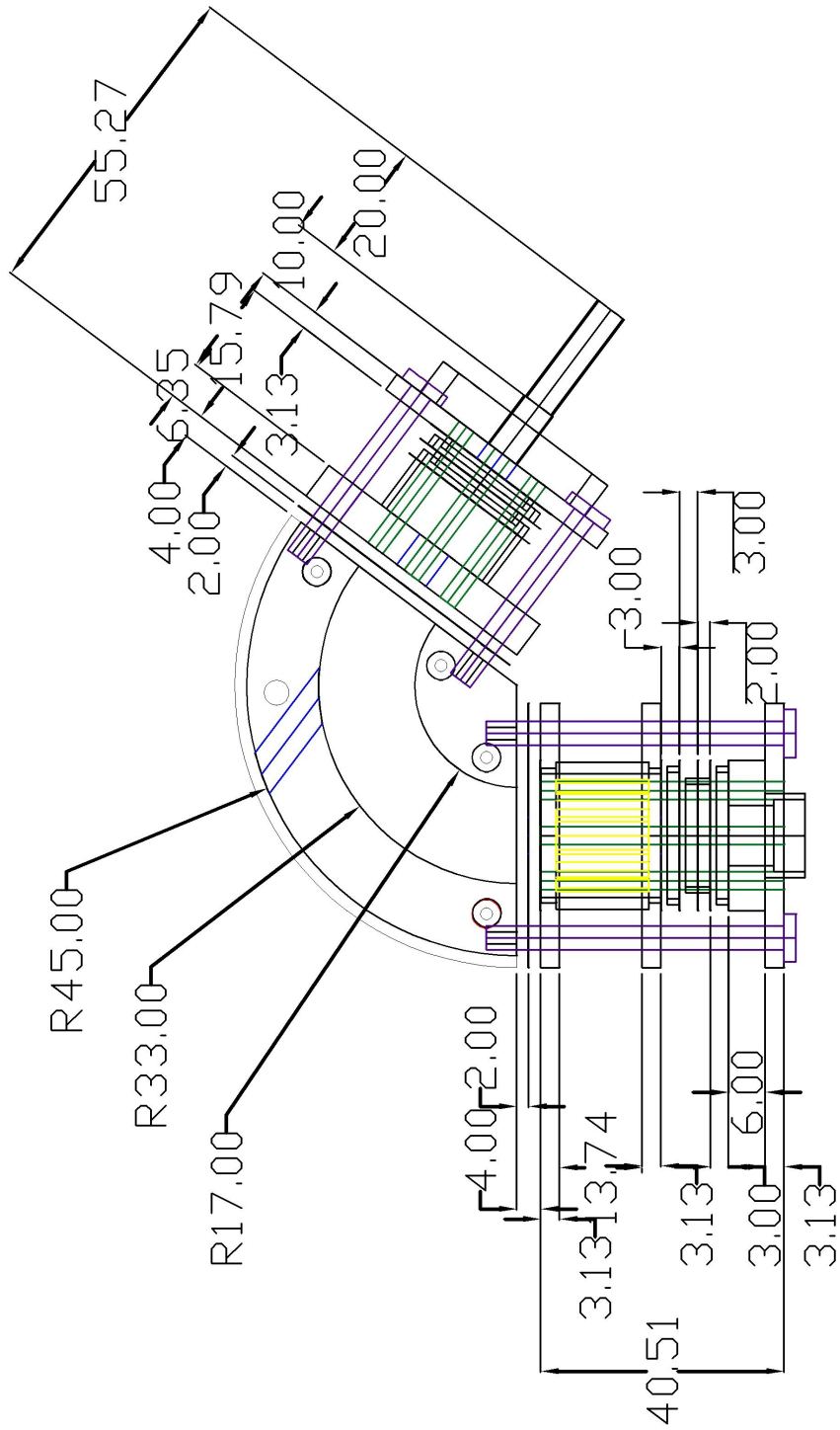


Figure 2.3 - Overall schematic of the electron gun. Measurements are in mm.

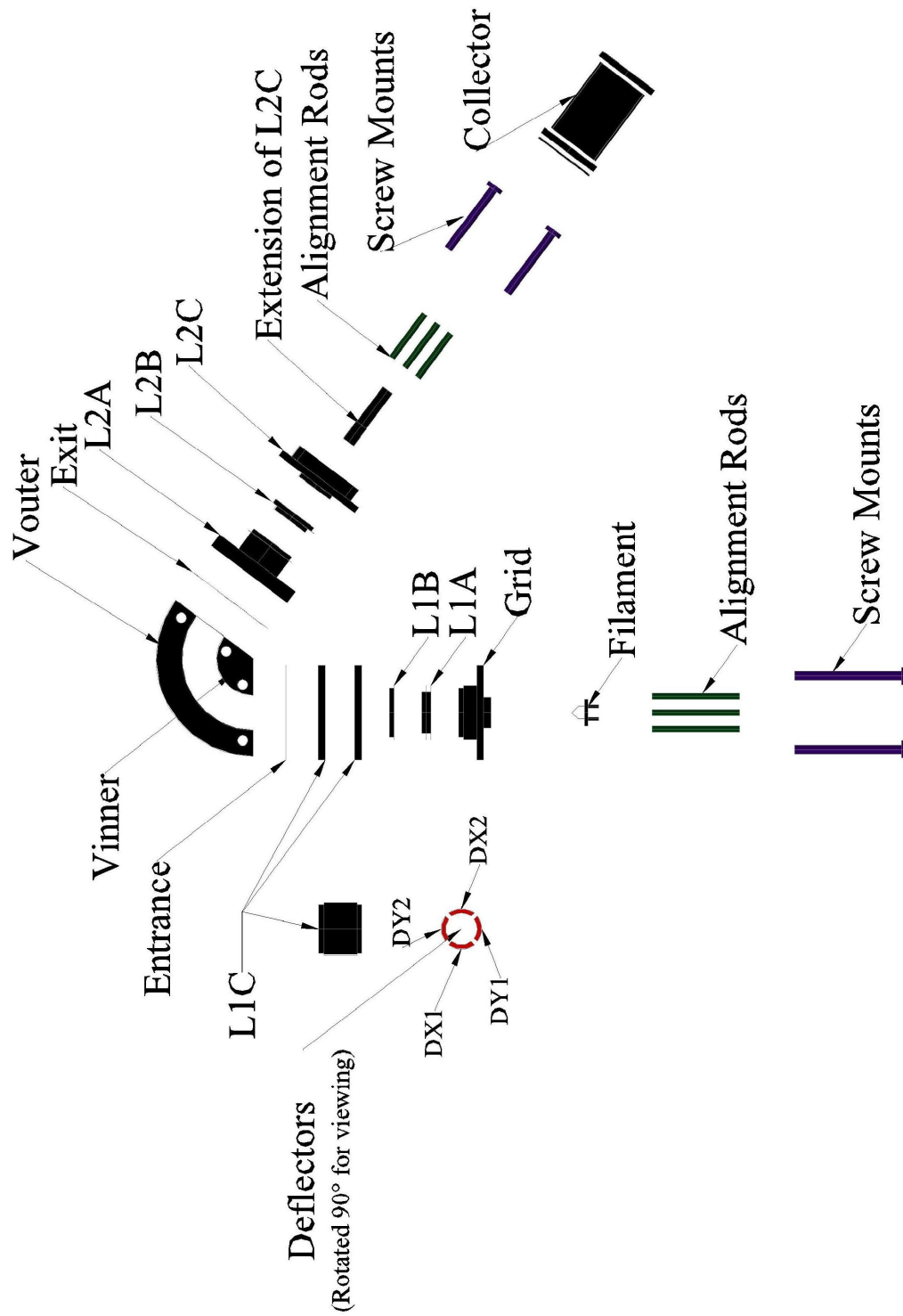


Figure 2.4 - An exploded view of the electron gun, with each piece labeled.

2.B.1. The Electron Gun

The lenses were designed using ratios based on Harting and Read's *Electrostatic Lenses* [Harting et al., (1976)]. A single set of deflectors, shown in Figure 2.4, was employed at the end of the first lens to provide steering.

2.B.2. The Electrostatic Analyzer

The design of the 127° analyzer is shown above in Figures 2.2, 2.3 and 2.4. An exploded view of the analyzer is included in Figure 2.5.

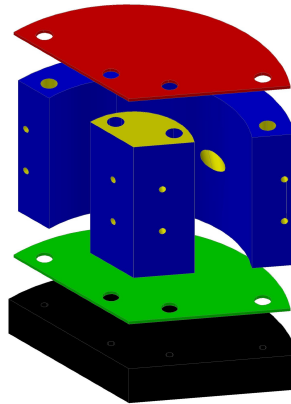


Figure 2.5 - Exploded view of the new analyzer.

2.B.3. The Collector

The cross-field collector was crucial as it not only measured the current, but permitted the path of the laser through the system. A comparative study between the cross-field collector and the previously used Faraday cups was done, verifying that this would be a suitable substitute for measuring the current. The schematics of the cross-field collector are included in Figures 2.6 and 2.7.

Tests done with different voltages on the collector revealed that optimum operation occurred when 100 V was used. There was sufficient penetration of this field through the grounded aperture on the front of the collector to encourage electrons to efficiently

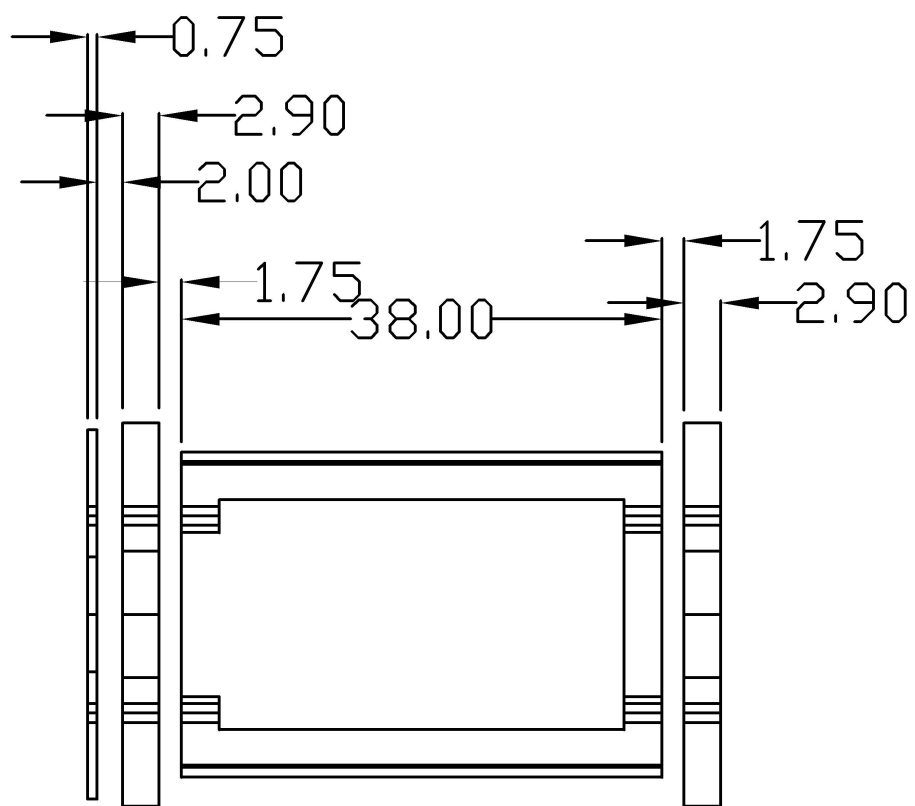
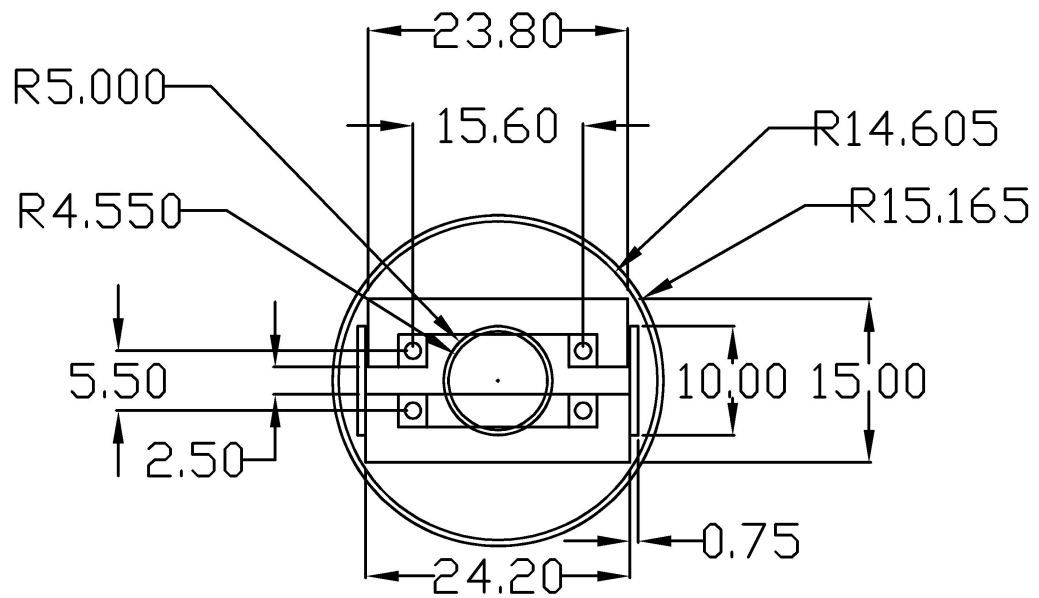


Figure 2.6 - Schematics from side and front view of the collectors. Measurements are listed in mm.

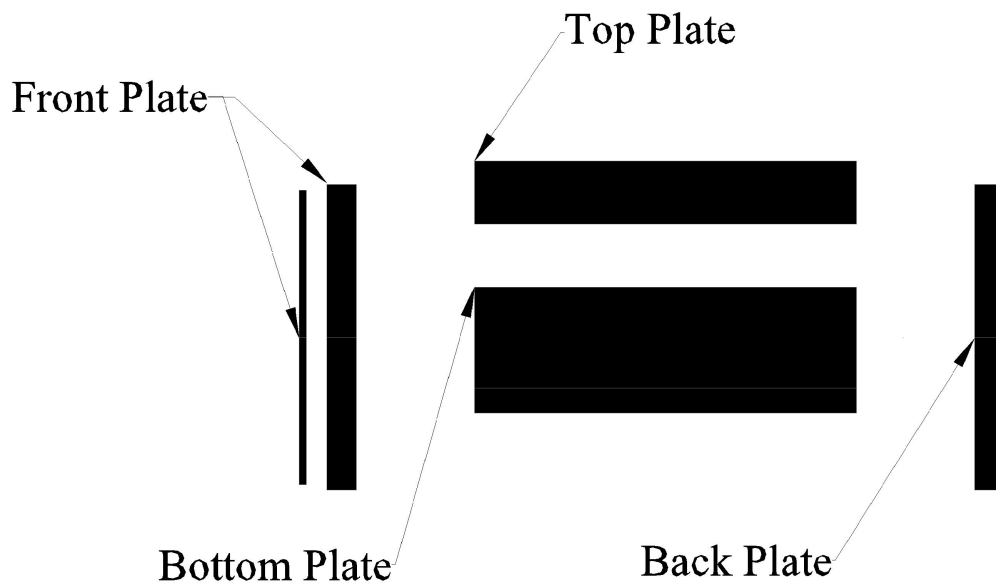
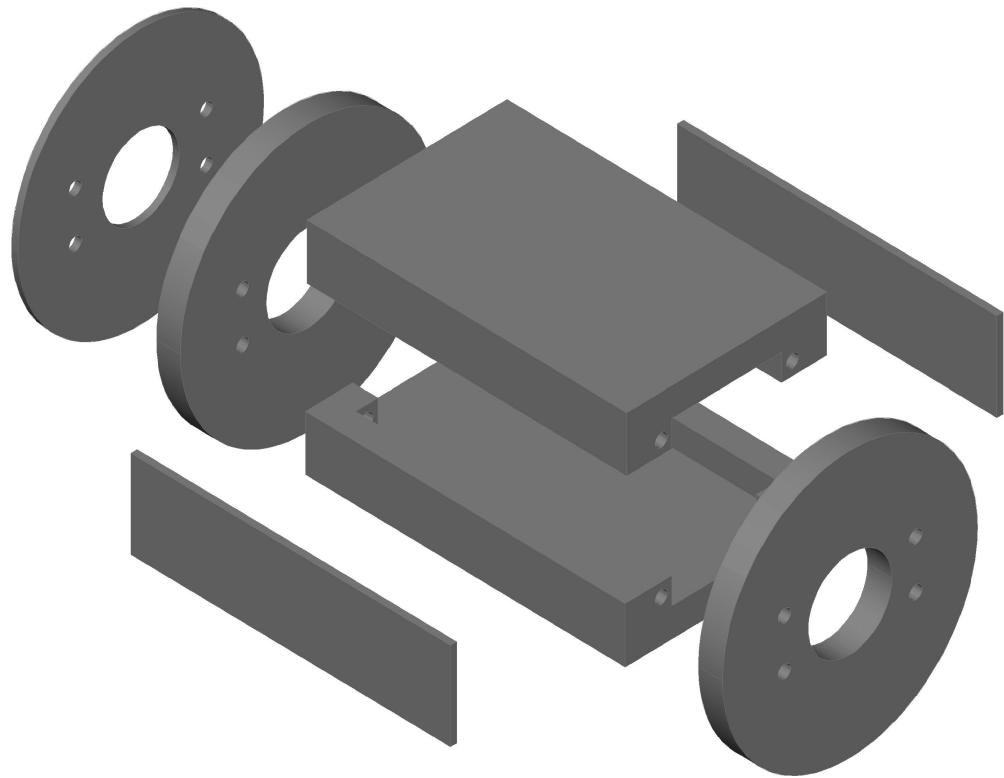


Figure 2.7 - Exploded and labeled view of the collectors.

traverse the interaction region independently of their energy. The known excitation function shape of the 427.8 nm N_2^+ emission was used as a standard in these tests. In practice batteries were used to supply this potential to avoid earth-loop problems and leakage currents.

2.C. The Electronics

2.C.1. Electron Gun Circuit

Figure 2.8 demonstrates the circuit diagram for the electron optical system. Five power supplies were used to operate the gun. The entire system floated off of a negative potential applied to the filament, provided by a 3-500 V home-made power supply. This defined the energy of the electrons in the interaction region. A Lambda power supply (Model# LPD-425A-FM) was used to power the lenses. Voltages were never allowed to exceed 350 V to prevent possible breakdown problems. Two 25 V Power-One Inc. power supplies (Model# HAA 24-.6) were used to power the X and Y deflectors, which were floating on the potential of the lens element named L1C. A 30 V Hewlett-Packard power supply (Model# 721A) was used to supply a negative potential to the grid. Finally, a 5 A home-made power supply was used to heat the filament. All of the power supplies had variable outputs, and each element was fed from a potentiometer which allowed independent adjustment of the element potential.

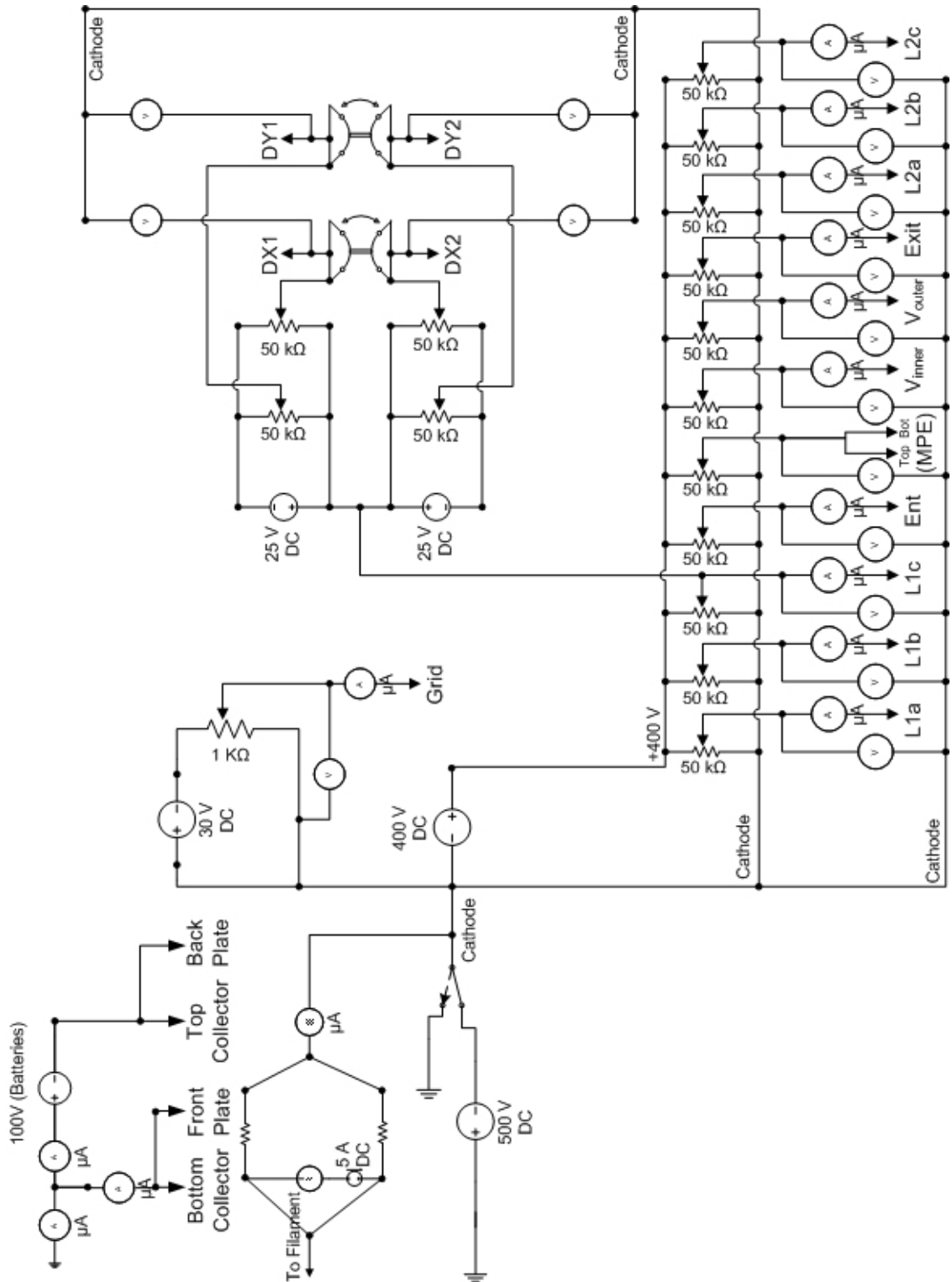


Figure 2.8 – Electric circuit diagram for the electron gun, used throughout the experiment. All power supplies could apply a varying voltage from 0 V up to its maximum. The 25 V power supplies provided a constant 25 V.

2.D. The Magnetic Field and Shielding

2.D.2. Magnetic Field

An average magnetic field of 150 Gauss along the electron beam direction was used to minimize the space charge effects which cause the electron beam to expand, especially at low energies. The magnetic field was essentially constant along the central axis, thus keeping the electrons in a well-focused beam.

2.D.3. Magnetic Shielding

To avoid the magnetic field adversely affecting the behaviour of the electron paths within the lenses and analyzer, the entire electron optical assembly was placed inside a mu-metal box, specially fabricated for this experiment. This box shielded the electrons until injected directly into the collimating magnetic field. Once injected, the magnetic field helped define the electron paths to the cross-field collector, which was also placed within the yoke. A diagram of the construction of the mu-metal box is included in Figure 2.9. This mu-metal box was clamped to a platform, aligning the system with the direct path of the laser.

2.E. Optimized System Operation

To assist in determining the optimized configuration for transmitting the electron beam from the filament through to the cross field collectors, a combination of tools were employed. Harting and Read's *Electrostatic Lenses* [Harting] was used in addition to the predictive formulae for a 127° Analyzer [Moore, et al., (2002)]. These helped determine appropriate lens voltage ratios based on the geometric configuration of the gun. Table 2.1 gives the predicted potential ratios from Harting and Read and the potentials for

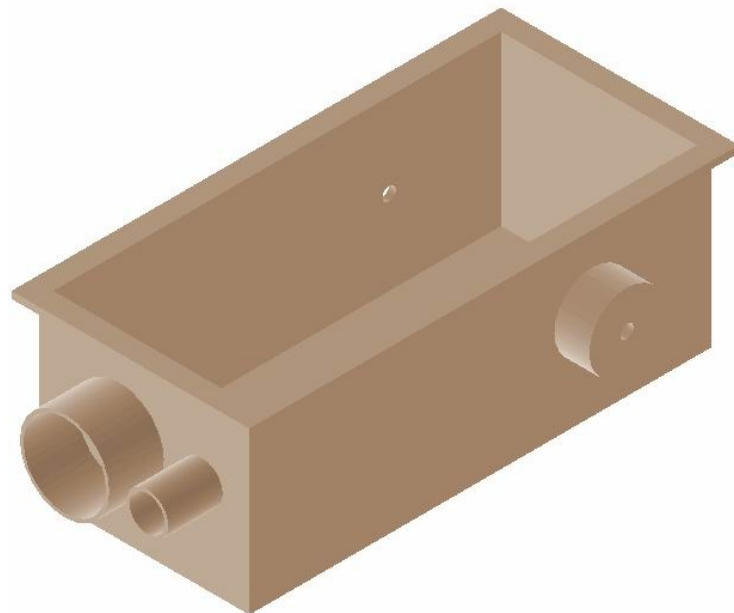
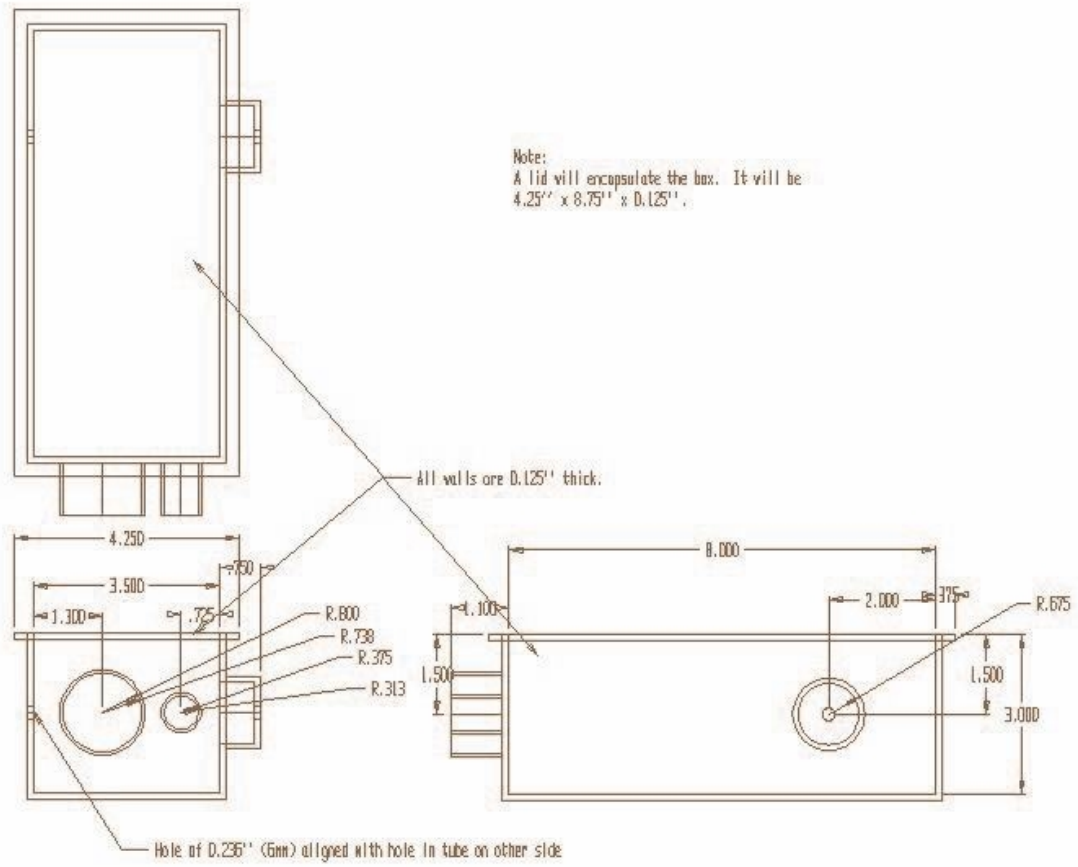


Figure 2.9 – Schematic and 3D view of the mu-metal box

various mean pass energies for the 127° analyzer used in this experiment. The formula for a 127° analyzer's inner- and outer-wall potentials, named V_{inner} and V_{outer} in this experiment, are included below:

$$V_{outer} = V_0 \left[1 + 2 \ln \frac{R_0}{R_2} \right] \quad (2.1) \text{ [Moore]}$$

and

$$V_{inner} = V_0 \left[1 + 2 \ln \frac{R_0}{R_1} \right] \quad (2.2) \text{ [Moore]}$$

where V_0 is the mean pass energy (fixed at 60.0 eV), R_0 is the mean radius (25.0 mm), R_2 is the outer radius (33.0 mm) and R_1 is the inner radius (17.0 mm). These resulted in theoretical values of 24.6 V and 106.3 V for the outer and inner voltages respectively.

V_0	V_{inner}	V_{outer}
25.00	44.28	11.11
30.00	53.14	13.34
32.00	56.68	14.23
50.00	88.56	22.23
60.00	106.30	24.60
70.00	123.99	31.13

Table 2.1 - Voltages for various transmission energies for the 127°, with R_0 , R_1 , and R_2 values 25.0, 17.0 and 33.0 mm respectively.

Most importantly, SIMION v 7.00 [Battelle, (2005)] was used as an accurate way to determine potentials for focusing. These potentials were used as a starting point when experimentally optimizing the system. Optimizing the current was the most critical component of success for this experiment. The optimized configuration, as will be shown in the following subsections, yielded a current of 0.64 μA for 3 eV electrons to 2.01 μA for 200.0 eV electrons where the total emission from the filament was 6.00 μA .

2.E.1 SIMION Model

SIMION version 7.00 [Battelle] was used to model the entire electron gun system. Potential settings were determined for the system using Equations (2.1) and (2.2) [Moore] above and the predicted ratios for the remaining elements based on published data appropriate to our electrode configuration from *Electrostatic Lenses* [Harting]. Because we were interested in total transmitted current and not high energy resolution, the mean pass energy of the 127° analyzer was set at 60.0 V. This minimized the acceleration ratio of the input lens, L1. The theoretical results of the SIMION model are graphically shown below in Figure 2.10. When the system was properly cleaned and tuned, results were found which were quite close to the predicted values. Using these lens voltages in the SIMION model yielded the results shown in Figure 2.11. It should be noted that the voltages for L2A and V_{inner} in the SIMION model are different than those applied experimentally. This optimized the transmission of the electrons through the simulated system. Table 2.2 demonstrates a comparison between the predicted and actual operating voltages. The present gun configuration, particularly the injection stage into the magnetic field, gave rise to some problems which will be discussed further in Chapter 6.

2.E.2. Configuration Potentials

Four critical factors were essential for proper operation of the electron beam. First the gun needed to behave consistently, regardless of any other variables. Second, potentials needed to be in alignment with what we expected from the SIMION model and the predictions of Harting and Read [Harting]. Third, it was hoped that at least 20% of the emission current could be transmitted successfully to the cross-field collectors.

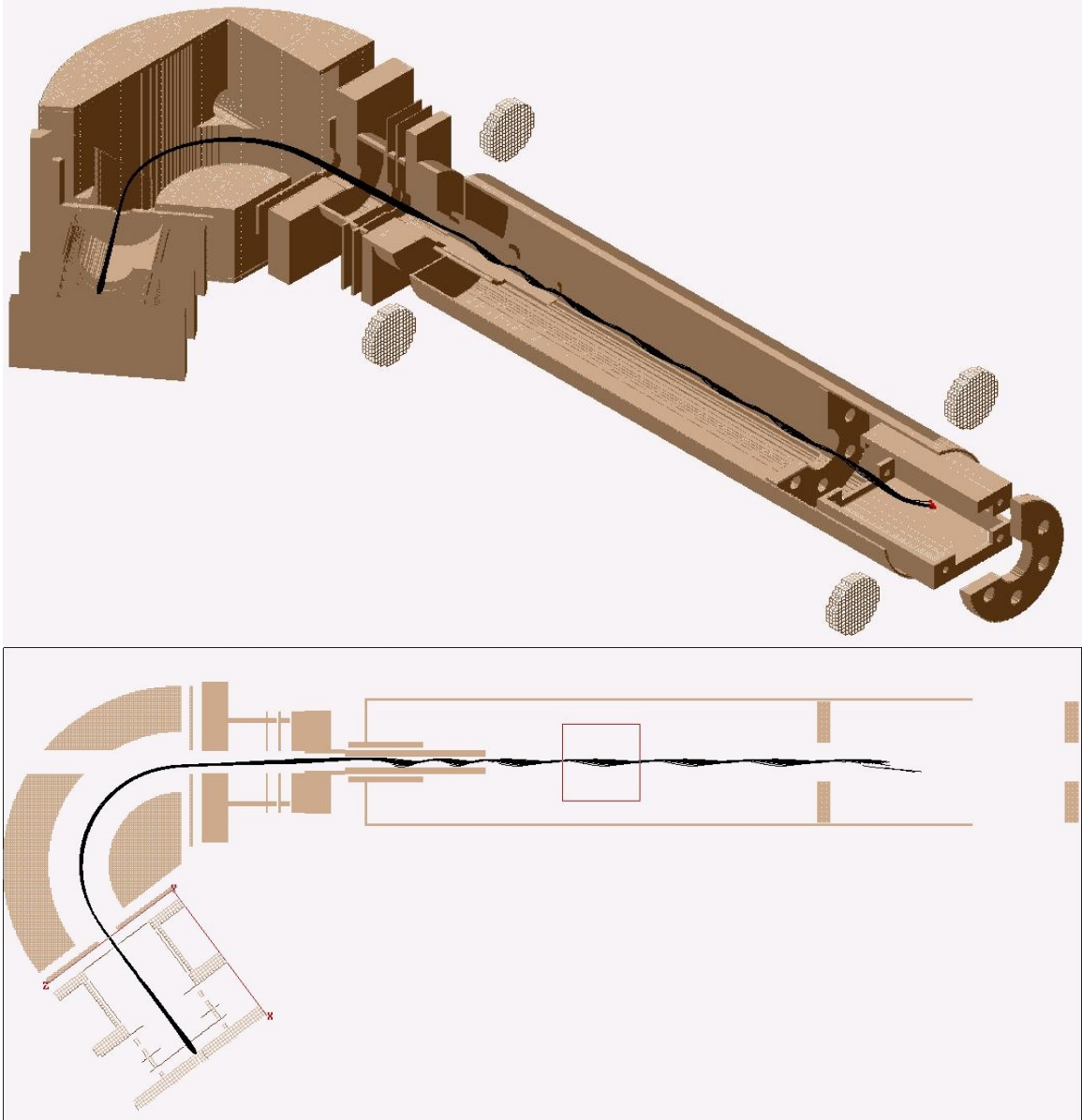


Figure 2.10 - 3D and 2D view respectively of electron trajectories obtained when using the theoretical values for potentials applied to the electron gun SIMION Model. The box shaded in the center of the 2D view represents the part of the interaction region focused by the lens onto the PMT cathode.

Lastly, the gun needed to be able to operate at low energies. All of these goals were accomplished as discussed below.

Table 2.2 lists the potentials applied to the various elements, relative to the cathode, which correspond to our SIMION model and are in alignment with the predictions found when using Harting and Read [Harting]. See Figure 2.4 for the locations of the listed lens elements.

Element Name	Theoretical Potentials Modeled in Figure 2.10	Potentials Modeled in Figure 2.11	Actual Experimental Potentials
Grid	0.00	-2.1	-2.1
L1A	15.00	60.5	60.5
L1B	400.00	176.9	176.9
L1C	60.00	60.0	60.1
DX1	55.00	70.5	70.5
DX2	65.00	60.0	60.1
DY1	60.00	60.0	60.0
DY2	60.00	60.0	60.0
Entrance	70.00	60.0	60.0
V _{inner}	106.30	64.7	94.7
V _{outer}	24.60	16.7	16.7
MPE	60.00	60.0	0.0
Exit	60.00	60.0	59.9
L2A	60.00	60.0	91.6
L2B	250.00	70.6	70.6
L2C	24.00	24.0	24.0
Collector	100.00	104.3	104.3

Table 2.2 - Comparison of theoretical and experimentally applied voltages. All values are listed in volts relative to the cathode with the exception of the collector where the potential is relative to earth. For the situations modeled in Figures 2.10 and 2.11, the cathode was 100 V relative to the interaction region. Note here that MPE means Mean Pass Energy plates and represents the plates above and below the analyzer.

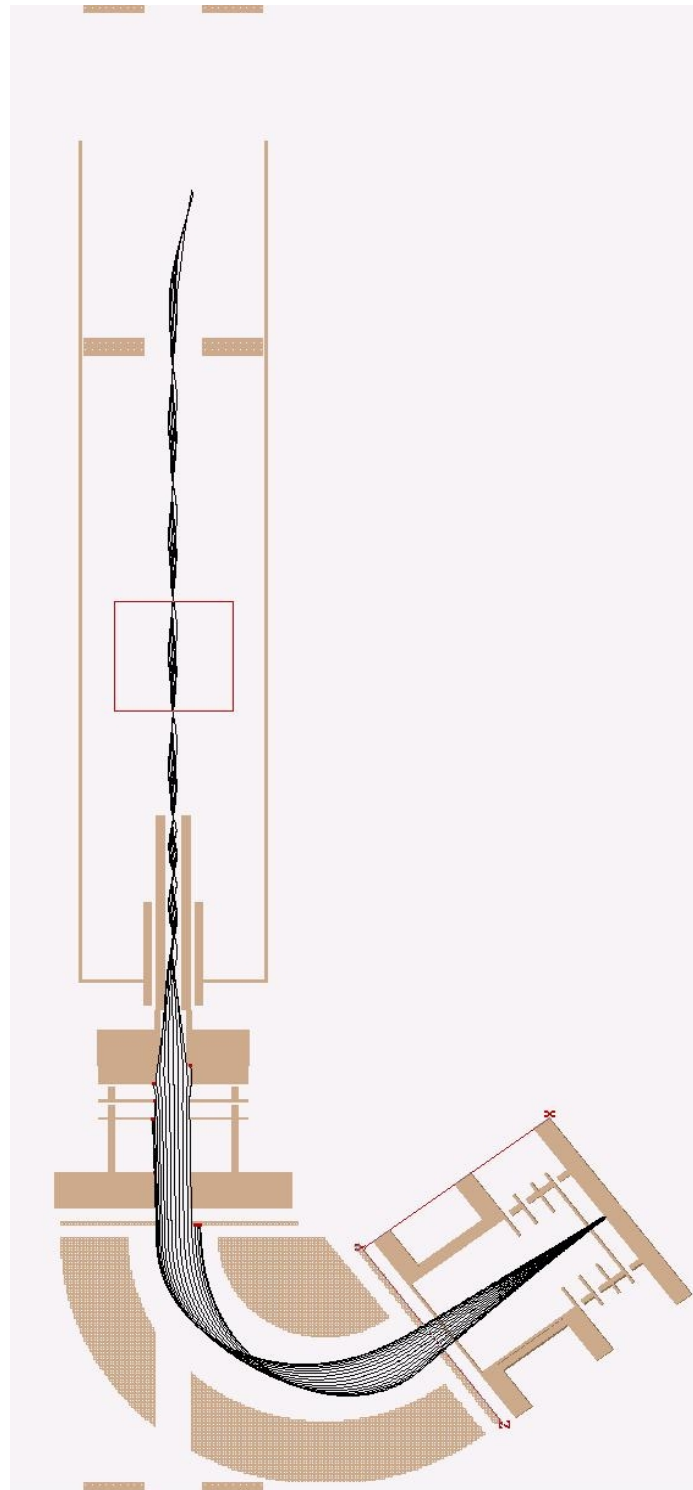


Figure 2.11 - 2D View of the electron trajectories using the voltages applied in SIMION as listed in Table 2.2, Column 3. The box outlined in the center of the beam path indicates the part of the interaction region focused by the lens onto the PMT cathode.

Some interesting facts emerge from a study of Figures 2.10 and 2.11. First it can be seen that ‘bunching’ of the electron beam occurs as it traverses the magnetic field region. The number of bunches is a function of the electron beam energy. This bunching is critical in that it demonstrates the need for a uniform target gas pressure throughout the interaction region when excitation function measurements of atomic emissions are being made. Otherwise, spurious features could be observed. Second it is noticeable that when maximum transmission of current is achieved, an intermediate focus occurs in the centre of the analyser. This may be the result of the rather large apertures which had to be used to accommodate the laser.

The analyzer made use of voltages that were very close to those predicted for a 127° analyzer at an analyzing energy of 60.0 eV, as shown above [Moore]. To obtain maximum passage of electrons through the analyzer, the plates known as Mean Pass Energy plates, or MPE, were given a potential value of 0 V relative to the cathode, as this provided some “squeezing” of the beam in the non-focusing plane.

The main downside of the present electron optical system is the fact that, over time, surface contamination of lens elements occurred with consequent charging of these elements with reduced gun performance. Fortunately, the gun would behave consistently for considerable periods of time, permitting the collection of data, and the changes that would take place would occur over several weeks. The emission current from the filament was kept at the low value of approximately 6 μA , so this process of charge buildup was delayed as much as possible. The best results were obtained when the gun was kept clean and the presence of pump oil vapours was minimized. Further

improvements that can be made on the geometric configuration of the electron optical system will be discussed in Chapter 6.

2.F. The Gas Injection

Previous work with this apparatus had used a pulsed target gas jet injection system. We initially intended to use a similar system but eventually decided on a static gas target where the interaction region would be longer and the constant target density throughout the interaction volume would avoid spurious data effects. However, for completeness, we give some details of the pulsed system. Thus, future applications will be able to make use of either configuration.

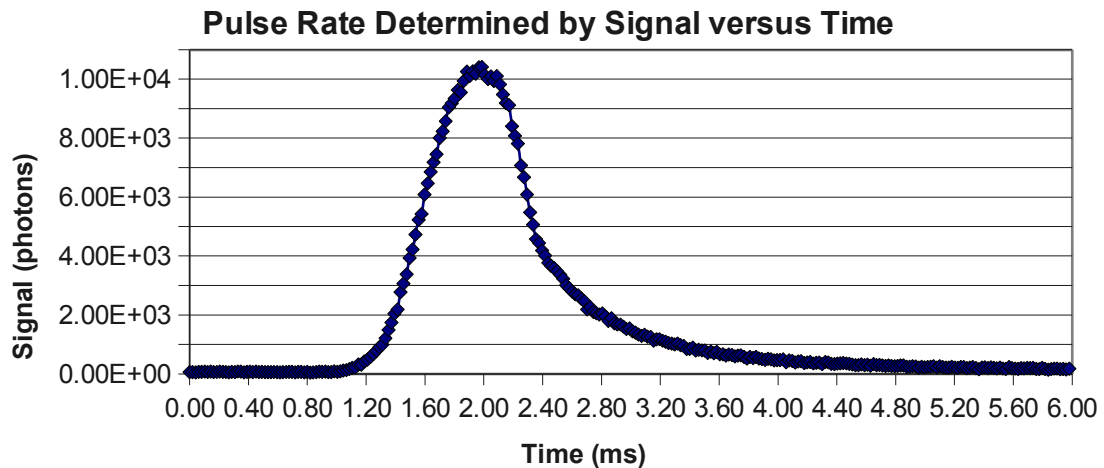


Figure 2.12 - The photon signal generated by a 800 μ s-width pulse valve.

2.F.1 Using a Pulsed Valve

A Parker Hannifin Corp. pulsed valve (Model # 9-181) was briefly explored and tested to find optimized settings. It was discovered that operating the valve with a pulse width, or full width half maximum value, of 800 μ s, at a maximum input voltage of 50V, provided optimum performance as determined by the shape of the gas pulse. This was determined by operating the electron gun and measuring photon signal versus time as the

valve was pulsed. The results of this study are shown above in Figure 2.12. This study was conducted using a photomultiplier (PMT) and a timing circuit which gated the fast multiscalar (A Standard Research Instruments SR430) synchronously with the pulsed valve at a rate of 2.5 Hz. The SR430 was used to record the signal versus time.

Various measurements were made comparing signal versus driving pressure, as well as signal versus chamber pressure. It was then determined that a driving pressure of 300 mtorr would create a sufficient amount of signal while also keeping the chamber pressure lower than 1.0×10^{-4} torr. Figure 2.13 illustrates the expected linear relationship between the signal versus the driving pressure for an energy of 100.0 eV.

Signal vs. Driving Pressure

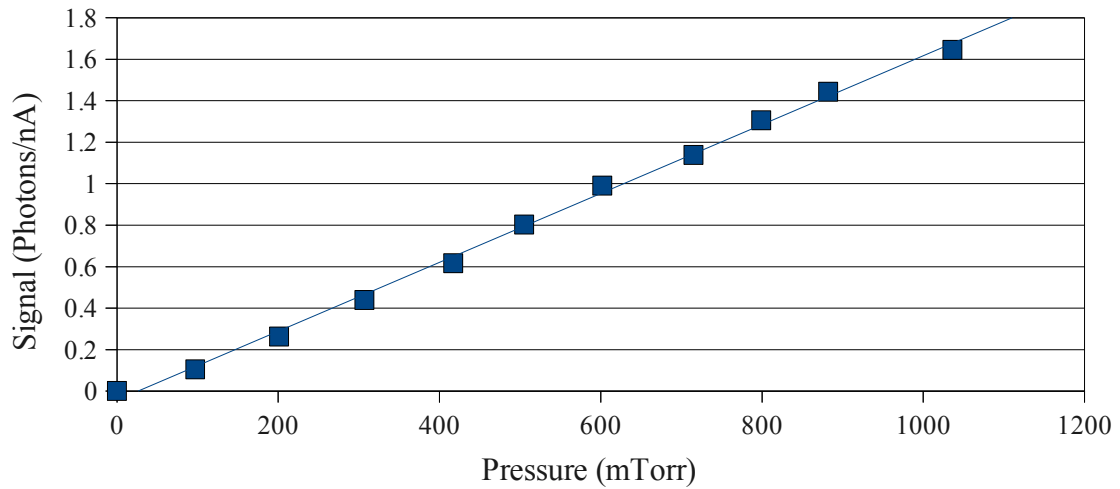


Figure 2.13 – A plot of photon signal from nitrogen versus driving pressure at 100.0 eV electron energy with a valve pulse-rate of 2.00 Hz.

2.F.2. Static Gas Setup

As discussed previously, it was found preferable to leak target gas at low pressure into the vacuum chamber containing the interaction region. It was found that a driving pressure of about 20 mtorr created a chamber pressure of 2.5×10^{-5} torr when the butterfly

valve to the diffusion pump was fully open. By partially closing the butterfly valve, so as to minimize pressure differentials in the chamber, the chamber pressure would rise to 1.9×10^{-4} torr, providing a great deal of signal for the tests conducted throughout the experiment.

2.G. The Light Collection

A XP2233B photomultiplier was used in series with several components to amplify and measure the signal. The variation of the quantum efficiency of the photomultiplier with wavelength is shown in Figure 2.14.

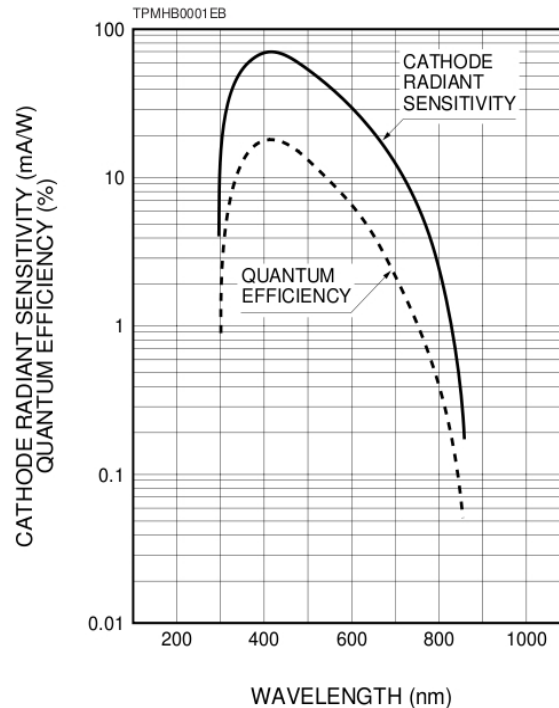


Figure 2.14 – Quantum efficiency curve given by Hamamatsu for the R7206-01 photocathode (similar to the XP2233B photocathode). [Hamamatsu, (1998)]

A block diagram of the light-collection system is included in Figure 2.15. A voltage of 1800 V was applied to the photomultiplier. A TE210RF, by Products for Research®, cooling system was applied to cool the PMT to temperatures around -20 °C.

It was necessary to use a lens to focus the light from the interaction region to the photomultiplier. With all conditions being kept equal between the data runs, the signal collected without the lens was approximately 1/5 of its value when the lens was used. Numerous optical filters were used throughout the experiment to isolate emissions of interest. Their transmission characteristics are shown in Chapter 4.

2.H. The Data Collection

A diagram of the data system is included as part of Figure 2.15. The signal from the photomultiplier was amplified by a home-made pre-amplifier in series with a timing filtering amplifier (Ortec Model 454). This amplifier was connected to a home-made master clock, whose delay was set at 0.0 ms and whose frequency was set at 10 Hz. The signal then passed to a Constant Fraction (C.F.) discriminator (Ortec Model 584) on the way to a photon counter (Ortec Model 9315) and a Standard Research Systems two-channel photon counter (SR400).

The SR400 was connected to a computer which was equipped with a 100-step multi-channel scaling software made previous [Harb, (2002)] in Quick Basic. The software was responsible for determining how many sweeps would be conducted as well as controlling the ramping voltage and monitoring the photon counts from the SR400. This program would ramp the energy, while simultaneously recording the photon counts from the SR400 and the current monitoring system. This provided the photon and current measurements.

The energy levels at each bin were determined by first determining the maximum and minimum voltages set by the ramping process and then dividing by 100 (the number of

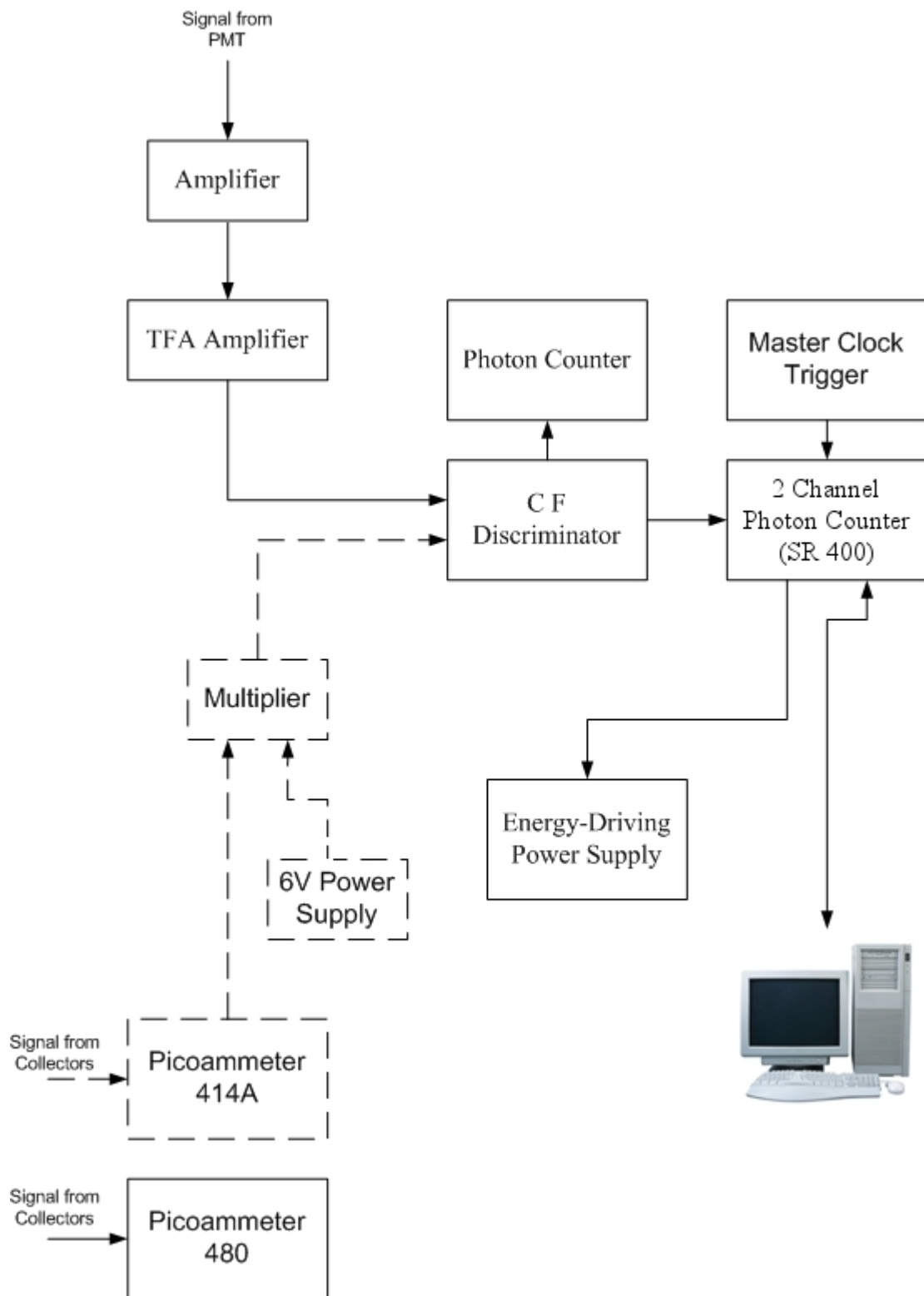


Figure 2.15 – Schematic of light and data collection. The dotted lines represent the schematic for digital current measurement.

bins used by the software).

The electron beam current was recorded manually using a Keithley Picoammeter (Model# 480A), which has a digital read-out and is accurate to 0.01 μA . Digital measurements of current were also made using a Keithley Picoammeter (Model# 414A). The process is shown by the path of dotted lines in Figure 2.15. This ammeter, which has an analog output, was connected, along with a constant 6 V power supply (Ortec Model 495), to a home-made analog multiplier which was also a voltage to frequency converter. The resultant signal was routed to the two-channel photon counter (SR400), which generated counts proportional to the current signal level. Figure 2.16 shows a typical plot of the current collected versus energy. The emission cross section data were created by dividing the photon counts by the current.

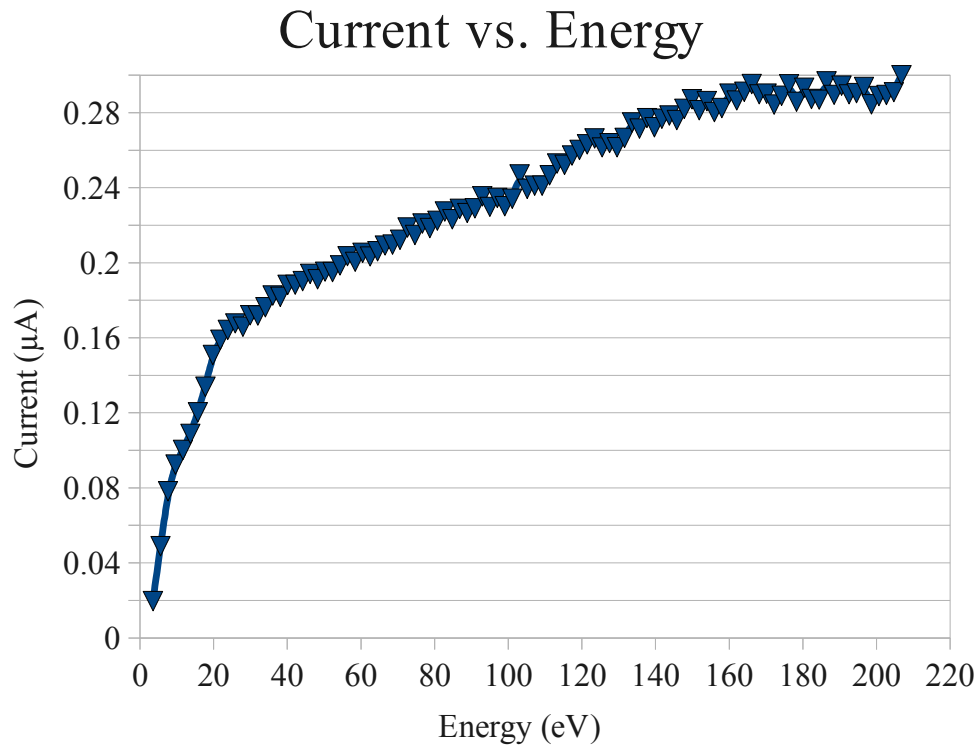


Figure 2.16 – Plot of collector current against electron beam energy.

2.I. The Laser

Laser induced fluorescence (LIF) was conducted by the use of a laser of wavelength 852.1443 nm (as measured in air). To accomplish this, a tunable-diode-laser by New Focus Inc. (Model# Velocity 6300) was used. To tune the laser and ensure that the wavelength was accurate, a series of mirrors and beam splitters were employed on the exit of the chamber where the beam was directed into a Burleigh WA-1500 wavemeter. Because the reading by the wavemeter did not match exactly the true wavelength, a two-stage method of calibration was employed.

First, a cesium cell was placed in the path of the laser, with an infrared camera aimed at the cell. When the laser was tuned to the wavelength of the $^2S_{1/2} \rightarrow ^2P_{3/2}$ resonance transition of cesium, 852.1149 nm, the cell would glow, and a reading was taken by the wavemeter. A full scan of the surrounding wavelengths was completed to determine the acceptable tolerance of the laser. Using the wavemeter, the laser was then adjusted by the difference (0.0294 nm) between the desired Ar and Cs wavelengths.

The second stage of calibration involved operating the electron gun in the presence of argon. The gun was operated at 12 eV, just above the threshold of the 794.8 nm excitation line (See Figure 4.2). When LIF was taking place, this photon signal would increase by over 40 % for a given fixed current. The Doppler broadening of the transitions in argon atoms was determined experimentally to agree with the following formula:

$$\Delta \nu_0 = \left(\frac{8 k_B T \ln(2)}{M c^2} \right)^{1/2} \nu_0 \quad (2.3) \text{ [Verdeyen, (1995)]}$$

where k_B was Boltzmann's Constant, T is the temperature in Kelvin, M is the atomic mass

in kilograms, c is the speed of light and ν_0 is the laser frequency. Experimentally it was found that the full width at half maximum was ± 0.0012 nm, compared with the theoretical 0.0016 nm. To maintain peak performance, the laser was tuned to the central wavelength, where the jitter was no more than ± 0.0005 nm. It was crucial to constantly monitor the wavelength as the laser was not stable for long time periods. More details on improvements to the laser system are included in Chapter 6.

Chapter 3 Measurement of Excitation of Nitrogen (N₂) by Electron Impact

3.A. Theory of Measurement and Error Budget

The optical emission cross section for a transition from level $i \rightarrow j$ (Q_{ij}^{Opt}) is given by the following formula, taken from Boffard et al.,

$$Q_{ij}^{Opt} = \frac{\Phi_{ij}}{n_0 I / e} \quad (3.1)$$

where Φ_{ij} is the number of photons emitted per unit time, per electron beam length at a wavelength λ_{ij} ; I is the electron beam current; e is the electron charge; and n_0 is the number density of atoms [Boffard]. Any excited level i can decay through many different transitions. Measured cross sections then are the sum of all optical emissions out of the excited level i . While direct excitation cross sections are of primary concern; the emissions cross sections measured could also include photons contributed by cascade [Boffard].

Normally all of the parameters in Equation 3.1 would need to be measured, excluding the constant e . Alternatively, one can use emissions from well-studied atoms and molecules as secondary standards and normalized to these. For this reason, possible systematic errors are not included in the present discussion. Statistical uncertainties were normally negligible due to the high signal rates obtained. Energies were normalized to the spectroscopic thresholds so uncertainties in this parameter were defined by the energy spread of the electron beam which was less than 1 eV (FWHM).

3.B. Introduction and Review of Previous Work

Nitrogen is the most prevalent gas in the Earth's atmosphere. Studies of the first negative band of N_2^+ (0,1) [Borst, et al., (1969)], and of the second positive band of N_2 (0,0) [Shemansky, et al., (1995)], are of particular importance in understanding auroral emissions from Earth's atmosphere [Borst]. The titles 'first negative' and 'second positive' are historical in origin and refer to excitation transitions illustrated below in Figure 3.B.1. The behaviour of the ionosphere due to auroral conditions can be studied through direct use of electron-impact excitation measurements of the first negative band [Borst]. The second positive band is of particular interest because its emission cross section peaks at low energy and because its excitation from ground state N_2 is optically forbidden; thus it is not naturally excited by solar photons [Shemansky]. Because these states are so well-studied, they serve as an excellent base for theoretical models of atmospheric processes. Nitrogen excitation and emission are also of interest in studies of celestial bodies such as planets and moons; further, the atmospheric properties of celestial bodies can be studied by these uniquely identifiable electron-impact transitions which naturally occur in atmospheres composed of nitrogen. These are of particular interest in the search for other earth-like environments [Malone, et al., (2009)].

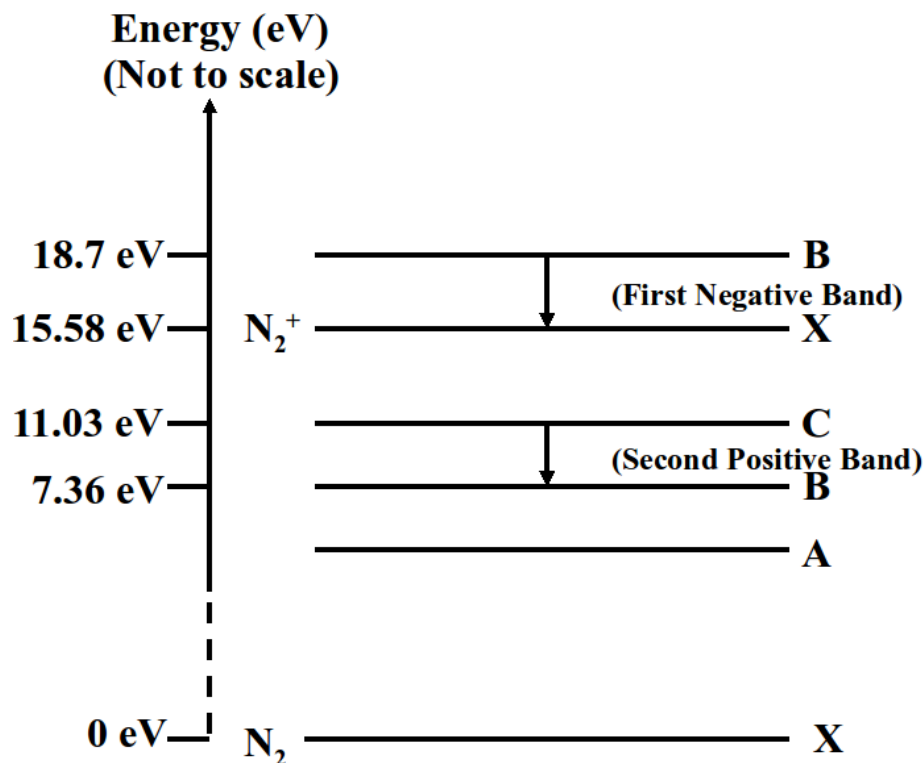
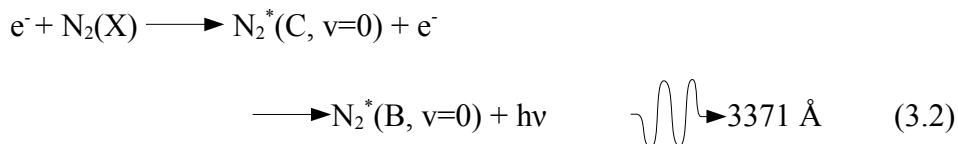
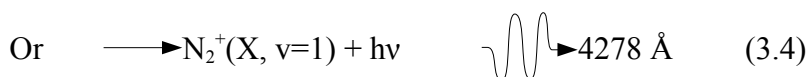
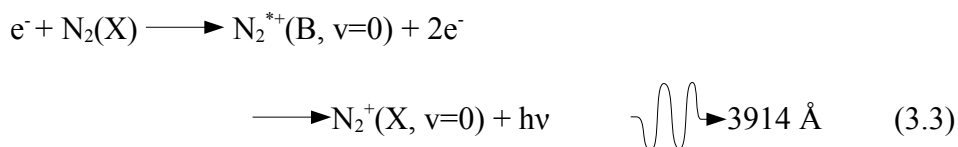


Figure 3.B.1 – A diagram of the excited states of N_2 and N_2^+ used in this work in relation to the ground state of nitrogen with the first negative and second positive bands indicated.

The (0,0) second positive band of N_2 occurs as the following process:



[Tyte, et al., (1965)]. This state has a peak in its cross section at an energy of 14.1 eV [Shemansky] and its threshold is at 11.03eV [Huber, et al., 1979]. Similarly, the (0,0) and (0,1) first negative bands of N_2^+ occur in the following manner:



[Tyte]. The cross sections of these states peak at an energy of about 100 eV [Borst] and their threshold is at 18.7 eV. Comprehensive studies of the cross section of the (0,0) second positive band of nitrogen have been carried out by Imami and Borst [Imami, et al., (1974)] and Shemansky et al. [Shemansky (1995)]. The cross sections of the first negative bands have been measured by numerous groups (See Borst [Borst] for detailed references).

3.C. Experimental Details

The setup for the cross section measurements in nitrogen was simple. The chamber was evacuated to a value of 3.0×10^{-6} torr. A nitrogen tank of “Ultra High Purity 5.0” was connected to the gas inlet system and nitrogen was leaked into the chamber as was shown in Figure 2.1 above. A needle valve controlled the flow such that, with the control valve opened, a pressure of 35 mtorr was observed in the input gas line. Under these conditions and with the butterfly partially closed, the pressure in the chamber rose to a value of 9.0×10^{-5} torr. Optical filters centered on 330 and 423 nm allowed the different features to be isolated. Electron currents through the interaction region were typically 1 μ A. The (0,0) second positive band was measured over the electron energy ranges of 3 eV to 25 eV, and 200 eV respectively. The (0,1) first negative band was measured over the ranges of 3 eV to 25 eV, and 200 eV respectively. The results are shown in Section 3.D below.

3.D. Results and Discussion

The data for the two bands measured are included below. The results of the measurement of the (0,0) second positive band were compared with the results from both Shemansky et al. [Shemansky] and Imami and Borst [Imami]. The measurement results

of the (0,1) first negative band were compared with the (0,0) first negative band cross section taken from Borst and Zipf [Borst]. The measurement of the second-positive band, because it was so sharply defined, was used as the primary calibrating point; the energy was shifted so that the appearance energy for our results agreed with the spectroscopic threshold. This shift in energy (2.93 eV) was then applied to subsequent data.

3.D.1. Excitation of the (0,0) Second Positive Band of N₂ (C→B)

The results of the present data collection were compared with previous work, [Shemansky, Imami] and are shown below in Figures 3.1 and 3.2. A shift of 2.93 eV in the energy of the data collected was made so as to align the spectroscopic threshold values between the three sets of data. This resulted in remarkable agreement between the present and previous data, particularly with Shemansky et al. [Shemansky]. The raw data are included in Table 3.1 below. The discrepancies found above 30 eV can be accounted for by the presence of low energy secondary electrons in the electron beam or by the fact that the interference filter was transmitting a component of the first negative N₂⁺ bands which possess a much broader excitation function.

The conclusion from these measurements was that the system behaved well in the range of 3-30 eV. For higher energy performance the 427.8 N₂⁺ band was used as a standard.

Present Work		Shemansky et. al.		Imami and Borst	
Energy (eV)	Cross Section (10^{-18} cm ²)	Energy (eV)	Cross Section (10^{-18} cm ²)	Energy (eV)	Cross Section (10^{-18} cm ²)
11.41	0.70	11.23	0.383	11	0
11.67	1.04	11.64	0.971	11.5	0.2
11.93	1.56	12.05	1.620	12.5	1.8
12.44	2.91	12.46	2.890	13.5	6.8
12.70	5.04	12.67	4.310	14	10
12.95	5.58	13.08	6.910	14.5	11
13.47	8.87	13.49	9.850	16	9.5
14.24	11.26	14.1	11.260	17	8
14.50	11.22	14.72	9.860	19	5.6
14.75	10.66	15.13	9.170	21	4.3
15.27	9.25	15.54	8.230	24	3.1
15.52	8.66	16.15	7.160	26	2.63
16.29	7.27	17.18	5.870	30	1.91
17.07	6.32	18.2	5.450	35	1.35
18.35	5.48	19.02	4.820	40	1.05
19.12	4.85	20.05	4.240	50	0.65
20.15	4.30	25.17	2.560	60	0.43
25.03	2.52	30.09	2.010	70	0.3
25.29	2.43	35.01	1.500	80	0.22
29.63	2.18	40.14	1.140	90	0.17
31.98	2.09	100	0.174	100	0.13
34.01	1.51	150	0.077	150	0.02
36.05	1.32	200	0.043	200	0.03
40.11	1.11				
44.17	0.92				
50.27	0.78				
54.34	0.73				
60.43	0.65				
64.50	0.59				
70.59	0.50				
80.75	0.43				
90.92	0.36				
101.08	0.38				
119.37	0.28				
139.69	0.27				
149.85	0.22				
160.01	0.22				
180.33	0.23				
200.66	0.17				

Table 3.1 – Comparison of present data for the N_2 ($C \rightarrow B$) second positive band (with peak value normalized to the peak value of Shemansky et al.) with the results from Shemansky et al. and Imami and Borst [Imami]. Note that the results from Shemansky et al. for 100, 150 and 200 eV are taken from theoretical models.

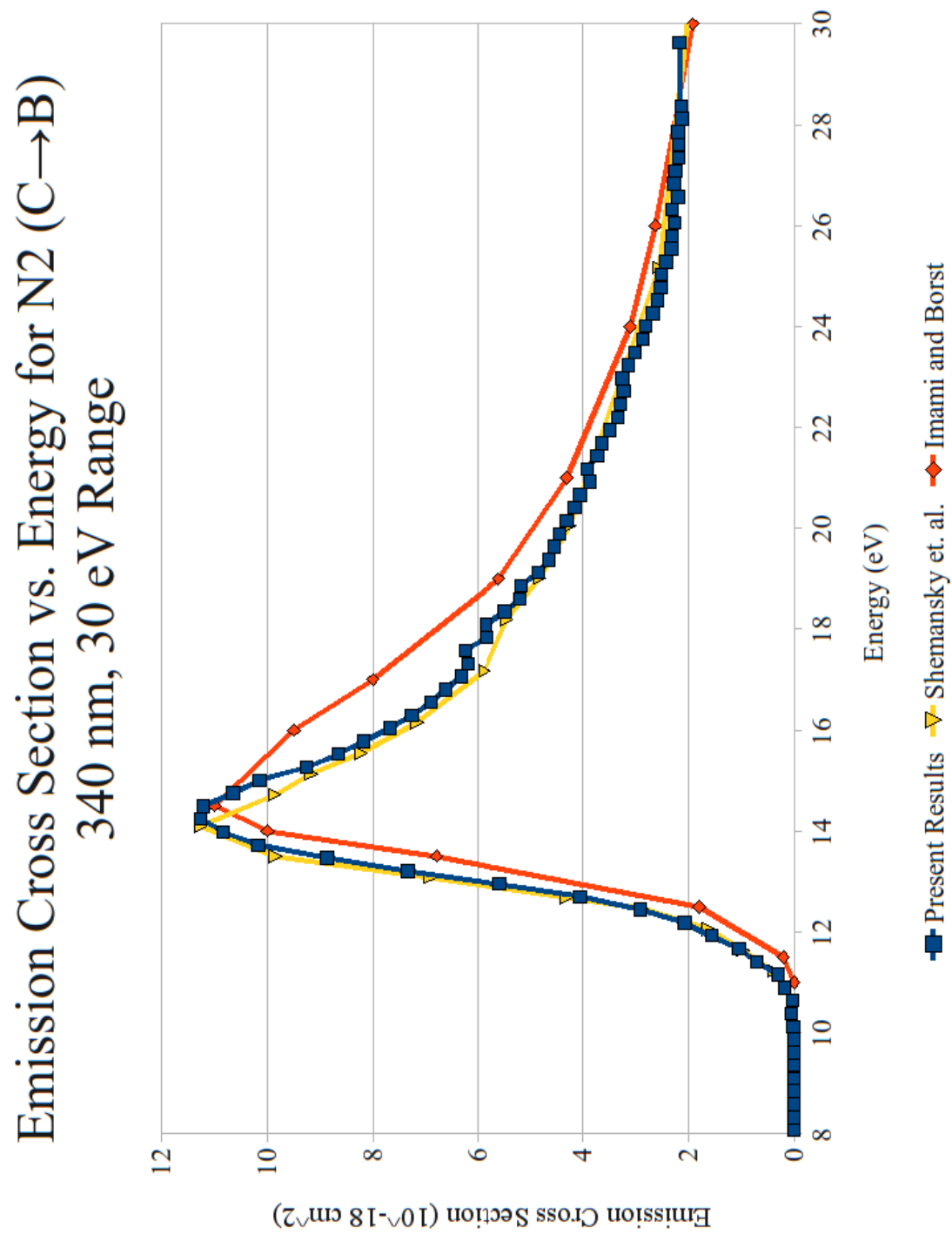


Figure 3.1 – Excitation function of the (0,0) second positive band of N₂ (C→B) comparing present data with previous results from Shemansky et al. and Imami and Borst [Imami] over the 3-30 eV range.

Emission Cross Section vs. Energy for N₂ (C→B) 340 nm, 200 eV Range

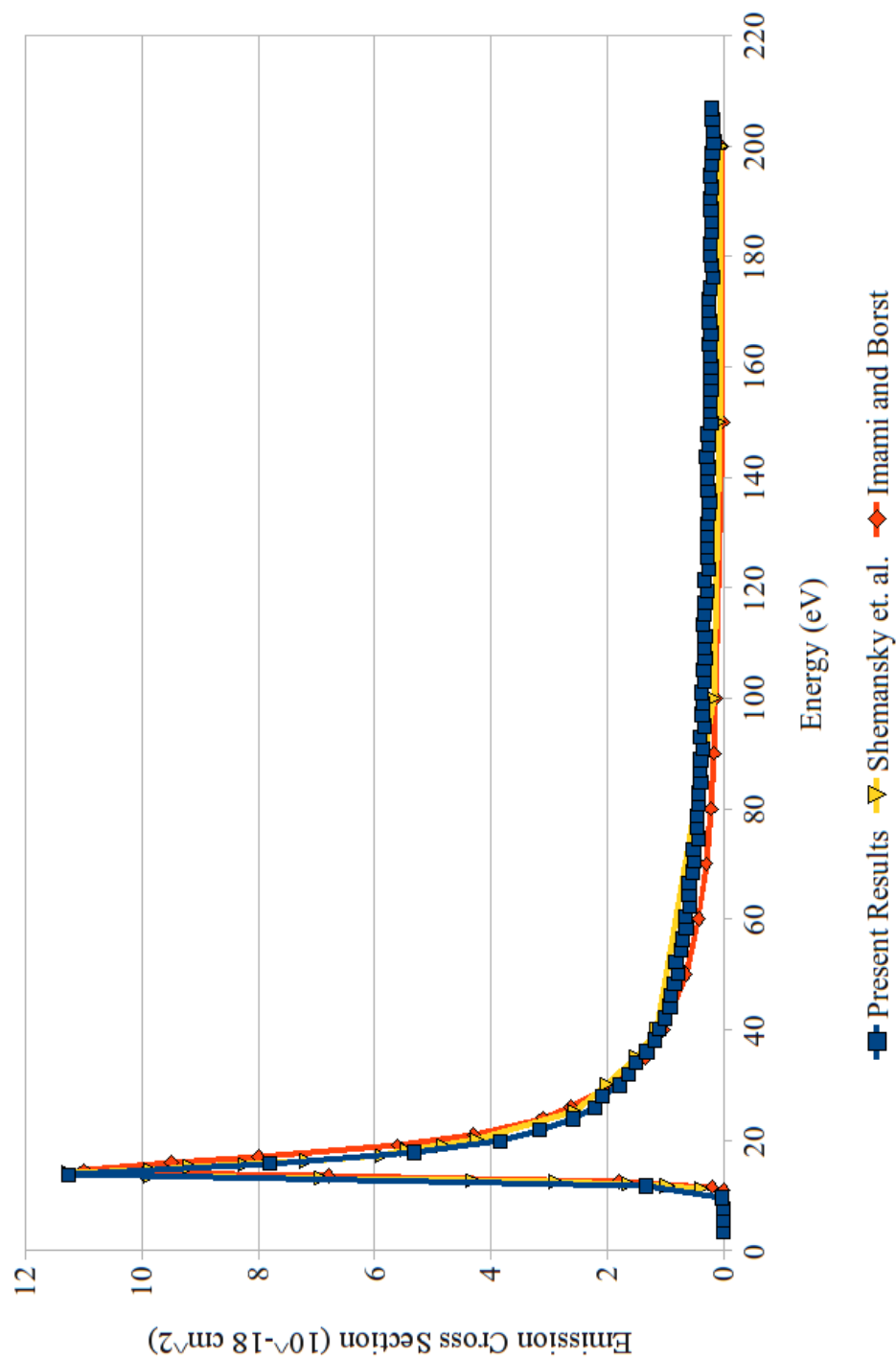


Figure 3.2 – Cross section of the (0,0) second positive band of N₂ (C→B) comparing present data with previous results from Shemansky et al. and Imami and Borst [Imami] over the 3-200 eV range. Note that the final 3 data points (100, 150 and 200 eV respectively) of Shemansky et al. were taken from their theoretical model.

3.D.2. Excitation of the (0,1) First Negative Band of N_2^+ (B \rightarrow X)

Present cross section data for the (0,1) first negative band are compared with previous work in Table 3.2 and Figures 3.3 and 3.4 below. The results were completely reproducible. Notice that there is an additional sharply peaked feature which occurs below the threshold of the first negative band. This is due to excitation of the ($\Delta v = 4$) second positive bands N_2 (C \rightarrow B), whose wavelengths are between 420 nm and 435 nm. The 423 nm filter, whose transmission half-width was ± 10 nm (see Figure 4.9), allowed some fraction of these bands to be detected. The threshold, for the (0,1) excitation of the first negative band of nitrogen was adjusted to the spectroscopic threshold (18.7 eV) utilizing the same energy shift as above (2.93 eV). The data was then normalized to the data by Borst and Zipf [Borst], who studied the (0,0) excitation of the first negative band. For accurate comparison, the data by Borst and Zipf [Borst] was multiplied by the ratio of the (0,1) to (0,0) first negative band (0.32:1) as determined by McConkey et al. [McConkey et al., (1965)]. By subtracting normalized data from the second positive band as observed in Section 3.D.1, the present data was adjusted to show remarkable agreement with the data found by Borst and Zipf [Borst]. These corrected results are demonstrated in Figure 3.3. When the previous work from Borst and Zipf [Borst] was compared with present data, it was seen that close agreement was obtained for energies up to 110 eV. For the future goals of this experiment, the functionality of the system in the range from 3 to 100 eV was of primary concern. The present results demonstrated clearly that this has been achieved.

Present Corrected Results (25 eV Range)		Present Uncorrected Results (100 eV Range)		Borst and Zipf	
Energy (eV)	Signal/Current (Arbitrary Units)	Energy (eV)	Cross Section (10^{-18}cm^2)	Energy (eV)	Cross Section (10^{-18}cm^2)
19.12	0.05	10.36	0.01	19	0.04
19.64	0.11	11.37	0.03	19.2	0.08
19.89	0.15	12.39	0.13	19.6	0.15
20.92	0.41	13.41	0.46	20	0.23
21.95	0.59	14.43	0.99	21	0.43
22.98	0.84	15.45	0.98	22	0.63
24.00	1.05	16.46	0.78	23	0.84
25.03	1.24	17.48	0.63	24	1.04
26.06	1.42	18.50	0.56	25	1.24
27.09	1.71	19.52	0.55	26	1.45
28.63	2.36	20.54	0.68	27	1.66
		21.55	0.89	30	2.29
		22.57	1.13	35	3.23
		23.59	1.34	40	3.87
		24.61	1.52	45	4.35
		25.63	1.71	50	4.7
		26.64	1.88	55	4.93
		27.66	2.13	60	5.12
		29.70	2.53	70	5.34
		34.79	3.59	80	5.47
		39.88	4.31	90	5.54
		44.97	4.55	100	5.57
		50.06	5.00	110	5.57
		55.15	5.24	120	5.54
		60.24	5.44	140	5.38
		70.42	5.42	160	5.22
		80.60	5.47	180	5.06
		90.78	5.40	200	4.86
		99.94	5.68		
		105.03	5.91		

Table 3.2 – Comparison of present data for the N_2^+ ($B \rightarrow X$) first negative band (Normalized to data from Borst and Zipf [Borst] multiplied by the ratio of 0.32, see text for more details) with the results of Borst and Zipf [Borst]. Data below 19 eV in Column 2 indicated the presence of second positive bands (See text for more details).

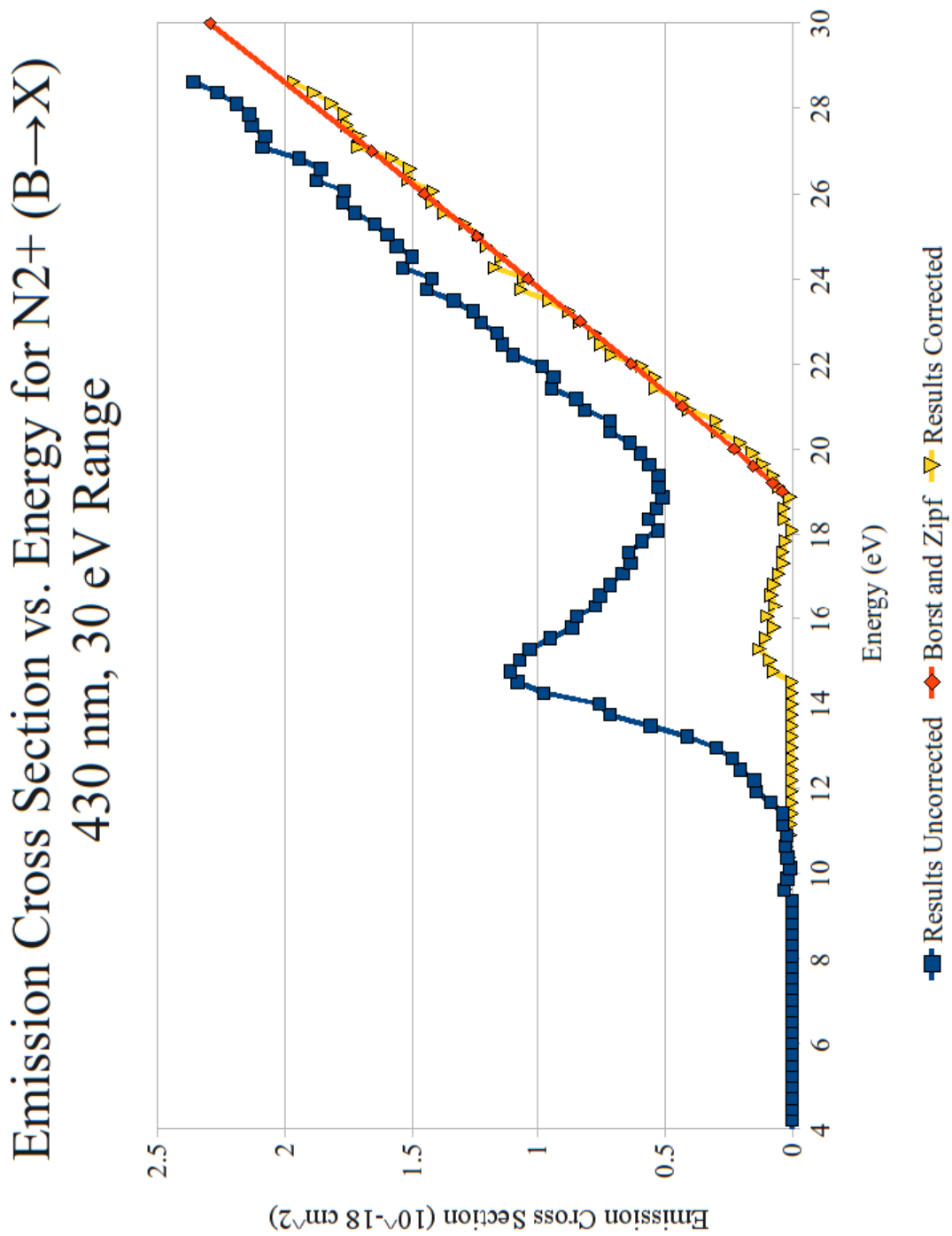


Figure 3.3 – Cross section of the (0,1) first negative band of N_2^+ ($B \rightarrow X$), over the 3-30 eV region, comparing present and corrected data with previous results by Borst and Zipf [Borst], corrected by the ratio from McConkey et al. [McConkey, (1965)] (See text for details).

Emission Cross Section vs. Energy for N_2^+ ($B \rightarrow X$)
 430 nm, 100 eV Range

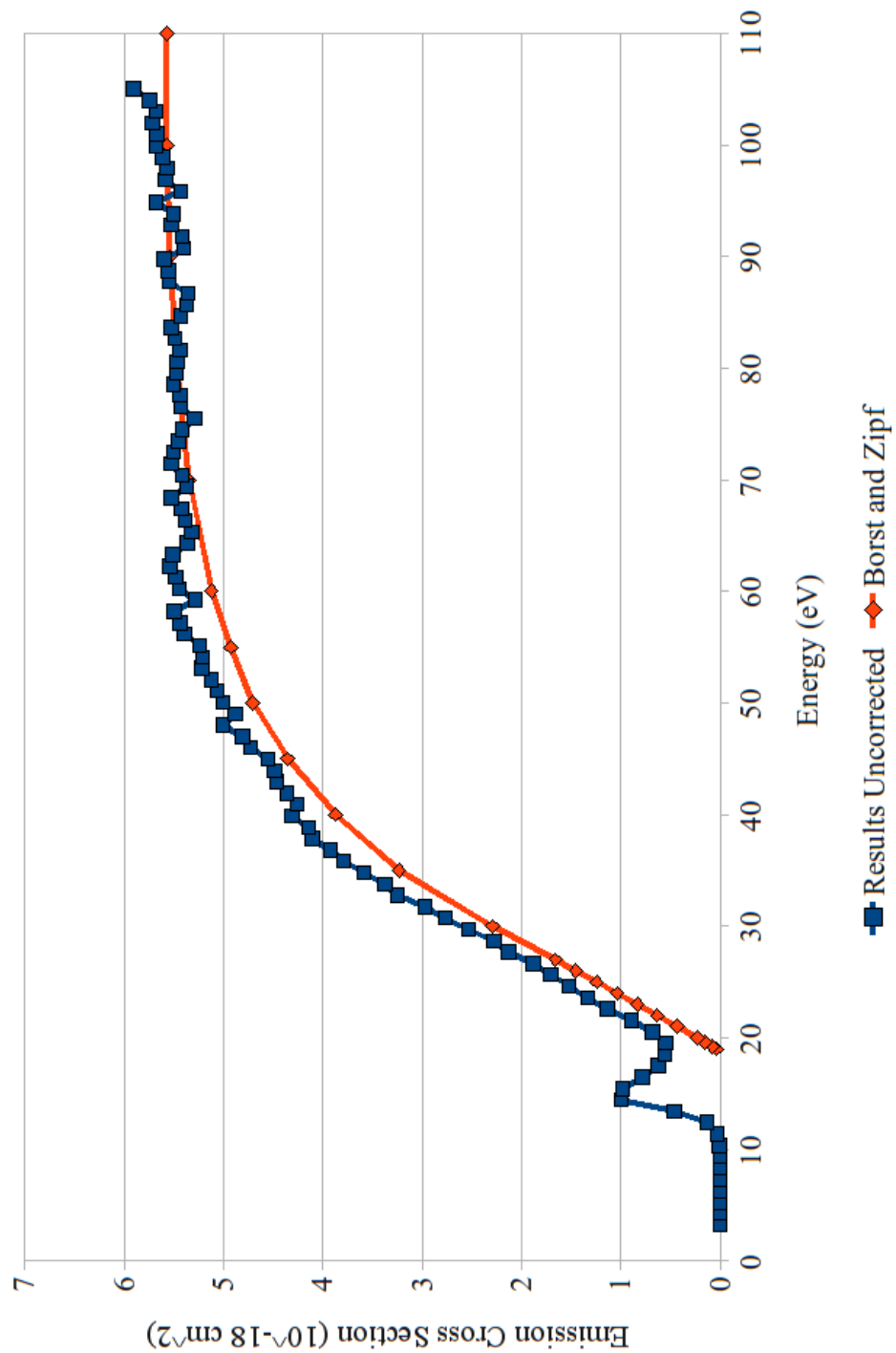


Figure 3.4 – Cross section of the (0,1) first negative band of N_2^+ ($B \rightarrow X$), over the 3-110 eV range, comparing present data with previous results by Borst and Zipf [Borst], corrected by the ratio from McConkey et al. [McConkey, (1965)] (See text for details).

3.E Summary and Conclusions

It was concluded from the nitrogen calibrations that an energy shift of approximately 3 eV should be applied to measured data. The (0,0) second positive band results demonstrated very close agreement with those previously measured [Shemansky]. A positive correlation was observed for the excitation function shapes between the present data and previous works [Borst, Imami, Shemansky] for the (0,0) second positive band and the (0,1) first negative band of nitrogen.

Furthermore, a significant amount of signal could be obtained in an extremely short period of time. The gate width was only 10 ms for the (0,0) second positive band, when it could easily have been increased to 90 ms; however the software could not handle the significantly higher counts that would occur. Similarly, the (0,1) first positive band was measured with a gate width of only 20 ms of the available 90 ms. Since these bands were particularly bright in intensity, these results showed excellent promise for high signal rates for the measurement of argon, and consequently also promise high signal rates for future measurements with other targets.

Chapter 4 Measurement of Excitation of Argon (Ar) by Electron Impact and LIF

4.A. Introduction and Review of Previous Work

Cross sectional data of argon play a critical role in industrial and experimental plasmas. Applications include lasers, fluorescent lighting and plasma displays [Boffard et al., (2007)]. Cross section information of argon is also very useful in understanding atomic structure and electron-atom interactions; the data are used to help create atomic models involving the many electron-electron interactions and the many possible angular-momentum vector couplings [Ballou et al., (1973)]. Strongly excited argon lines also are also used to detect planetary formation in celestial bodies in addition to many other space applications [Ajello, et al., (1990)]. LIF measurements of argon in particular have been used in plasma physics measurements [Severn, et al. (1998)].

In this experiment, the cross sections of a number of Ar emissions were measured by electron-impact techniques using the optical method [Boffard]. Following this, LIF involving the $3p^54p [1 \frac{1}{2}] (J=1) \rightarrow 3p^54s [\frac{1}{2}] (J=1)$ transition of argon (Highlighted in Figure 4.1) was used to probe the excitation of the $3p^54s [\frac{1}{2}] (J=1)$ level (The number in square brackets refers to the total angular momentum of the core). Comprehensive studies have been conducted on the electron-impact excitation of argon; most recently these have been summarized thoroughly by J.B. Boffard et al. and J.E. Chilton et al. [Chilton, et al., (1998)]. LIF techniques involving the metastable states have been explored by Schappe et al. [Schappe, et al. (1994)].

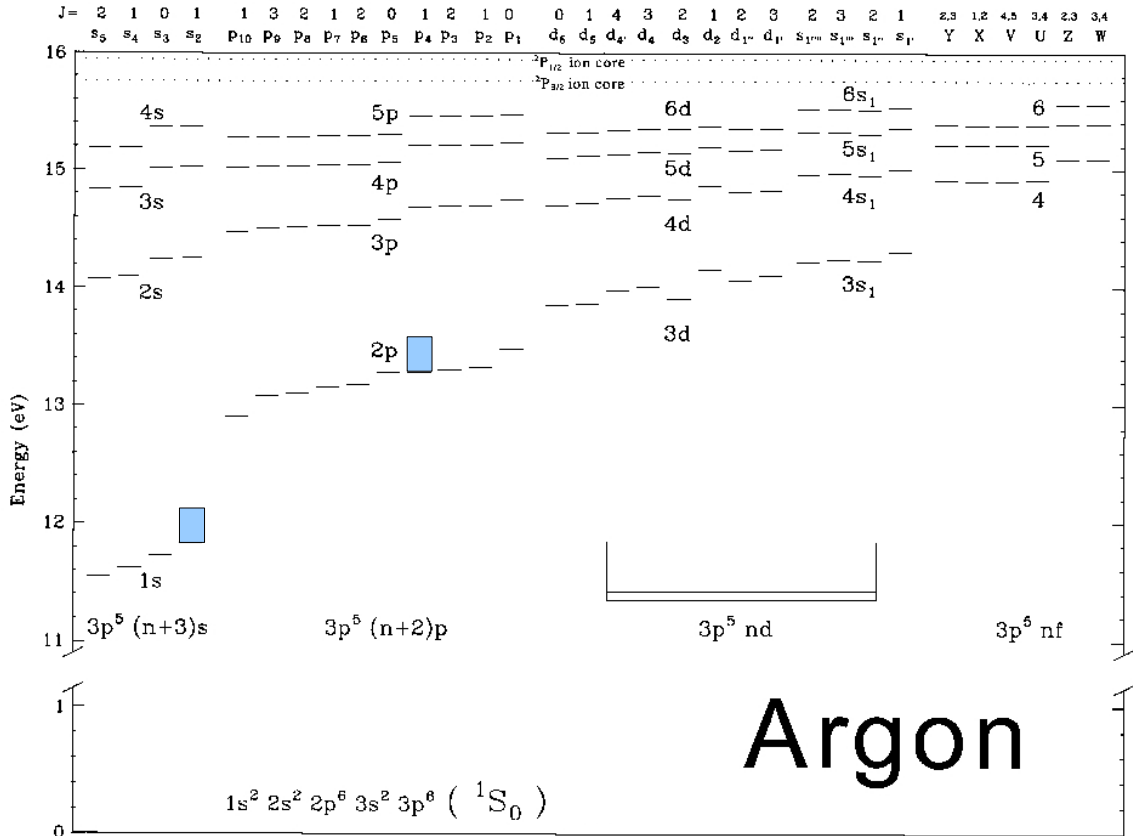


Figure 4.1 – Energy level diagram for argon. The top features the J-value, under which is the Paschen's notation for the excited state. The conversion to configuration notation is provided at the bottom. [Chilton] The states involved in the LIF measurements are indicated by the boxes.

4.B. LIF

The process of Laser Induced Fluorescence (LIF) is explained in Figure 4.2 below. It is a process whereby an atom, in this case argon, is excited by a laser of a specific wavelength from a lower state, shown as state “a”, to a higher excited state, shown as state “b”. Spontaneous emission will occur as the excited atom descends to a different state, shown as state “c”. It is the emission to this final state that is measured. The electrons begin to excite the atom to state “a” at a threshold energy of approximately 11.72 eV [Ralchenko et al., (2001)], where a laser of wavelength 852.1443 nm

[Ralchenko] excites the atoms to state “b”. Through spontaneous emission, the atom descends to a resonant state “c”, emitting a photon of wavelength 794.8176 nm [Ralchenko].

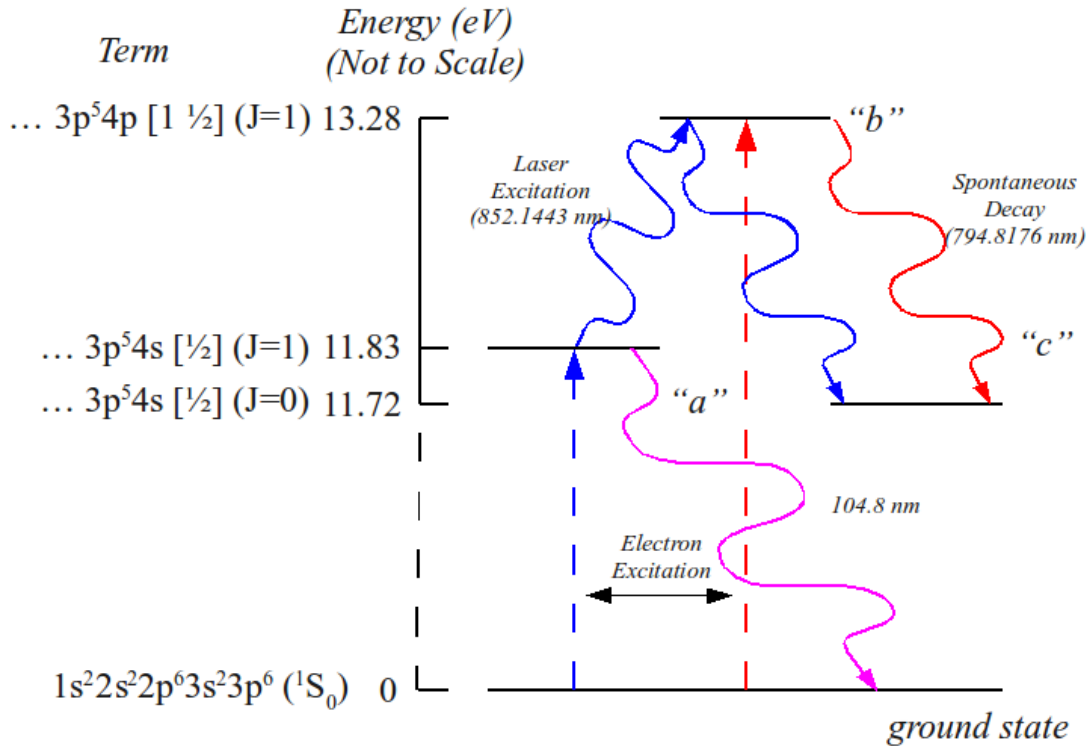


Figure 4.2 - Schematic diagram of the LIF process used in this experiment for argon. The solid lines indicate the LIF process, while the dotted line indicates the electron-impact excitation. The term on the left has been listed in configuration notation. The energies listed for the energy level have been taken from NIST [Ralchenko]. The lifetimes of the “a” and “b” states are 2 ns and 31 ns respectively.

4.C. Experimental Details

The setup for the cross sectional measurements in argon by electron excitation was very similar to that for nitrogen. The chamber was pressurized to a value of 5×10^{-5} torr to 9×10^{-4} torr using argon gas of 99.95% purity. The gas inlet control system was identical to that used for nitrogen (See Figure 2.1). Appropriate filters were used to isolate the different transitions or groups of transitions as discussed in detail below.

An identical setup as above was used for the implementation of LIF techniques, only the addition of a laser, as described in Section 2.I above, was made to the setup as shown in Figure 2.1. The diode laser was tuned to 852.1442 nm, and was monitored by the Burleigh Wavemeter as described in Section 2.I above. This wavelength matched the argon $3p^54s [1/2] (J=1) \rightarrow 3p^54p [1/2] (J=1)$ transition.

4.D. Results and Discussion

4.D.1. The $3p^54p [1/2] (J=1) \rightarrow 3p^54s [1/2] (J=0)$ (“794.8 nm”) Transition

This transition was of particular interest because its complete excitation function had not been published previously and because it was the test transition for which LIF excitation was possible. A special narrowband filter centered on 793 nm was used. Figure 4.3 shows the transmission function of the filter and also indicates which Ar lines in addition to 794.8 nm might also be partially transmitted. From the anticipated intensity of these lines, based on cross section data of Boffard et al., the 794.8 nm emission was expected to dominate the observed signal. We note that the reduced sensitivity of the photomultiplier for wavelengths longer than 800 nm also helped to discriminate against the two very intense lines above this wavelength.

Excitation data for this transition was obtained over the impact energy ranges of 3 to 25 eV, and 100 eV respectively. These results are shown in Figures 4.4, and 4.5 below and compared with previous results. The threshold has been adjusted to the spectroscopic threshold of 13.28 eV. Here the peak cross section was normalized by considering the Boffard et al. data for all excitations which fell within the range of the filter. Analytical equations were provided by Boffard et al. from which any emission line excitation

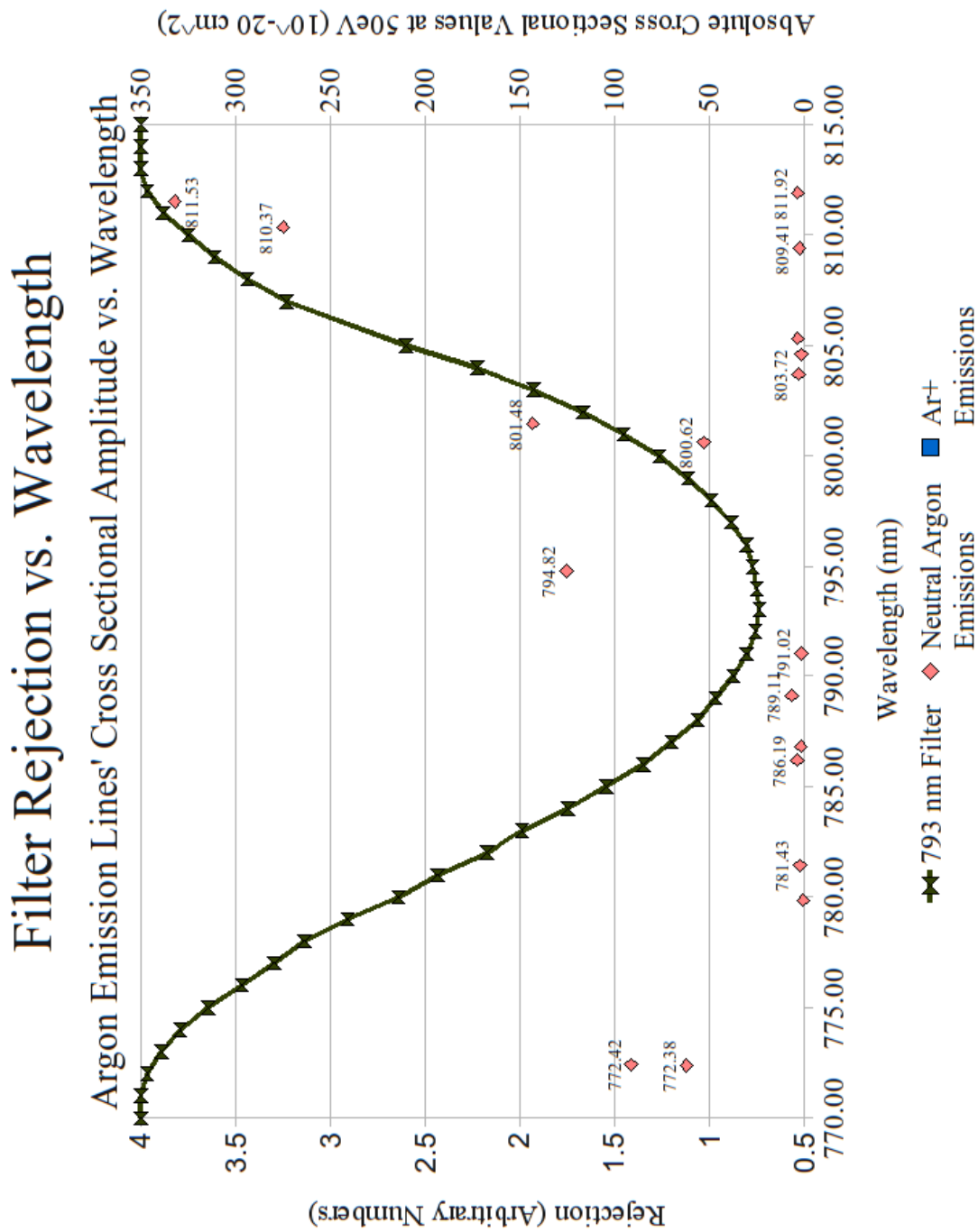


Figure 4.3 – Filter rejection as a function of wavelength for the narrowband filter centered at 793 nm (A filter rejection of 4 corresponds to 100% rejection). The cross-sectional values from Boffard et al. at an energy of 50 eV have been included as diamonds and squares [for magnitudes refer to the second y-axis on the right of the diagram].

function could be reproduced. For a complete listing of the data from Boffard et al., see the Appendix. An excitation was selected if a value of 5% of the maximum amplitude or greater was obtained when multiplying the cross sectional value at 50 eV by the transmittance. The results were also compared with direct excitation results from Tsurubuchi et al. [Tsurubuchi, et al., (1996)] The shapes of these excitations are compared in Figures 4.4 and 4.5 where very good agreement is demonstrated. Our data has much higher statistical significance than the earlier Wisconsin results.

Boffard et al., recorded the excitation functions at a pressure of 5 mtorr, while Tsurubuchi et al. recorded results at pressures lower than 1×10^{-4} torr. Present results were recorded at pressures between 5×10^{-4} torr and 9×10^{-4} torr. Although there is very positive agreement between the present results and the previous data, particularly the results from Tsurubuchi in Figure 4.4 for the range of 3 to 30 eV, differences in the shape of the high energy ‘tails’ were observed in Figure 4.5. This can readily be accounted for by the increased signal due to low energy secondary electrons at higher nominal energies. This effect is exaggerated as the pressure is increased. The present results which lie between Tsurubuchi and Boffard reflect the different pressures used but also suggest that our electron beam has a significant low energy secondary-electron component. From the rather sharply peaked nature of the excitation function one can conclude that the initial excitation of the state from the 1S_0 ground state is not dipole allowed (as expected since there is no change in parity). However the peak is not as sharp as, for example, the shape of the N_2 second positive excitation function (see Figure 3.2). This means that electron exchange is not playing the same dominant role in the excitation as it does in the N_2 case.

Direct Excitation of "794.8nm" Transition of Ar

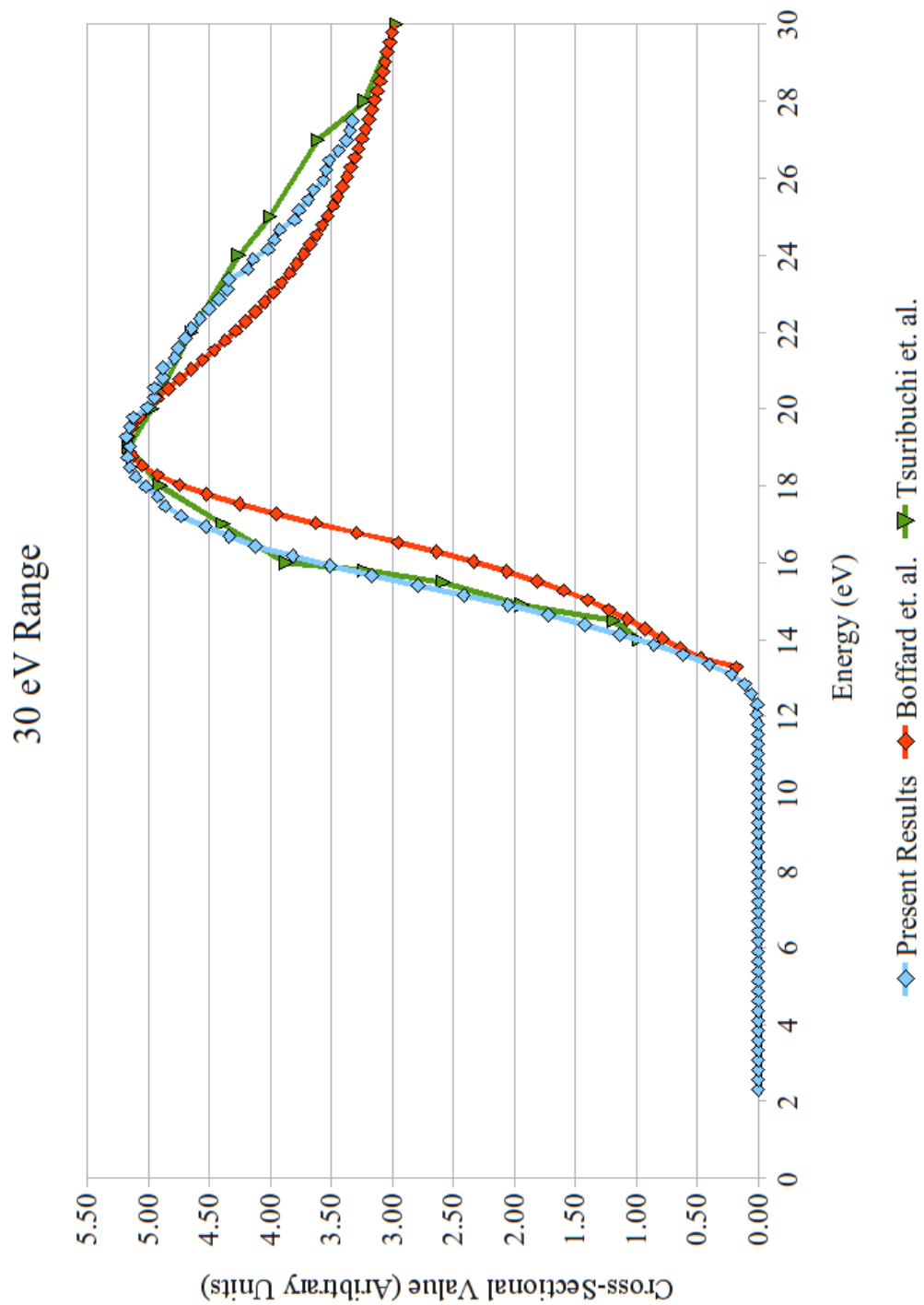


Figure 4.4 – Present cross section results for the 794.8 transition in the range from 3-30 eV compared with Tsurubuchi et al. and the compilation of signal from Boffard et al. The data sets have been normalized at 19 eV.

Direct Excitation of "794.8nm" Transition of Ar

100 eV Range

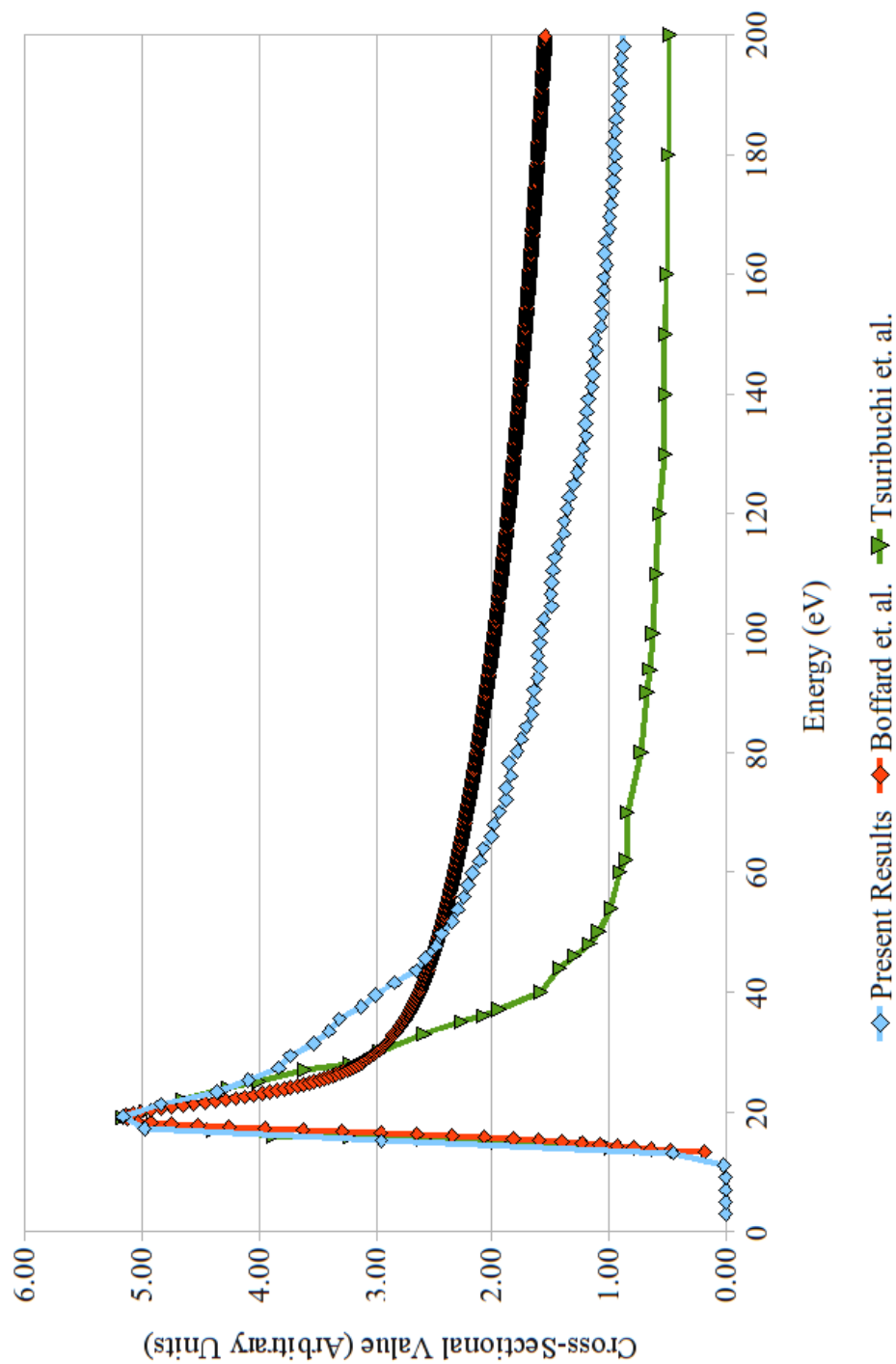


Figure 4.5 – Present cross section results for the 794.8 transition in the range from 3 to 200 eV compared with Tsurubuchi et al. and the compilation of signal from Boffard et al. The data sets have been normalized at 19 eV.

4.D.2. 340nm Emissions

Emission lines which occurred in the neighbourhood of 340 nm are identifiable in Figure 4.6 below. As can be seen, a large number of Ar emissions occur in this region though most of them have rather low intensity. The data in the table from Boffard et al. in the Appendix indicate which transitions correspond to the listed wavelengths in Figure 4.6, as well as giving the emission cross section values at 50 eV. The shape of the integrated emission cross section from all the significant emission lines was evaluated from Boffard et al. in the same way as for Section 4.D.1 above. The summation of these emission lines from Boffard et al. is shown in Figures 4.7 and 4.8.

As is shown in Figure 4.6, the primary sources of emission when using this filter, were argon ions, whose thresholds begin at 38 eV. However, as is clear from Figure 4.6 and as the results from Boffard confirm, a fraction of the signal also comes from excited neutral argon, with thresholds around 15 eV in this wavelength region. The argon ion emissions are due mainly to contributions from many $4d \rightarrow 4p$ as well as some $4f \rightarrow 4p$ transitions. The significant neutral argon emission lines result from a combination of $np \rightarrow 4s$ and $4d \rightarrow 4s$ transitions, where the core ion is $3p^5 \ ^2P_{3/2}$. The results demonstrate remarkable agreement with the data of Boffard et al. in the overall shape of the emission cross section. At the highest energies, our data fall off more rapidly than those of Boffard et al. suggesting a smaller secondary electron component in our electron beam. This is consistent with our finding for the 794.8 nm line (see Section 4.D.1).

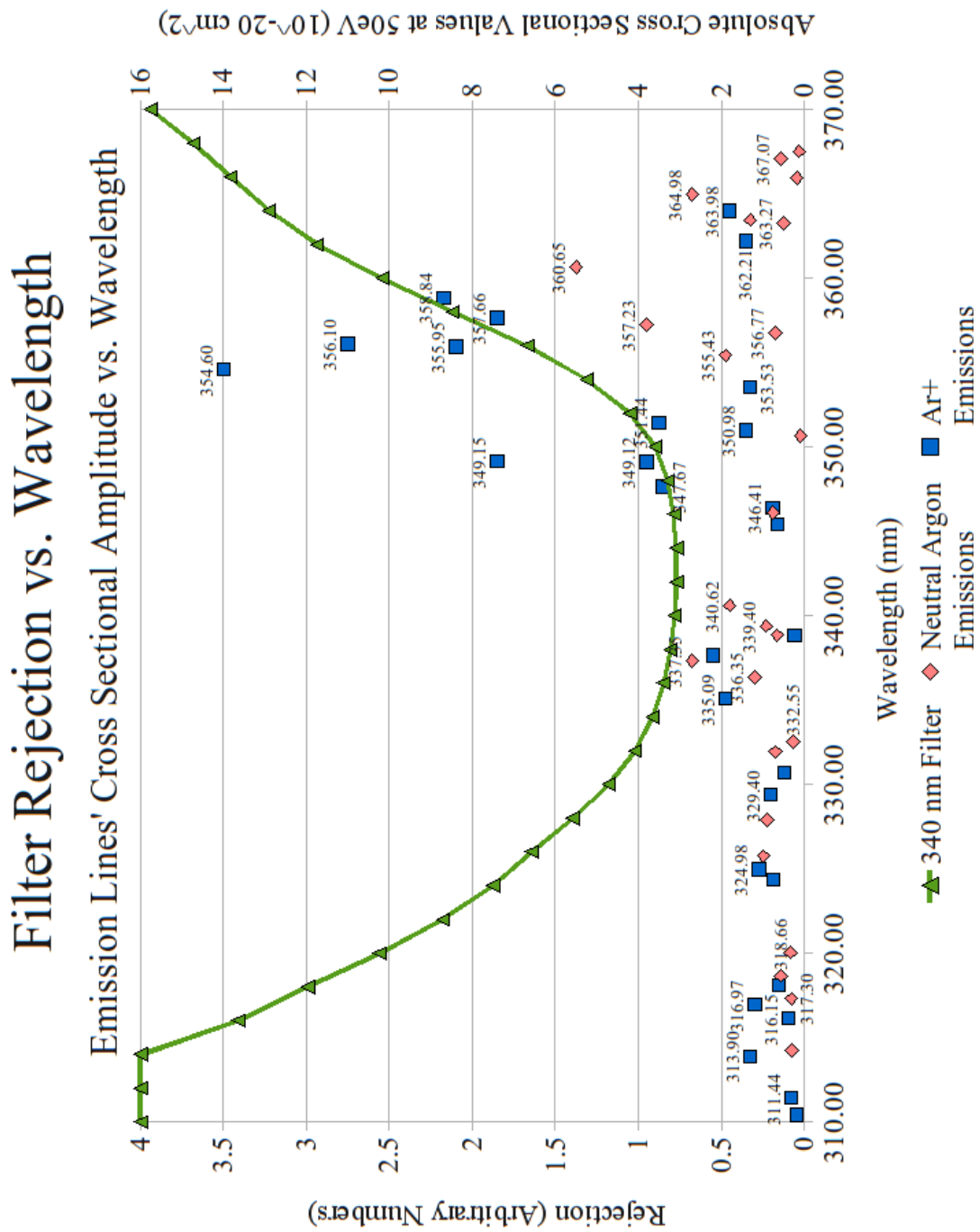


Figure 4.6 – Filter rejection as a function of wavelength for the narrowband filter centered at 340 nm (A filter rejection of 4 corresponds to 100% rejection). The cross-sectional values from Boffard et al. at an energy of 50 eV have been included as diamonds and squares [for magnitudes refer to the second y-axis on the right of the diagram].

Emission Cross Section vs. Energy for Argon 340 nm, 30 eV Range

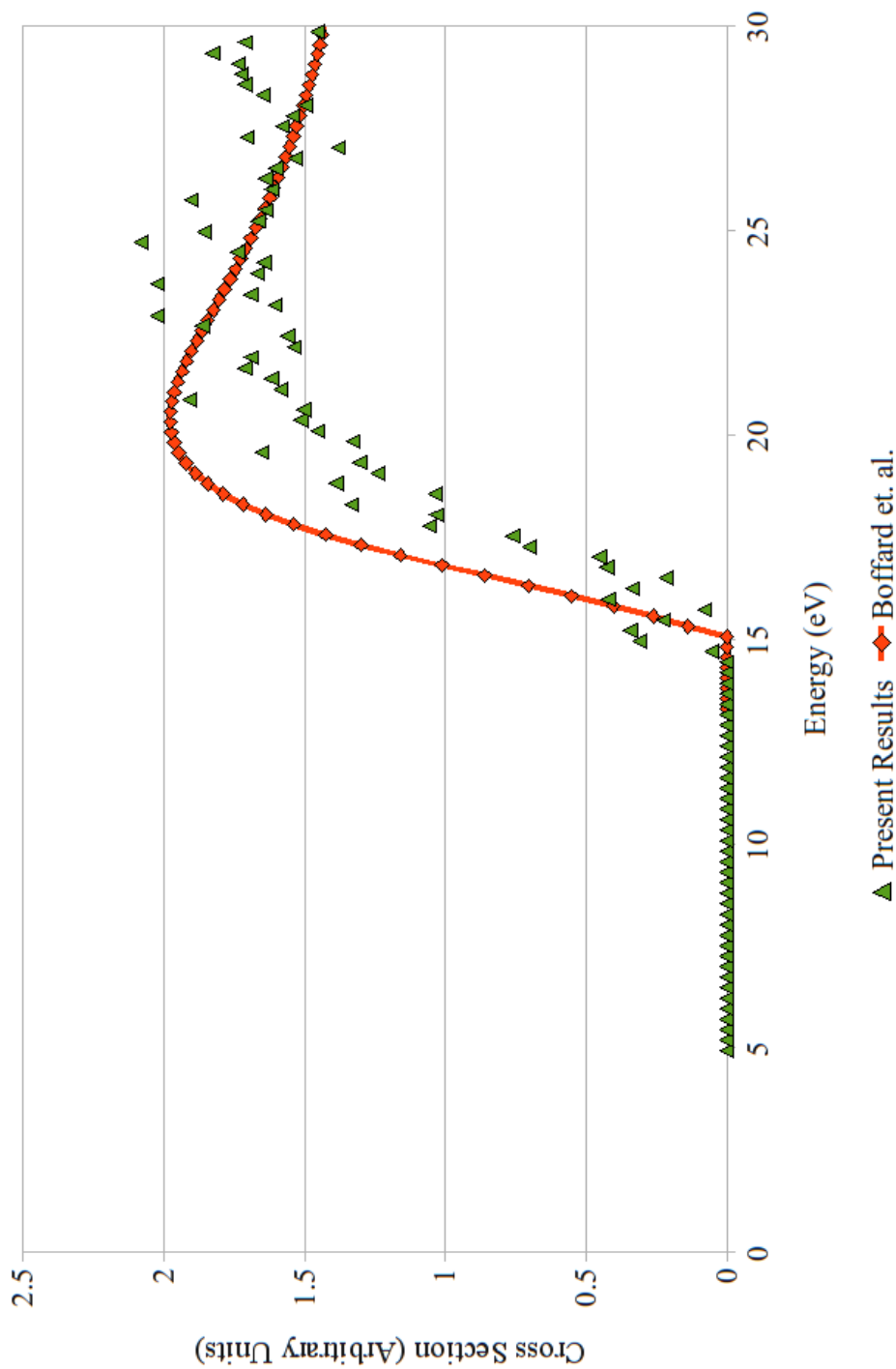


Figure 4.7 – Present cross section results for 340 nm excitations in the range from 3 to 30 eV. The combination of emission cross sections from Boffard et al. is included for comparison. The two data sets have been normalized at 22.5 eV.

Emission Cross Section vs. Energy for Argon 340 nm Filter, 200 eV Range

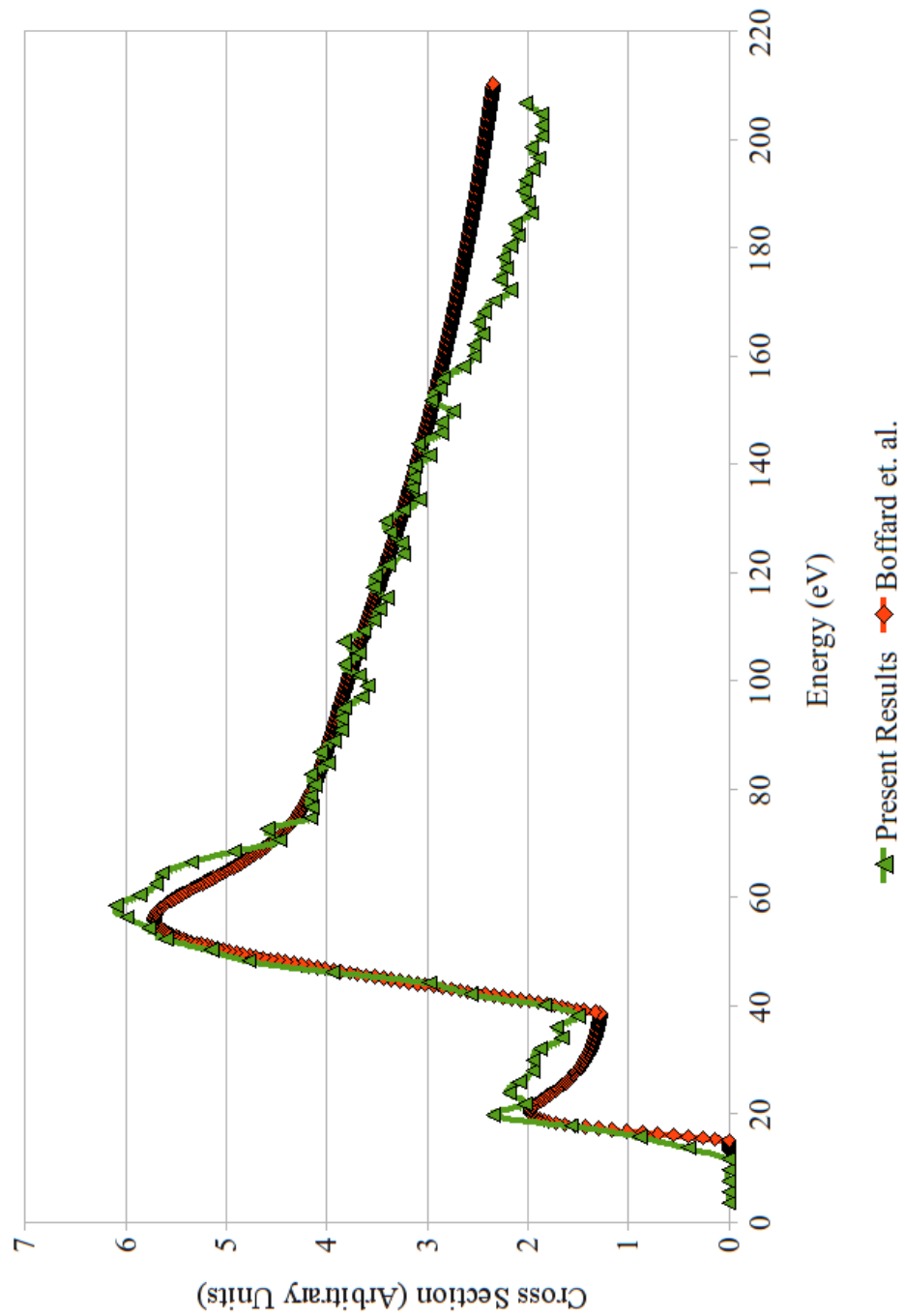


Figure 4.8 – Present cross section results for 340 nm excitations in the range from 3 to 200 eV. The combination of emission cross sections from Boffard et al. is included for comparison. The two data sets have been normalized at 80 eV.

4.D.3. 423 nm Emissions

Emission lines near 423 nm are identified in Figure 4.9 below. The data in the table from Boffard et al. in the Appendix indicate the transitions involved. As before, the total observable cross section from Boffard et al. was calculated and used as a basis of comparison with present results, shown in Figures 4.10 and 4.11 below.

Figures 4.9 and 4.11 illustrate a stronger presence of neutral argon emissions relative to the argon ion emissions when compared with the 340 nm emissions in Section 4.D.2. If we normalize our data and the results from Boffard et al. at energies around 20 eV, where only neutral Ar excitation is involved we see that the general shape in this low energy region shows excellent agreement with Boffard et al., as is demonstrated in Figure 4.10. The neutral emissions are dominated by $5p \rightarrow 4s$ transitions with a $3p^5\ ^2P_{3/2}$ core. At higher energies, above 35eV, Ar^+ emissions occur strongly, contributing to the second peak seen in Fig 4.11. Here the major transitions are of $4p \rightarrow 4s$ in nature with both doublet and quartet excitations being involved. We note however that some of the neutral Ar emissions, e.g. at 419.83 nm, have been shown by Boffard et al. to have a second broad peak around 70 eV which would contribute to the overall shape of the excitation function. The existence of two peaks in the excitation function could be due to dipole-forbidden spin-allowed excitation giving the sharp initial peak together with cascade from a dipole allowed level which peaks at the higher energy (See Boffard et al.). Once again the present results demonstrate a reduction in signal for energies beyond 140 eV when compared with those of Boffard et al. suggesting that Boffard et al. had more secondary electrons in their beam at higher energies.

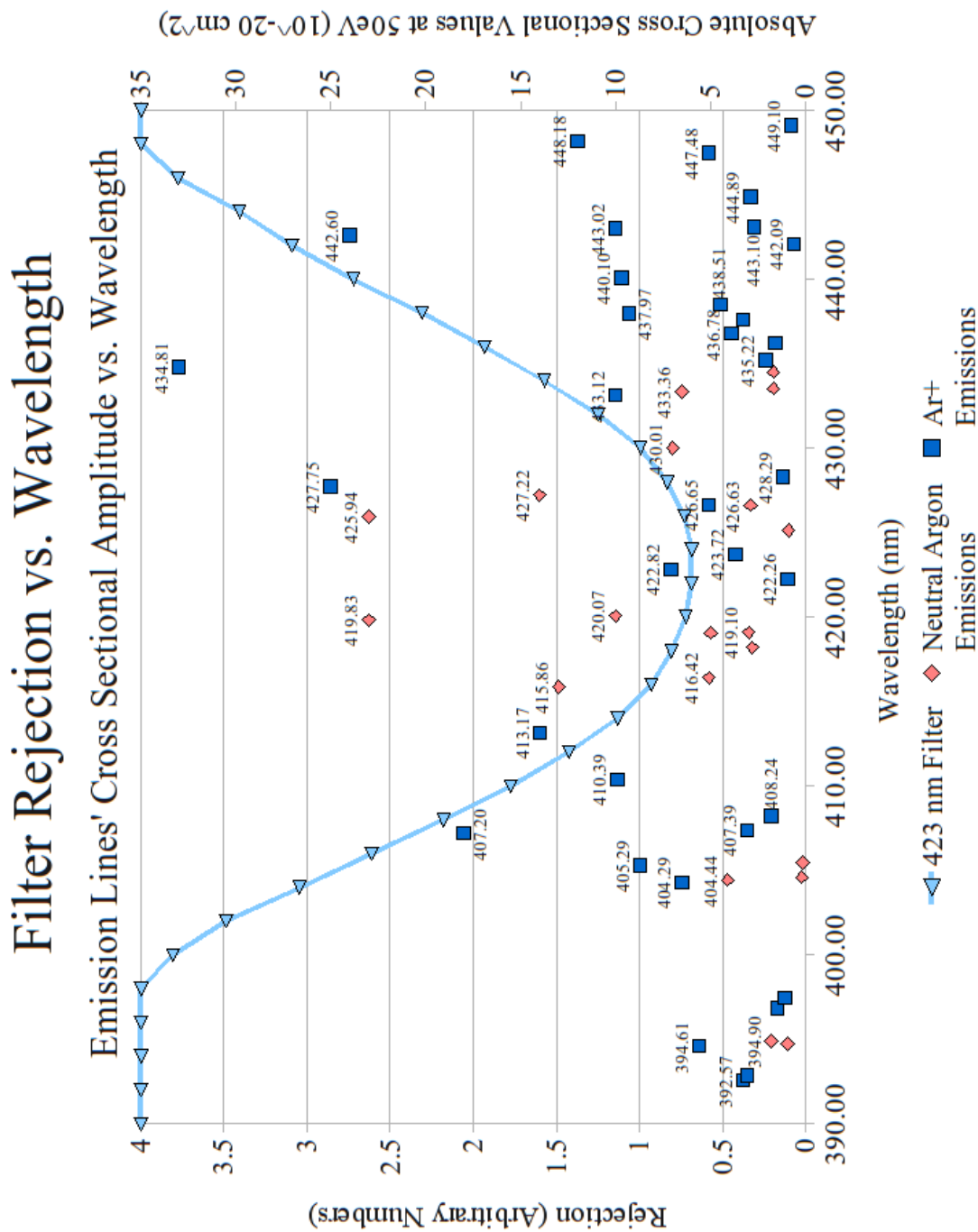


Figure 4.9 – Filter rejection as a function of wavelength for the narrowband filter centered at 423 nm (A filter rejection of 4 corresponds to 100% rejection). The cross-sectional values from Boffard et al. at an energy of 50 eV have been included as diamonds and squares [for magnitudes refer to the second y-axis on the right of the diagram].

Emission Cross Section vs. Energy for Argon

423 nm, 30 eV Range

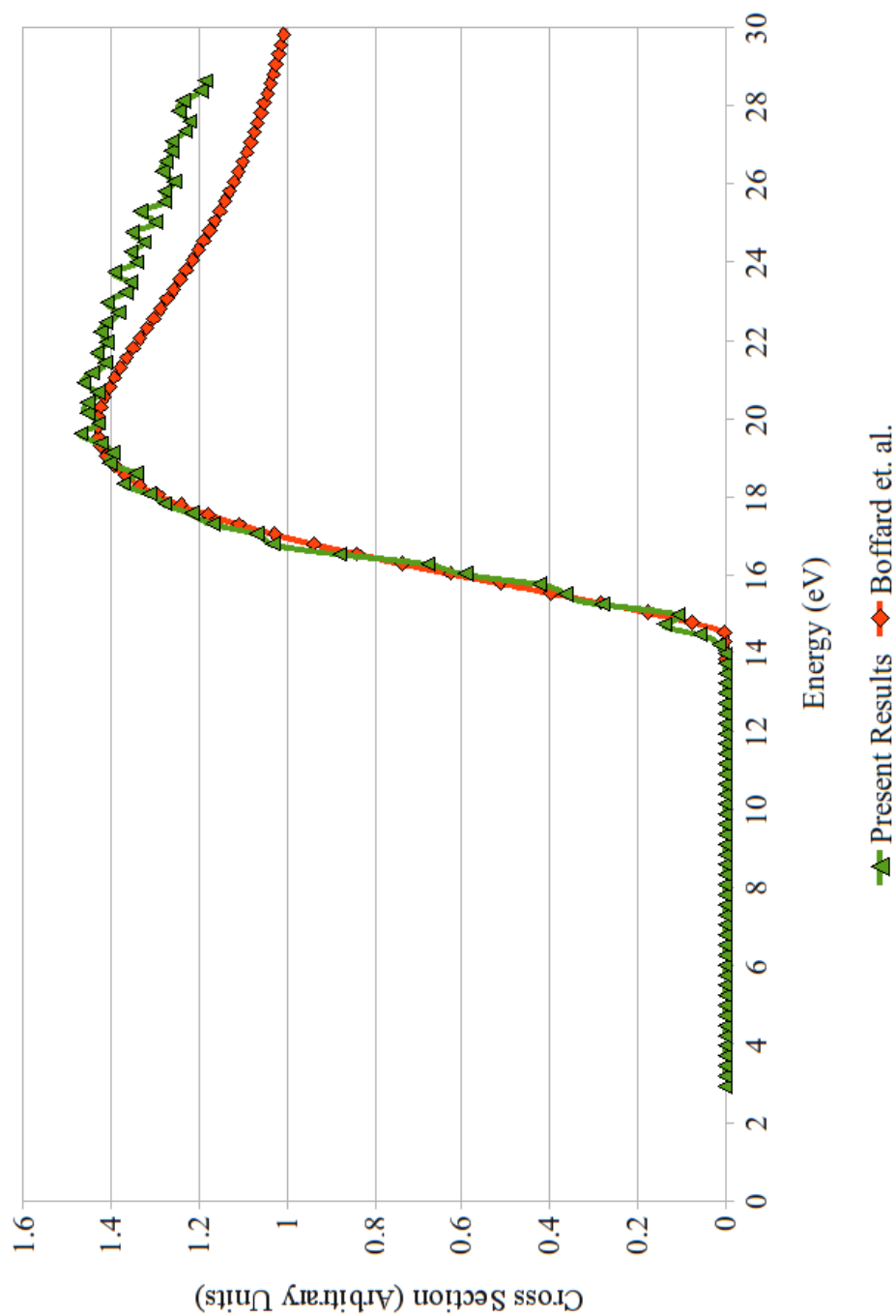


Figure 4.10 – Present cross section results for 423 nm excitations in the range from 3 to 30 eV. The combination of emission cross sections from Boffard et al. is included for comparison. The two data sets have been normalized at 19 eV.

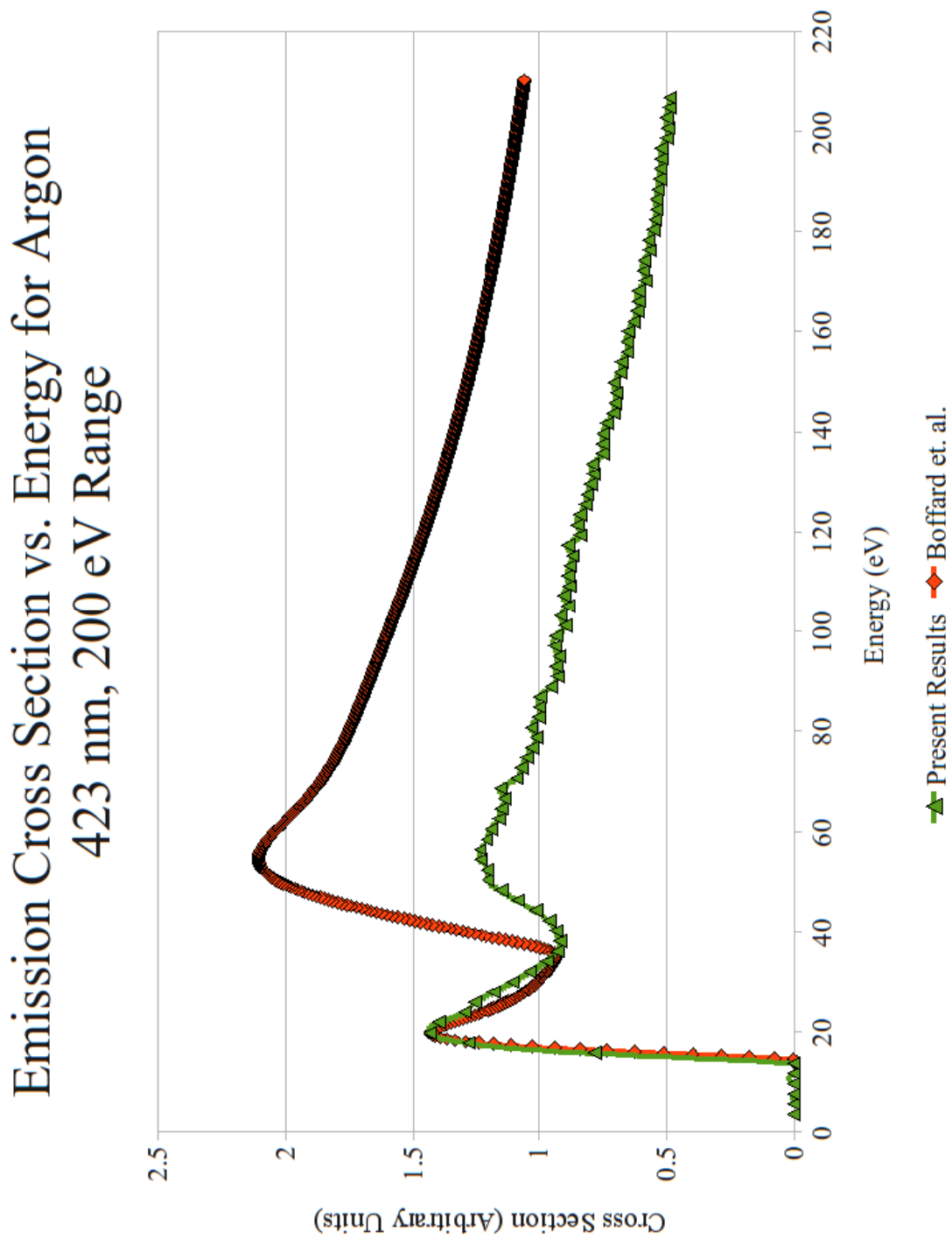


Figure 4.11 – Present cross section results for 423 nm excitations in the range from 3 to 200 eV. The combination of emission cross sections from Boffard et al. is included for comparison. The two data sets have been normalized at 20 eV.

4.D.4. 470 nm Emissions

The identifiable emission lines near 470 nm are shown in Figure 4.12 below. The data in the table from Boffard et al. in the Appendix shows the corresponding transitions. Neutral and ion lines are identified on Figure 4.12. Since all the dominant lines are from Ar^+ , we anticipate that the integrated excitation functions will be similarly dominated. As before, the integrated observable cross section based on the data of Boffard et al. was calculated. The resultant curves are compared with present results in Figure 4.13 below. These data were the poorest statistically of all the results but it was verified that the observed features were present on all data runs taken.

Figure 4.13 demonstrates the presence of signal from neutral argon excitation (threshold of approx. 15 eV) and also shows principally excited Ar^+ emissions (threshold of approx. 38 eV). Some of the differences in peak signal values may be due to geometrical effects in the electron gun, as will be discussed later. Comparisons with the Boffard et al. results are poorer than with some of the other filters though similar structures are observed. The argon ions' excitation is due to $4p \rightarrow 4s$ transitions, within both doublet and quartet manifolds. The neutral argon contributions result from $5p \rightarrow 4s$ transitions, where the core is $3p^5 \ ^2P_{3/2}$.

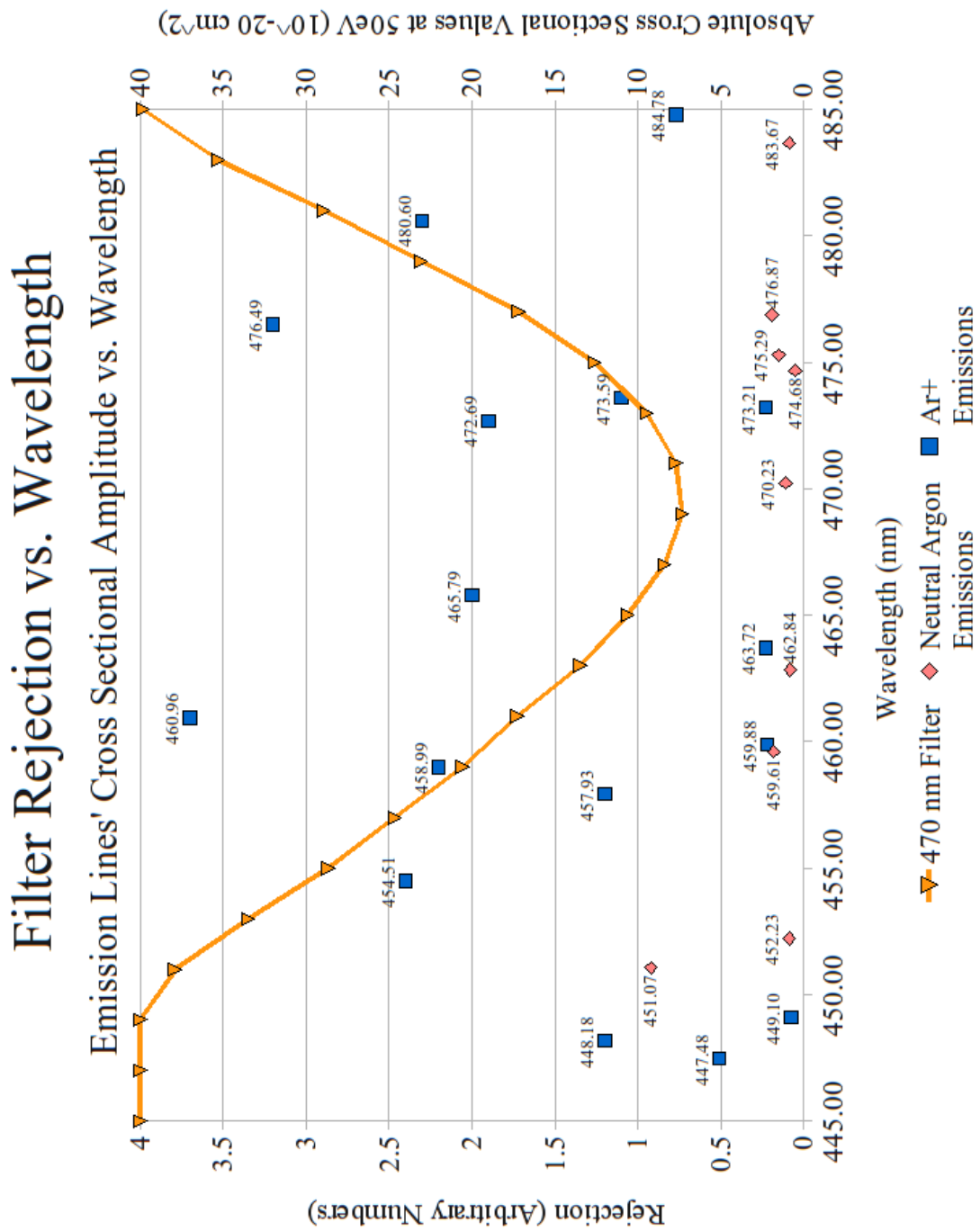


Figure 4.12 – Filter rejection as a function of wavelength for the narrowband filter centered at 470 nm (A filter rejection of 4 corresponds to 100% rejection). The cross-sectional values from Boffard et al. at an energy of 50 eV have been included as diamonds and squares [for magnitudes refer to the second y-axis on the right of the diagram].

Emission Cross Section vs. Energy for Argon 470 nm, 200 eV Range

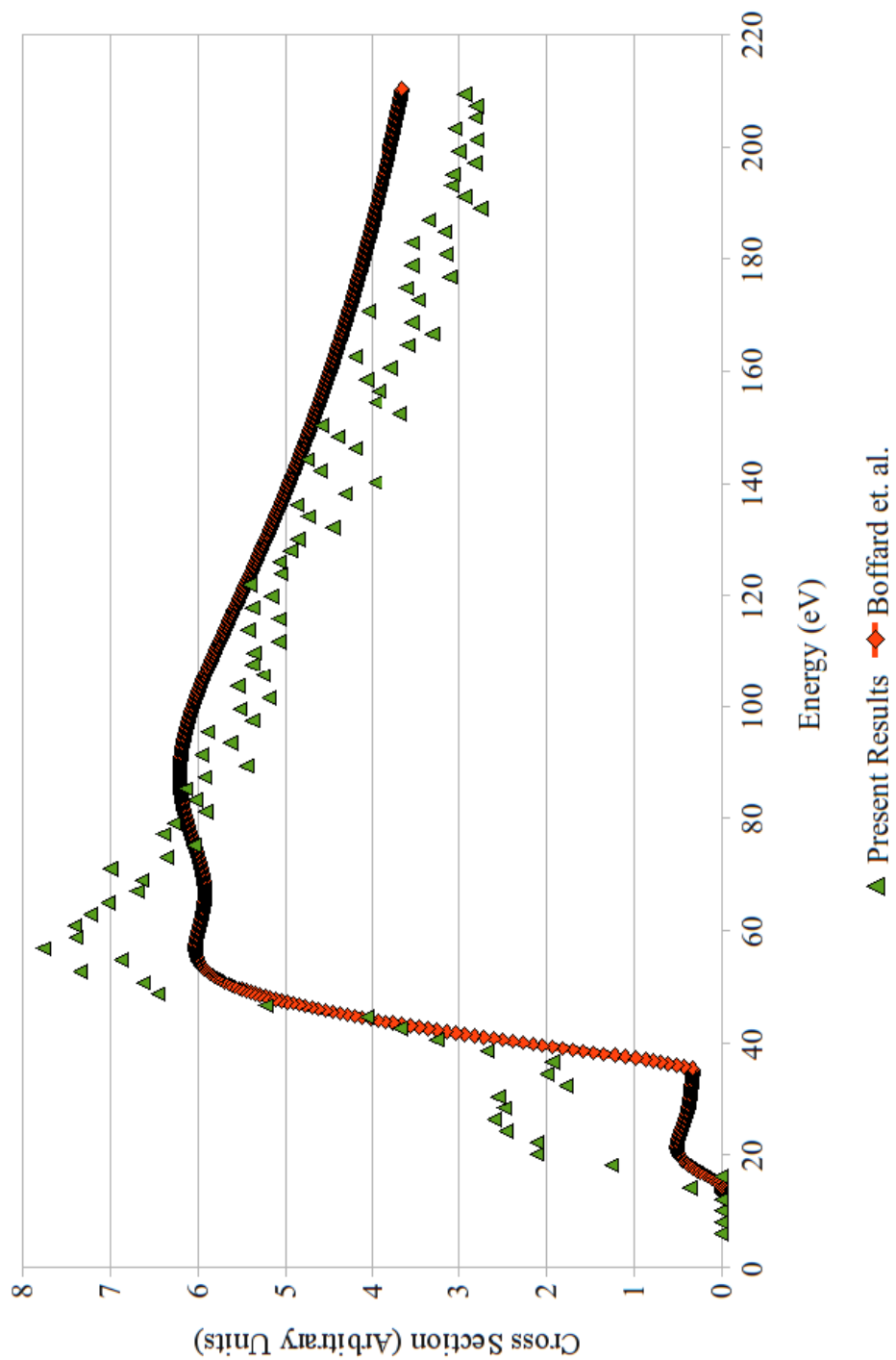


Figure 4.13 – Present cross section results for 470 nm excitations in the range from 3 to 200 eV. The combination of emission cross sections from Boffard et al. is included for comparison. The two data sets have been normalized at 57 eV.

4.D.5. 620 nm Emissions

The emission lines at 620 nm were identified as shown in Figure 4.14 below. The table in the Appendix, taken from Boffard et al., indicates the corresponding emission lines. Section 4.D.1 above illustrates the process by which the total observable cross section was created from the data from Boffard et al. The present results are compared with the resultant curves in Figure 4.15 below.

Figure 4.15 demonstrates remarkable agreement between the present results and those compiled from Boffard et al. Both neutral and ion emissions are clearly visible from their threshold signatures at 15 and 37 eV respectively. The 37 eV feature indicated the presence of the very strong argon ion emission lines – the $3d' G_{7/2} \rightarrow 4p' ^2F_{5/2}$ and $3d' G_{9/2} \rightarrow 4p' ^2F_{7/2}$ which take place at 611.49 nm and 617.23 nm respectively with thresholds of 36.90 and 36.89 eV respectively. Here the “ ' ” symbol indicates a 1D core. The remaining signal is due to the combination of signal resulting from the emission of neutral argon, primarily $5d \rightarrow 4p$ and $7s \rightarrow 4p$ transitions, where the core is again $3p^5 ^2P_{3/2}$. Despite the difference in peak signals, there is reasonable agreement between the curve shapes for the present results and those expected from Boffard et al.

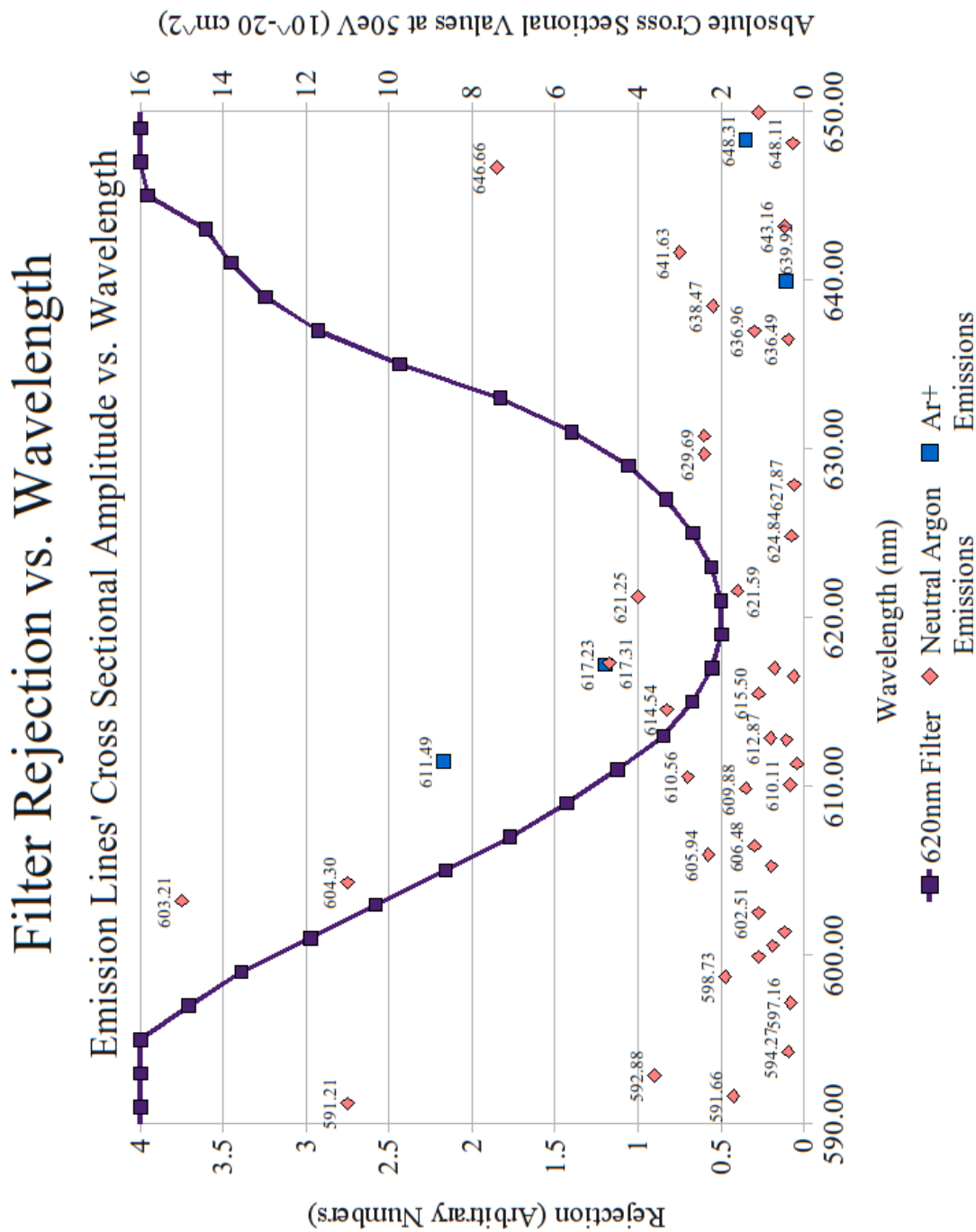


Figure 4.14 – Filter rejection as a function of wavelength for the narrowband filter centered at 620 nm (A filter rejection of 4 corresponds to 100% rejection). The cross-sectional values from Boffard et al. at an energy of 50 eV have been included as diamonds and squares [for magnitudes refer to the second y-axis on the right of the diagram].

Emission Cross Section vs. Energy for Argon 620 nm, 200 eV Range

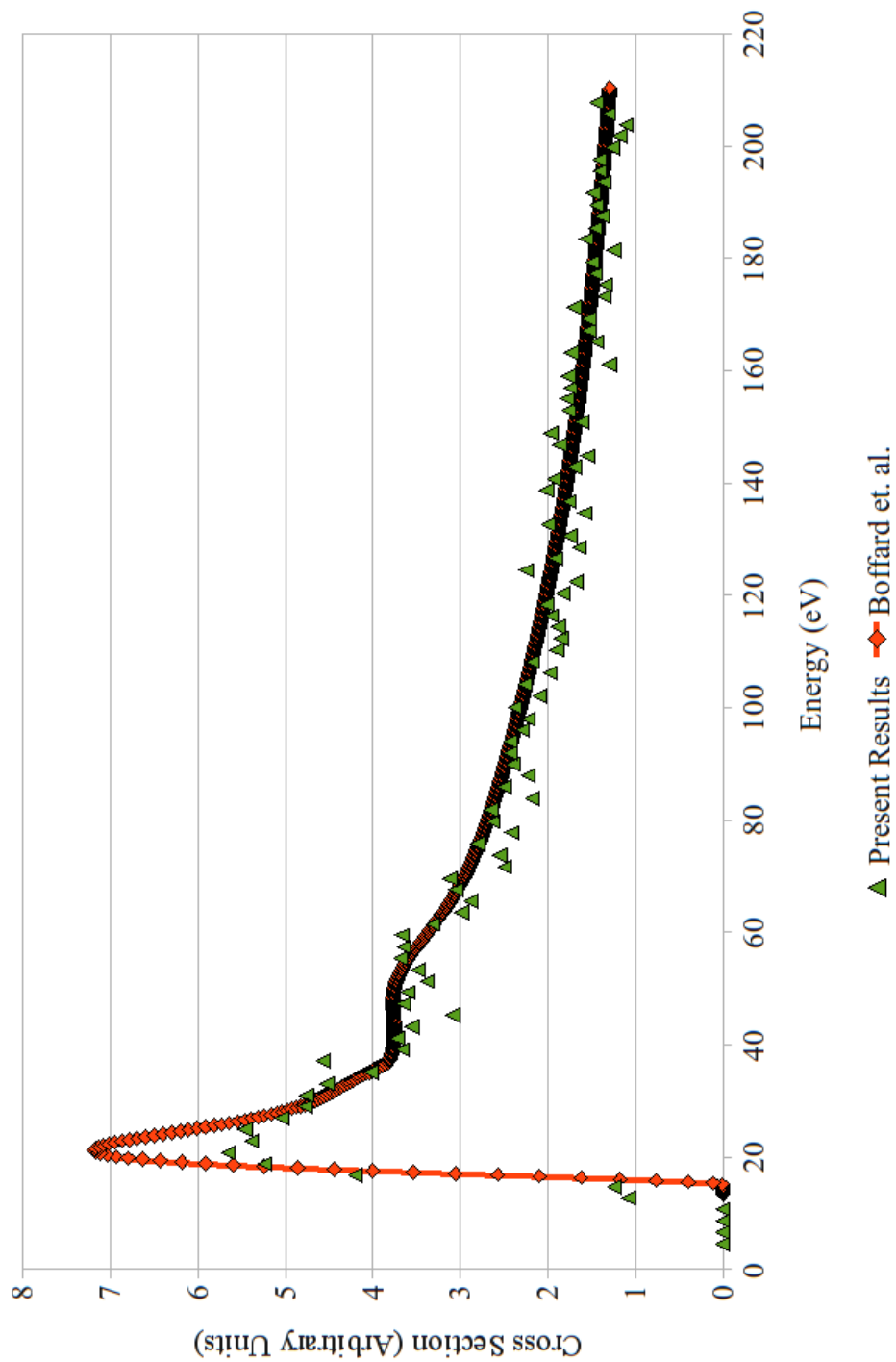


Figure 4.15 – Present cross section results for 620 nm excitations in the range from 3 to 200 eV. The combination of emission cross sections from Boffard et al. is included for comparison. The two data sets have been normalized at 82 eV.

4.D.6. 710 nm Emissions

The identifiable emission lines at 710 nm are shown in Figure 4.16 below. Data taken from the table by Boffard et al. in the Appendix indicates corresponding emission lines. The process for determining the total observable cross section was created as outlined in Section 4.D.2 above. The curves created from this process were then compared with the present results and are shown in Figures 4.17 and 4.18 below.

There is remarkable agreement between the results from Boffard et al. and the present results, as is shown in Figure 4.18. The threshold and peak energies occur at the same points, however Boffard et al. has higher signals at higher energies. Again, the presence of secondary electrons at higher pressures explains Boffard's increased results at higher energies when compared with the present results. The signal is entirely dominated by the presence of neutral argon emission lines, most significantly the $4p \rightarrow 4d$ and $4p \rightarrow 6s$ transitions, with a core of $3p^5 \ ^2P_{3/2}$. A single argon ion emission is contained within this filter, but is not observable due to a low proportion of signal. Despite the difference in signals for higher energies, the present results show reasonable agreement with those expected from Boffard et al.

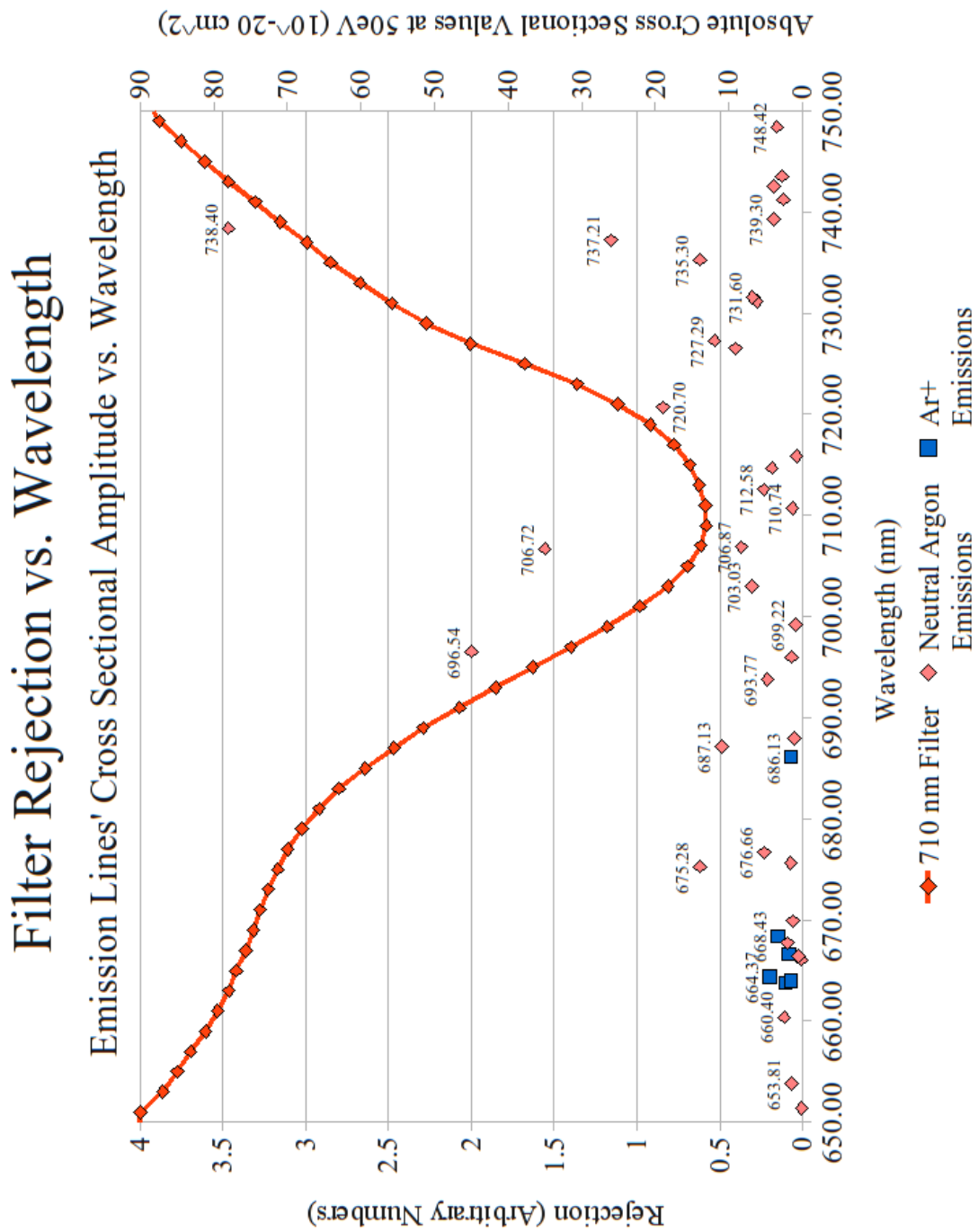


Figure 4.16 – Filter rejection as a function of wavelength for the narrowband filter centered at 710 nm (A filter rejection of 4 corresponds to 100% rejection). The cross-sectional values from Boffard et al. at an energy of 50 eV have been included as diamonds and squares [for magnitudes refer to the second y-axis on the right of the diagram].

Emission Cross Section vs. Energy for Argon 710 nm, 30 eV Range

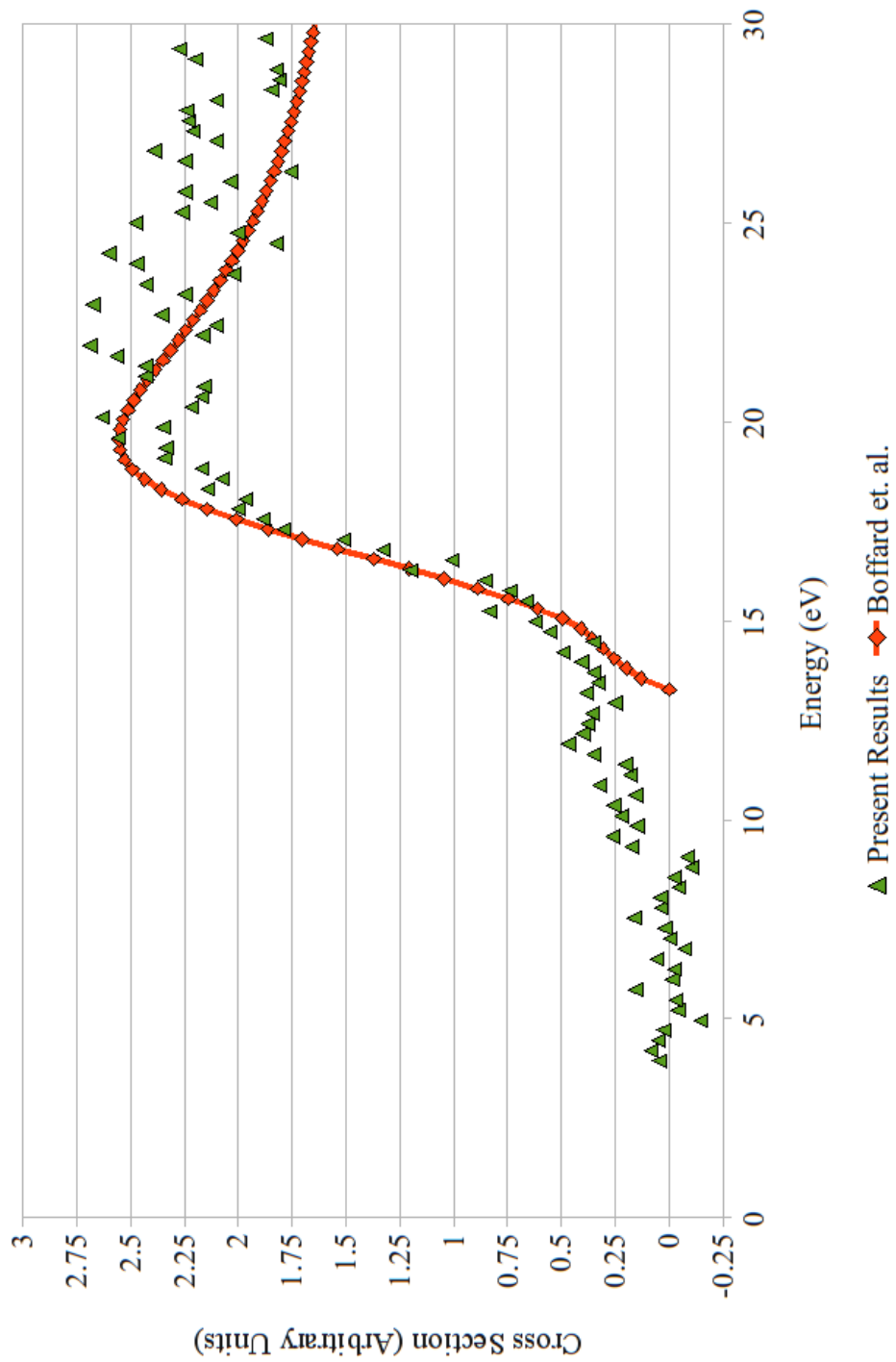


Figure 4.17 – Present cross section results for 710 nm excitations in the range from 3 to 30 eV. The combination of emission cross sections from Boffard et al. is included for comparison. The two data sets have been normalized at 19.5 eV

Emission Cross Section vs. Energy for Argon 710 nm, 200 eV Range

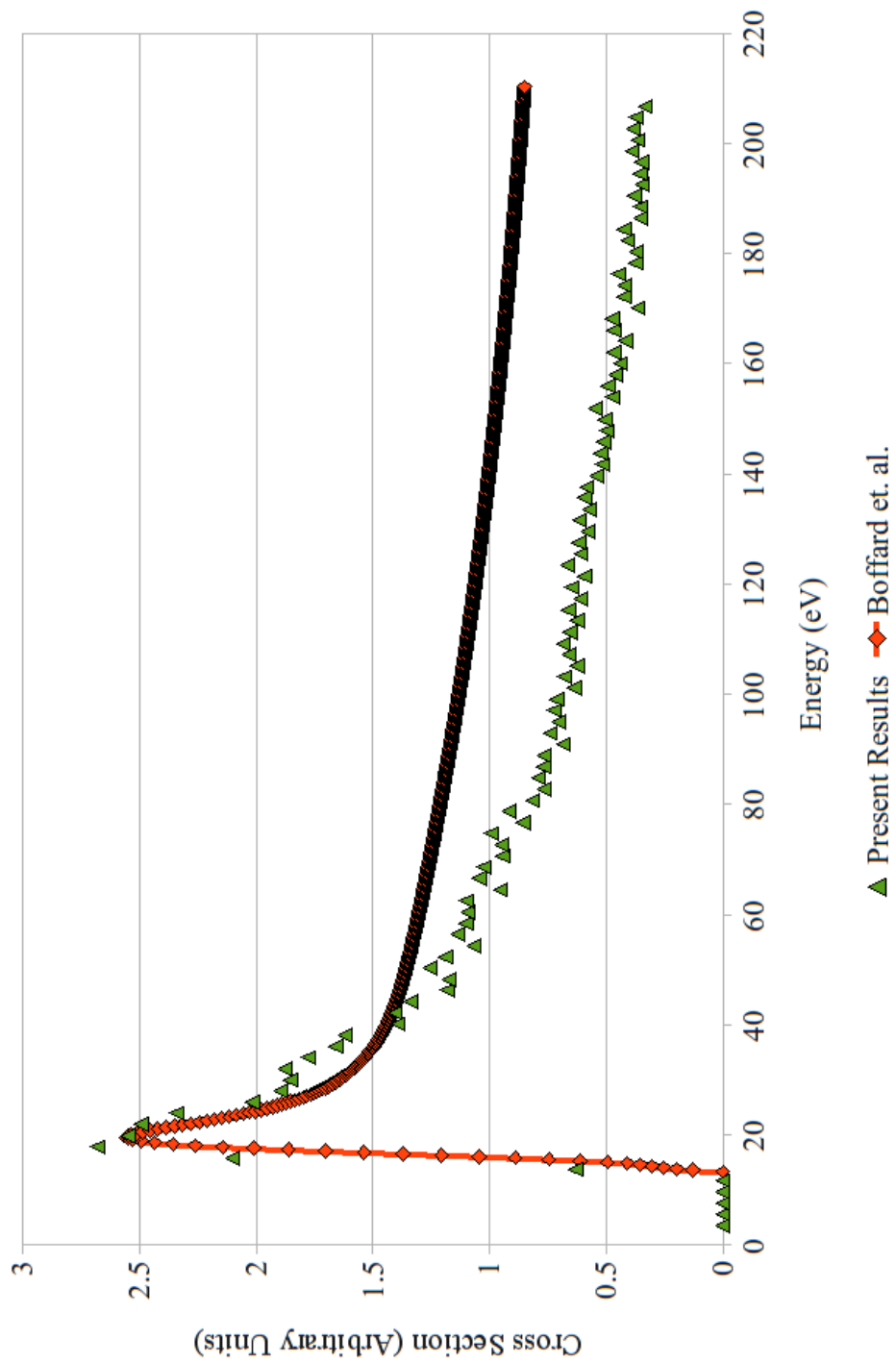


Figure 4.18 – Present cross section results for 710 nm excitations in the range from 3 to 200 eV. The combination of emission cross sections from Boffard et al. is included for comparison. The two data sets have been normalized at 20 eV.

4.D.7 Excitation by LIF

Section 4.D.1 above illustrates a detailed measurement of the “794.8 nm” transition, whereby the $3p^5 4p [1 \frac{1}{2}] (J=1) \rightarrow 3p^5 4s [\frac{1}{2}] (J=0)$ transition could be measured. The results of this study were shown in Figures 4.4 and 4.5 where good agreement between previous results from Tsurubuchi et al. and Boffard et al. were demonstrated. As Figure 4.2 illustrates, by tuning a laser to the specific wavelength of 852.1443 nm, the excitation of the $3p^5 4s [\frac{1}{2}] (J=1)$ level could be measured. The threshold energy of this level was expected to occur at 11.83 eV, while the excitation by electron impact of the $3p^5 4p [1 \frac{1}{2}] (J=1)$ level had a threshold of 13.28 eV. Furthermore, based on previous measurements of the relevant cross sections, it was expected that the photon signal would increase by a significant factor when the laser was tuned to the appropriate wavelength.

Figures 4.19 to 4.24 below demonstrate the results of using LIF techniques. Figures 4.19 and 4.20 illustrate the difference in signal between direct excitation and the summation of direct and LIF signals. These were adjusted to the appropriate spectroscopic thresholds. Figure 4.19 demonstrates the shift in threshold energies of 1.45 eV, as expected, between the use of LIF and direct excitation. Figure 4.20 illustrates the significant 40% increase in signal that was observed when LIF was achieved.

Figures 4.21 to 4.24 are a result of the subtraction of the two signals shown in Figures 4.19 and 4.20. By subtracting the direct excitation signals from the summation of direct and LIF signals, the resultant curve was expected to yield the shape of the excitation from the ground state, $3p^6 (^1S_0)$, to the excited state $3p^5 4s [\frac{1}{2}] (J=1)$, whose decay wavelength

Direct Excitation of Argon at 8.8×10^{-4} torr

Electron Excitation and Laser Induced Fluorescence

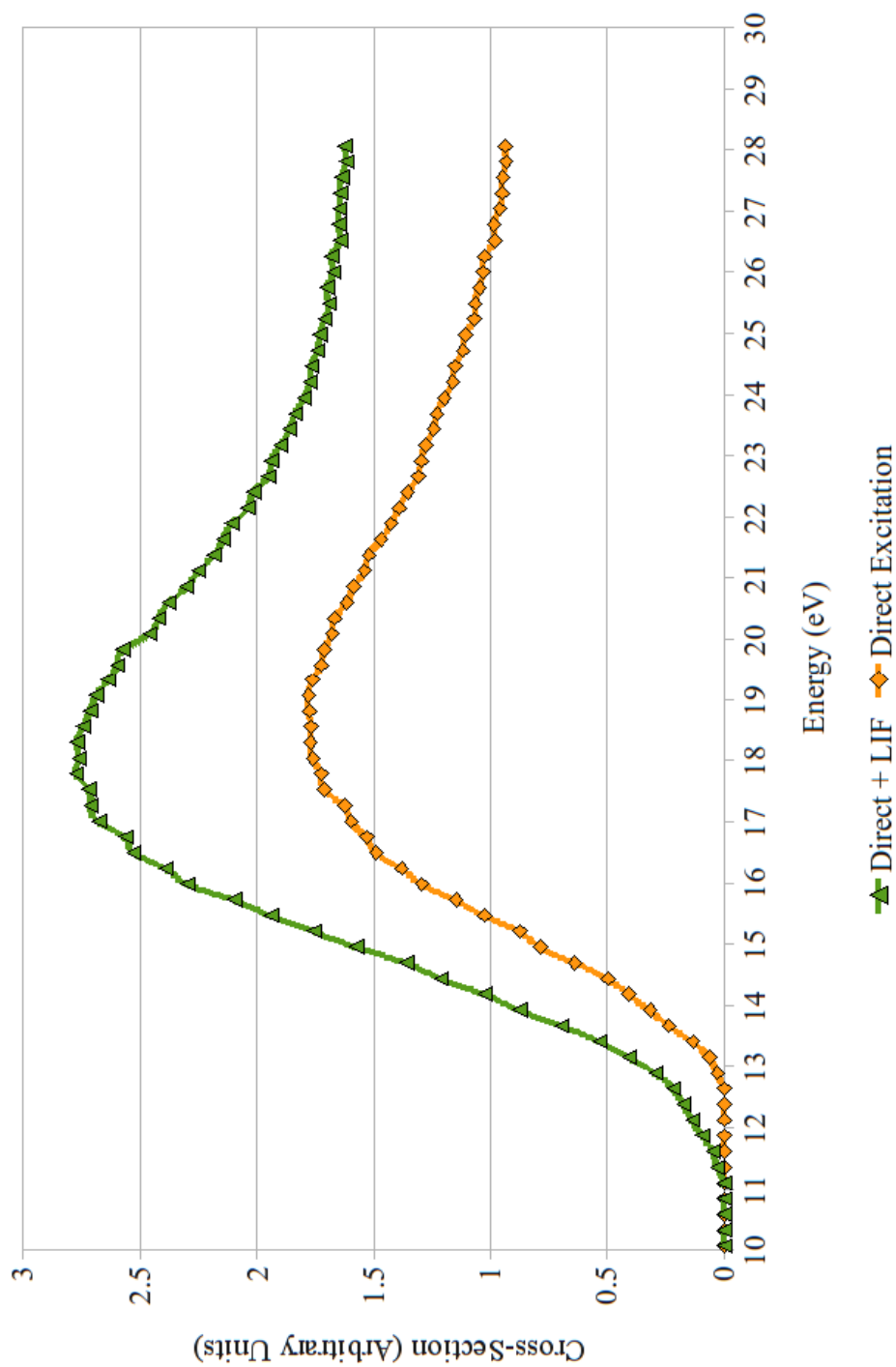


Figure 4.19 – Comparison of direct excitation with direct + LIF excitation for the 794.8 nm emission line for the 3-30 eV Range. Note the expected threshold energy shift of 1.45 eV.

Direct Excitation of Argon at 8.8×10^{-4} torr

Electron Excitation and Laser Induced Fluorescence

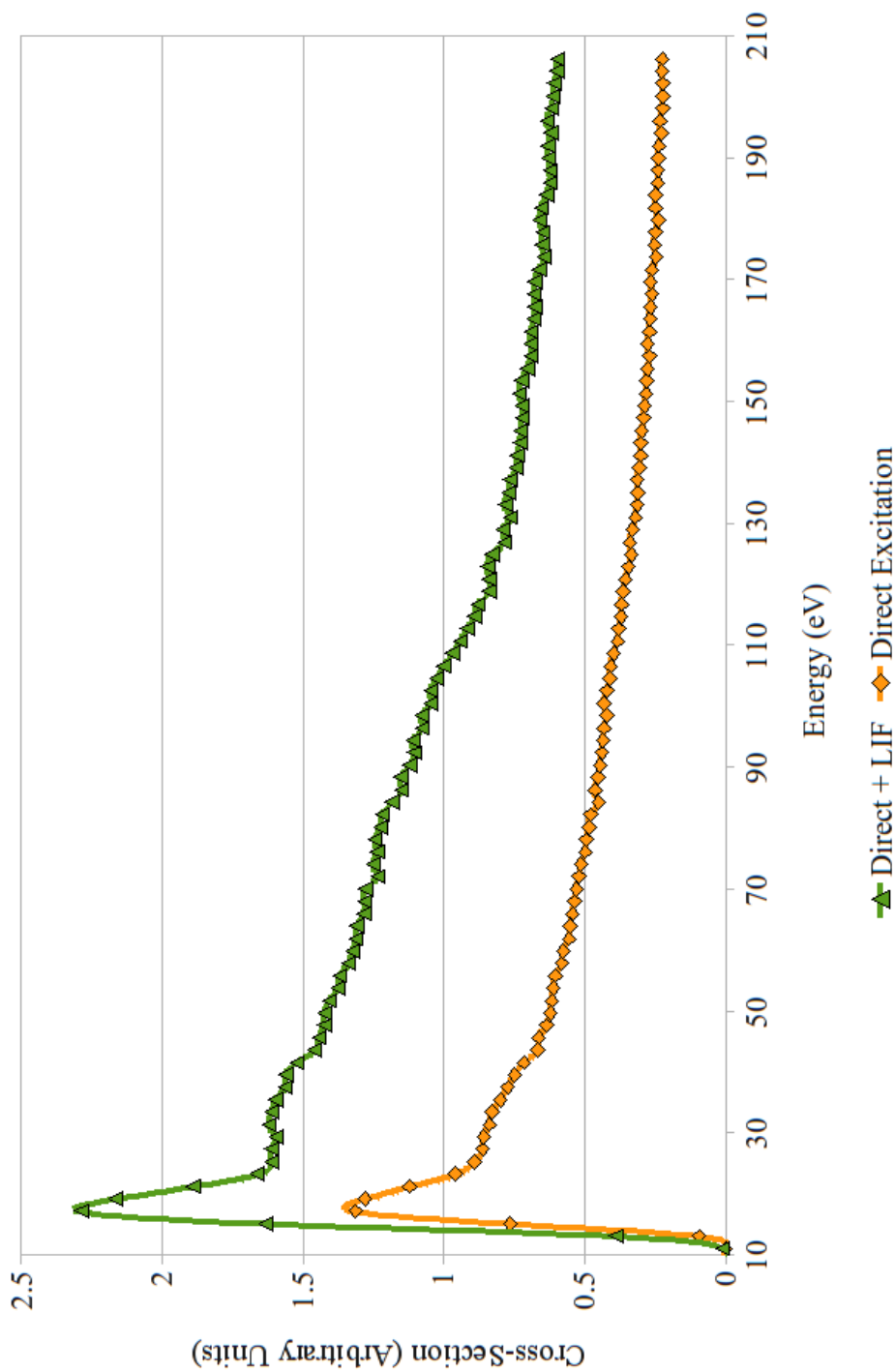


Figure 4.20 – Comparison of direct excitation with direct + LIF excitation for the 794.8 nm emission line for the 3-200 eV Range. Note the dramatic increase in signal, by approximately 40%, when the LIF signal is also present.

was at 104.8 nm in the VUV, and thus not measurable directly using the current photomultiplier. The excitation of this level has been studied through direct excitation and VUV spectroscopy by McConkey et al. [McConkey, (1973)], and by Tsurubuchi et al. Their results are included in Figures 4.21 to 4.24. The present experiment marks the first time, however, that this energy level has been studied using LIF. The experiment was conducted at different pressures, as it was noticed that the signal shape of the LIF changed with pressure. The present setup was unable to produce reliable signal at pressures lower than 5×10^{-4} torr. Figures 4.21 and 4.23 provide the results of LIF at a pressure of 8.8×10^{-4} torr, in comparison with direct measurements made previously, while Figures 4.22 and 4.24 illustrate the results of LIF at a pressure of 5.0×10^{-4} torr.

The reason why LIF did not work at lower pressures is because of the short lifetime of the $3p^5 4s [^1/2] (J=1)$ level. However, as the pressure is increased trapping of 104.8 nm radiation occurs. This is a process where neutral atoms absorb the photons emitted by nearby excited atoms, effectively lengthening the lifetime of the state and allowing a population build-up to occur. Thus, the higher the pressure the better chance that LIF will be observed.

It can be observed through a comparison of Figures 4.21 with 4.22, and Figures 4.23 with 4.24, that at lower pressures the relative height of the 'peak' signal that occurs at approx. 16 eV is reduced when the pressure is lowered. Because of 'bunching' in the electron beam the effective overlap of the laser and electron beams could change with energy and with pressure, possibly leading to the low energy enhancement observed. This geometrical effect has been mentioned for a number of the sections above, and a study

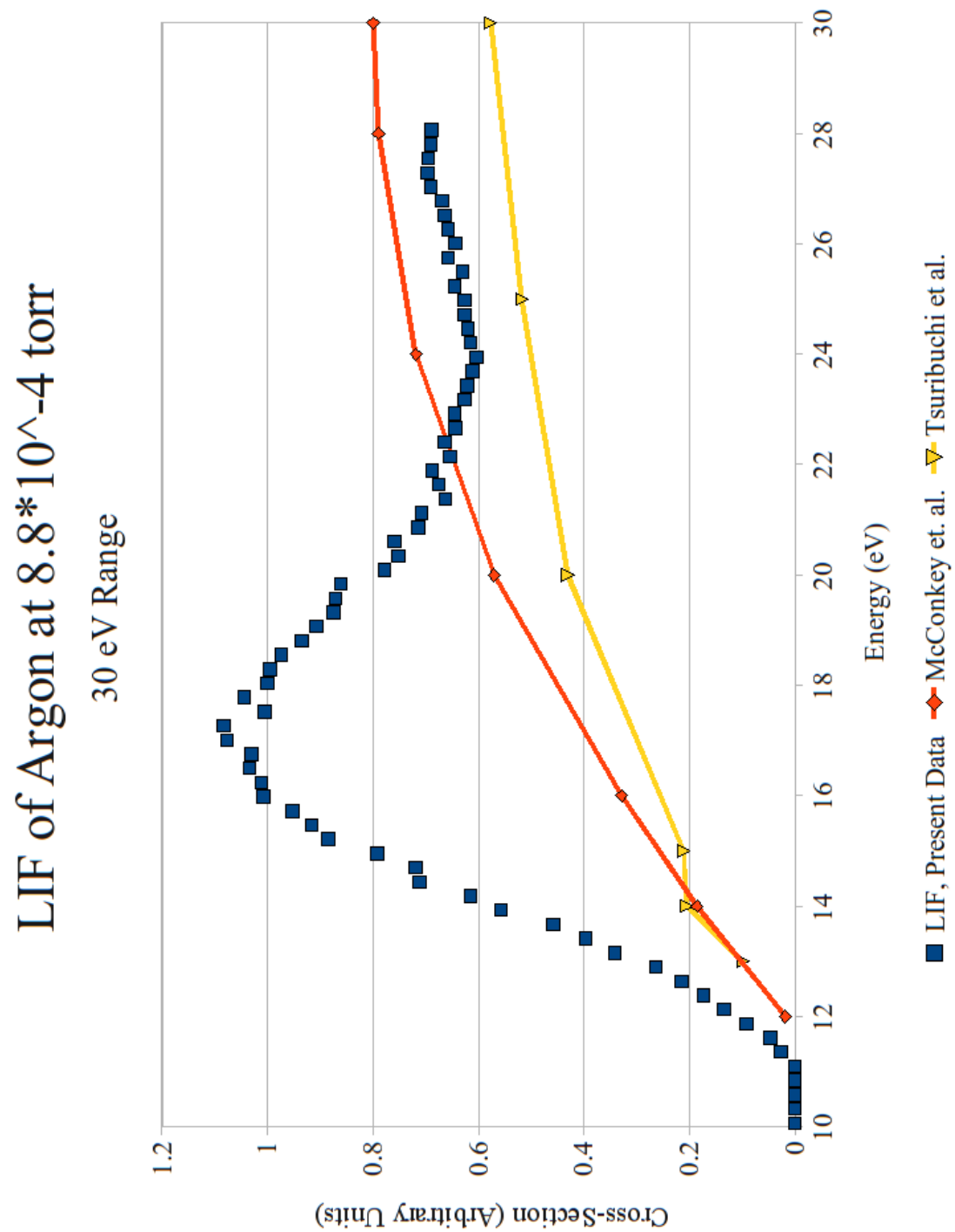


Figure 2.21 – Comparison of LIF signal (the “1048 nm” line) with previous results made by direct excitation by McConkey et al. [McConkey, (1973)] and Tsurubuchi et al. at 8.8×10^{-4} torr over the range 10-30 eV.

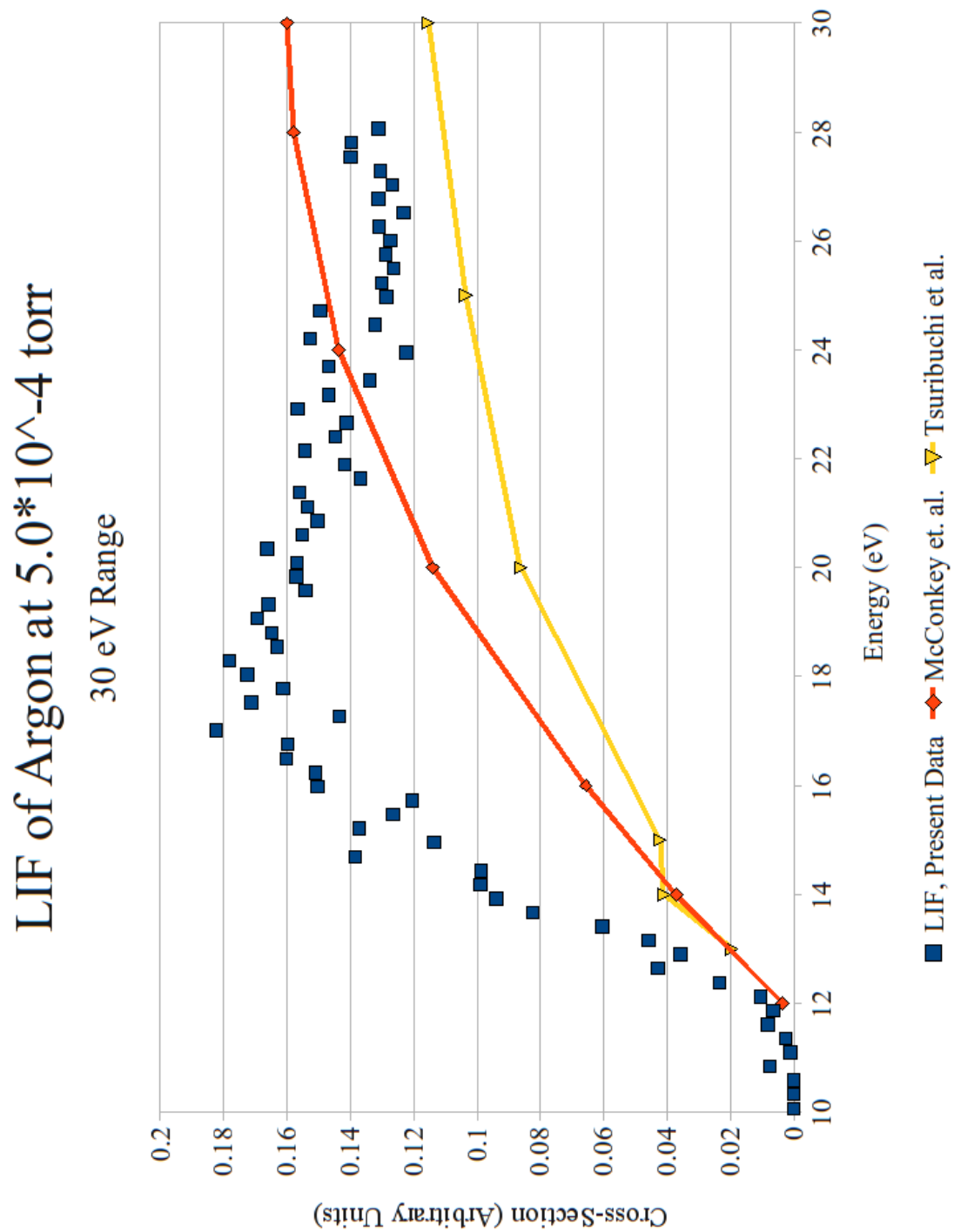


Figure 2.22 – Comparison of LIF signal (the “1048 nm” line) with previous results made by direct excitation by McConkey et al. [McConkey, (1973)] and Tsurubuchi et al. at 5.0×10^{-4} torr over the range 10-30 eV. Note the reduction in the signal peak at 15 eV with the results at 8.8×10^{-4} torr.

was conducted, comparing LIF signals with different injection energies on the final lens element of the electron gun, (labeled L2C in Figure 2.4 in Chapter 2 above). It became clear, when this voltage was changed from the present 24.0V, to 35.0 V and 50.0 V, that this peak feature changed as well. As the potential on L2C increased, the width of the peak broadened and its relative height increased. Additional features were observed at 50 eV as well. More details on improvements for the design of the electron gun will be discussed in Chapter 6.

Therefore, Figures 4.22 and 4.24 are the best final results that were obtained from this experiment and are used as the results for comparison with the previous direct excitations made by McConkey et al. and Tsurubuchi et al. The results from each were normalized to the arbitrary units used for the present results. An analysis of Figure 4.24 reveals that for energies higher than 40 eV, there is good agreement between all three results, although the agreement between the present and Tsurubuchi et al. results is closer. An observation of Figures 4.22 and 4.25 reveals a disagreement however, in the peak position between all three sets of data – Tsurubuchi et al. shows the highest energy peak, while McConkey et al. [McConkey et al. (1973)] shows the lowest peak energy. The present results lie between these with a maximum value of 40 eV (ignoring the variable peak data at 16 eV). Tsurubuchi et al. conducted the study by direct impact at pressures a factor of 10 lower than those currently used, so some of the differences may be attributed to this.

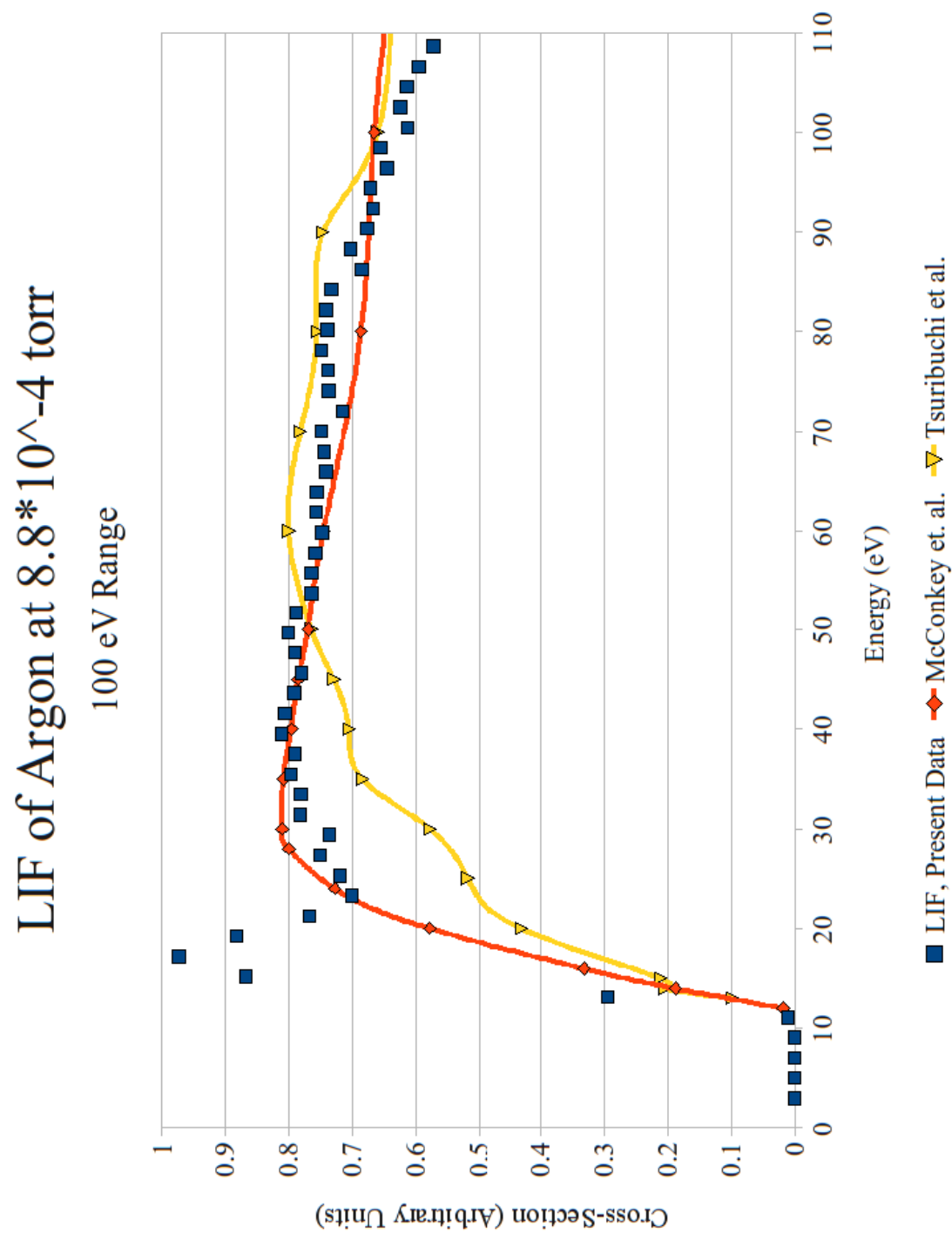


Figure 2.23 – Comparison of LIF signal (the “1048 nm” line) with previous results made by direct excitation by McConkey et al. [McConkey, (1973)] and Tsurubuchi et al. at 8.8×10^{-4} torr over the range 3-220 eV.

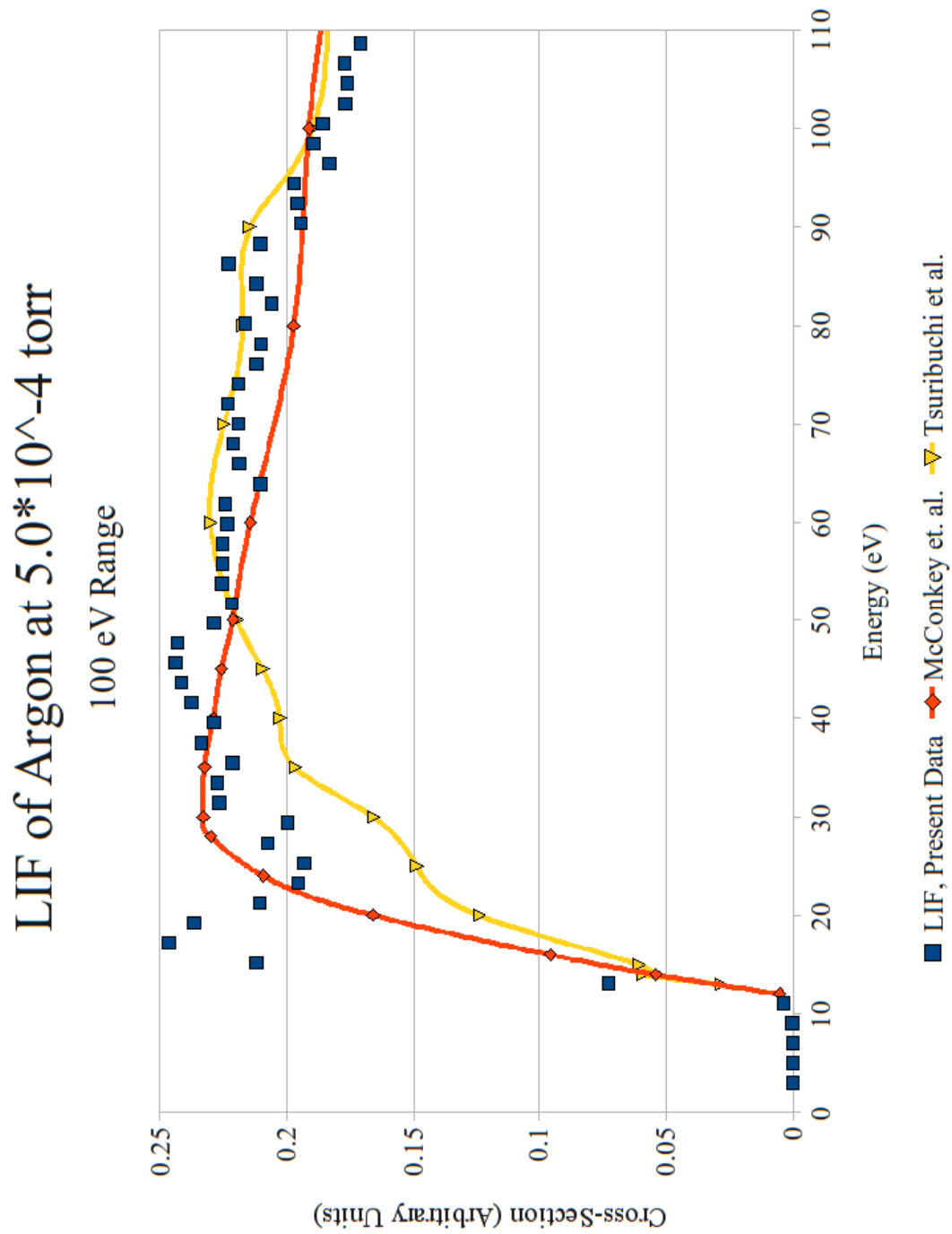


Figure 2.24 – Comparison of LIF signal (the “1048 nm” line) with previous results by McConkey et al. [McConkey, (1973)] and Tsurubuchi et al. at 5.0×10^{-4} torr over the range 3-220 eV. Note the reduction of signal peak at 15 eV with the results at 8.8×10^{-4} torr.

4.E. Summary and Conclusions

Direct excitation by electron impact of the “794.8 nm” transition line showed excellent agreement with previous results of Boffard et al. and Tsurubuchi et al. A comparative analysis between the present results and those by Boffard et al. showed very good agreement for the 340 nm, 423 nm, 470 nm, 620 nm, and 710 nm groups of emission lines. Our results demonstrated much higher statistical significance than the earlier data. A faster fall off with increasing energy compared to the results from Boffard et al. indicated a lower secondary electron component in our electron beam. The current data indicates that our setup provides an excellent instrument for the direct measurement of emission cross sections.

LIF measurements of the $3p^54s [1/2] (J=1)$ level were made for the first time. Near threshold measurements were possible because of the high signal levels obtained but target pressures of at least 5×10^{-4} torr were necessary. The threshold energy was demonstrably correct in relation to the threshold of the $3p^54p [1 \ 1/2] (J=1)$ level. The shape of the resultant LIF curve, giving the “104.8 nm” line excitation function, was compared with direct excitation results and demonstrated reasonable agreement at energies higher than 40 eV. The results suggested that the setup in this experiment could be used for the purpose of LIF of molecules, most importantly of H_2O , once necessary adaptations had been made to the system. For further details on the improvements and uses of this experiment, see Chapter 6.

Chapter 5 Overall Summary and Conclusions

A system which propagated an electron beam coaxially with a laser beam was successfully developed and tested. The present results for the (0,0) second positive band of N_2 agree strongly with the data by Shemansky et al. for energies up to 30 eV. Strong agreement was also observed between the present results and those of Borst and Zipf [Borst] for the (0,1) first negative band of N_2^+ . The $3p^54p [1 \frac{1}{2}] (J=1) \rightarrow 3p^54s [\frac{1}{2}] (J=0)$ transition of argon was measured with good agreement between the present results and those by Boffard et al. and Tsurubuchi et al. Additional emission cross sections of argon were studied and compared with previous results, the most notable of which were the emission lines measured for the 340 nm and 620 nm filters. Lastly, the $3p^54s [\frac{1}{2}] (J=1)$ cross section was measured using Laser Induced Fluorescence. The results of this initial study were compared with direct excitation cross section measurements made by McConkey et al. [McConkey, (1973)] and Tsurubuchi et al. Excellent agreement between the present results and those by Tsurubuchi et al. were demonstrated at energies higher than 40 eV. Suggested modifications for future development of the experiment are included in Chapter 6.

Chapter 6

Suggested Future Modifications and Developments

6.A. Present State

As has been illustrated in this thesis, the present state of the system provides an excellent instrument for the measurement of direct excitation by electron impact of a variety of atoms and molecules provided they are available in gaseous form. Of notable interest would be atmospheric gases such as O₂ or CO₂.

Regarding future LIF measurements, Krypton could readily be studied, using the current system with no changes. Excitation of the 5s'[1/2] (J=1) → 5p'[1/2] (J=1) transition using light of wavelength 850.8870 nm, is well within the operating range of the current laser. This system has remarkable resolution with a great quantity of signal, keeping data collection times short while maintaining accurate results.

6.B. Electron Optics Developments

The accurate determination of Laser Induced Fluorescence requires several modifications to the electron optical system. Firstly, the 'bunching' of the electrons in the magnetic field needs to be addressed. Secondly, the effective energy at the interaction region is affected by the potential of the final lens element and so the injection of the electron beam into the magnetic field needs to be improved. Lastly, the gun gets dirty over time, adversely affecting the quality of focusing and beam steering. Each of these issues can be addressed by appropriate modifications.

To resolve the bunching of electrons, the optimal solution would be to have the focal point of the final lens at infinity so that a parallel beam of electrons is ejected from the electron optical system. This is not possible with a single lens. The addition of a second

lens to the output stage of the electron optical system should solve this problem

This second lens would also contribute to reducing the final injection potential. Currently the system is operated with a final lens element at 24 V, however an additional lens would allow the final element to be operated at 10 V or lower. This would reduce any shift in effective energy observed at the earthed interaction region.

A set of deflectors added to the system in the output stack is essential to enable proper steering of the electron beam. This would allow operation of the gun using potentials closer to theoretical values. With these changes, the present limitations of the electron optical system could be greatly reduced, thereby dramatically improving the accuracy of the results.

In addition with more efficient operation of the gun, the analyser voltages could be reduced giving much higher energy resolution than was achieved with the present set-up. This would open up the system to studies of resonance phenomena or other such effects.

6.C. Laser Developments

The experiment suffered from long wait times in between collections of data. The Velocity Tunable Diode Laser by New Focus Inc. proved to be very unstable for long operations. It could sustain a particular wavelength for 20 minutes to one hour at a time, and would take a great deal of time to re-attain the desired wavelength. The addition of a more stable, reliable laser, would greatly improve the data collection time of the experiment. The optimal solution would be a laser with a built-in feedback mechanism, which would maintain the laser at the desired wavelength for live operation. This was done by hand in the present system which was far from ideal. For the study of more

complex molecules where the present diode laser does not provide the desired wavelengths, the inclusion of a YAG dye laser (currently available in the laboratory) would be necessary.

To further increase the accuracy of cross-sections, there are two suggestions which arise from this experiment. First, narrowband filters of the desired wavelength, with a width of no more than ± 1 nm at FWHM would be ideal for collecting accurate data. This would be an expensive addition, but would greatly improve the experiment as it would eliminate the unnecessary emission lines from the current observation.

Secondly, when the laser was turned on, an increase in background signal was observed. This was greatly minimized in this experiment because of low scattering of the laser off surfaces within the chamber. However to further minimize its effects a notch filter of the wavelength of the laser being used would minimize background signal being measured, thereby increasing the accuracy of LIF results.

6.D. Vacuum Developments

The present system utilizes a 6" Diffstak Turbo Pump. This causes some issue with the present system as the oil vapours tend to condense on the surfaces within the electron optics, thereby increasing the possibility of surface charging. This decreases the net time of operation of the gun before cleaning becomes necessary. This is in itself a lengthy process. This could be reduced by the addition of a Turbo Pump instead of the Diffstak. As the turbo pump would be oil-free, it could keep the system operating for a much more extensive period of time than the present system allows.

Also, the addition of heating coils to the mu-metal box, where the electron optics are

contained, would assist in keeping the lensing elements free from contaminants, extending the lifetime of the gun before a cleaning would be necessary.

6.E. Data Collection Developments

The final modification suggested for this system lies in switching the controls. The system is presently operated by a very old Quick Basic program, written for DOS and recorded on 3½" floppy disks before being transferred to a modern computer. This control system is limited in its ability to vary the energy, and has an upper limit on the total number of counts permitted for recording.

A switch to Labview as a control system would enable a user to increase the total number of bins, thereby increasing resolution. It could record the output signals generated in a more complete fashion. By recording each sweep of data separately, better statistics could be generated.

Labview would also permit the simultaneous control of the vacuum system, the electron optics and the laser. When the system is refitted for the measurement of water or more complex molecules, proper control of the YAG laser will be crucial for operation, This can best be accomplished with Labview.

Finally, the inclusion of Labview into the experiment would assist in the modernization of the control system. It has been fortunate that a functioning computer that is capable of running the present control software was available, however future progress of this experiment will involve the inclusion of more up-to-date technology.

Chapter 7 References

Ajello, J.M., et al., “Study of electron impact excitation of argon in the extreme ultraviolet: emission cross section of resonance lines of Ar I, Ar II”, J. Phys. B: At. Mol. Opt. Phys. **23** 4355-4376, (1990).

Ballou, J.K., and C.C. Lin, “Electron-Impact Excitation of the Argon Atom”, Phys. Rev. A, **8**, 4, (1973).

Battelle Energy Alliance, LLC (BEA) on behalf of Idaho National Labs (INL), “SIMION, v. 7.00”, software, (2005).

Becker, K., et al, “Electron-driven processes: scientific challenges and technological opportunities”, US Dept of Energy Report, (2000).

Boffard, J.B. et al., “Electron-impact excitation of argon: Optical emission cross-sections in the range of 300–2500 nm”, Atomic Data and Nuclear Data Tables **93**, 831-863 (2007).

Borst, W.L., and E.C. Zipf, “Cross Section for Electron-Impact Excitation of the (0,0) First Negative Band of N₂⁺ from Threshold to 3 keV”, Phys. Rev. A., **1**, 3 (1969).

Chilton, J.E., J.B. Boffard, R.S. Schappe, and C.C. Lin, “Measurement of Electron-impact excitation into the 3p⁵4p levels of Argons using Fourier-transform spectroscopy”, Phys. Rev. A, **57**, 1, (1998).

Hamamatsu Photonics K. K., “*Photomultiplier Tube, R7206-01*”, <http://sales.hamamatsu.com> Manual, Published 1998, (Available 2010, Apr. 1).

Harb, T., et al. “Laser Induced Fluorescence Studies of Molecular Dissociation by Electron Impact”, J Chem. Phys., **115**, 5507 (2001).

Harb, T., “Laser Induced Fluorescence Studies of Molecular Dissociation by Electron Impact”, Ph. D Thesis, University of Windsor (2002).

Harting, E., F.H. Read, *Electrostatic Lenses*, (Elsevier, N.Y., 1976).

Huber, K.P., and G. Herzberg, *Constants of Diatomic Molecules*, (New York: Van Nostrand), (1979).

Imami, M. and W. Borst, “Electron excitation of the (0,0) second positive band of nitrogen from threshold to 1000eV”, *J. Chem. Phys.*, 61, 3 (1974).

Itikawa, Y., N. Mason, “Cross Sections for Electron Collisions with Water Molecules”, *J. Phys. Chem.* **34**, 1, (2005).

Melton, C.E., “Cross Sections and Interpretation of Dissociative Attachment Reactions Producing OH⁻, O⁻, and H⁻ in H₂O”, *J. Chem. Phys.* **57**, 4218 (1972).

Malone, C.P., et al., “Integral Cross Sections for electron-impact excitation of the C3Πu, E3Σg+ states of N₂”, *J. Phys. B: At Mol. Opt. Phys.* 42, 1-8 (2009).

McConkey, J.W., et al., “Absolute cross section for simultaneous ionization and excitation of N₂ by electron impact”, *Proc. Phys. Soc.*, **86**, 463-466, (1965).

McConkey, J. W., and F. G. Donaldson, “Excitation of the Resonance Lines of Ar by Electrons”, *Can. J. Phys.*, **51**, 914-921, (1973).

Moore, J. H., C. C. Davis, M. Coplan. *Building Scientific Apparatus*. (Westview Press, 2002).

Ralchenko, Y., A. E. Kramida, J. Reader, and NIST ASD Team (2008). *NIST Atomic “Spectra Database”*, (version 3.1.5), <http://physics.nist.gov/asd3>, National Institute of Standards and Technology, (Available 2010, Feb 26).

Schappe, R.S., M.B. Schulman, L.W. Anderson and C.C. Lin, “Measurements of cross sections for electron-impact excitation into the metastable levels of argon and number densities of metastable argon atoms”, *Phys. Rev. A*, **50**, 444, (1994).

Severn, G.D., et al., “Argon ion laser-induced fluorescence with diode lasers”, *Rev. Sci. Instrum.* **69**, 1, (1998).

Shemansky, D.E., J.M. Ajello, I. Kanik, “Electron Excitation Functions of the N₂ Second Positive System”, *The Astro. J.*, **452**, , 472-479 (1995).

Taylor, F. W., “The greenhouse effect and climate change revisited”, *Rep. Prog. Phys.* **65**, 1 (2002).

Tsurubuchi, S., et al., “Electron-impact emission cross sections of Ar”, *J. Phys. B: At. Mol. Opt. Phys.* **29** 1785–1801 (1996).

Tyte, D.C., and R.W. Nicholls, “Identification Atlas of Molecular Spectra”, The University of Western Ontario, Dept of Physics, Molecular Excitation Group, (1965).

Verdeyen, J. T., *Laser Electronics 3rd Edition*, (Prentice Hall, Inc., 1995).

Zetner, P., “The Application of Laser Induced Fluorescence to the Study of Electron Impact Excitation of Atoms and Molecules”, Ph. D Thesis, University of Windsor (1985).

Appendix

J.B. Boffard et al. / Atomic Data and Nuclear Data Tables 93 (2007) 831–863

849

Table 1
Optical emission cross sections measured at a target gas pressure of 5 mTorr. See page 847 for Explanation of Tables

Wavelength (nm)	Levels	E_{th} (eV)	A_{ij} (10^6 s $^{-1}$)	$Q^{opt}(E)$ (10^{-20} cm 2)			Notes
				25 eV	50 eV	100 eV	
301.00	Ar ²⁺	3d ⁿ 3D ₂ ^o -4p ⁿ 3P ₂	73.57	—	—	0.18	
303.35	Ar ⁺	4s 2P _{1/2} -4p' 2P _{3/2}	37.11	9.9	—	3.0	4.3
305.48	Ar ²⁺	4s ⁿ 3P ₁ ^o -4p ⁿ 3D ₂	73.18	190	—	—	0.27
307.82	Ar ²⁺	4s ⁿ 3P ₀ ^o -4p ⁿ 3D ₁	73.16	140	—	—	0.16
309.34	Ar ⁺	4p 2P _{3/2} ^o -4d 2D _{5/2}	39.63	—	—	0.60	1.4
309.99	Ar ⁺	3d' 2D _{3/2} -5f[2] _{5/2}	41.18	—	—	0.54	1.2
310.44	Ar ⁺	4p' 2P _{3/2} ^o -5d 2D _{3/2}	41.10	—	—	0.19	0.53
311.44	Ar ⁺	3d' 2D _{3/2} -6p 2S _{1/2}	41.17	—	—	0.31	0.64
313.90	Ar ⁺	4p 4P _{5/2} ^o -4d 4P _{5/2}	38.93	52	—	1.3	0.61
314.26	Ar ⁺	4s[3/2] ₁ ^o -10p[1/2] ₀	15.57	—	0.37	0.30	0.25
316.15	Ar ⁺	3d' 2F _{7/2} -4f[5] _{9/2}	39.95	—	—	0.39	0.67
316.97	Ar ⁺	4p 4P _{3/2} ^o -4d 4P _{5/2}	38.93	49	—	1.2	0.53
317.30	Ar ⁺	4s[3/2] ₂ ^o -7p[1/2] ₁	15.45	—	0.74	0.31	0.21
318.10	Ar ⁺	4p 4P _{5/2} ^o -4d 4P _{3/2}	38.88	37	—	0.61	0.39
318.66	Ar ⁺	4s[3/2] ₁ ^o -9p[1/2] ₀	15.51	—	0.73	0.56	0.43
320.04	Ar ⁺	4s[3/2] ₂ ^o -8p[3/2] ₂	15.42	—	0.55	0.33	0.21
324.37	Ar ⁺	4p 4P _{3/2} ^o -4d 4P _{1/2}	38.84	106	—	0.75	1.3
324.98	Ar ⁺	4p 4P _{1/2} ^o -4d 4P _{3/2}	38.88	63	—	1.1	0.73
325.76	Ar ⁺	4s[3/2] ₁ ^o -8p[1/2] ₀	15.43	—	1.2	0.98	0.81
327.89	Ar ⁺	4s'[1/2] ₁ ^o -11p[1/2] ₀	15.61	—	1.3	0.90	0.69
328.59	Ar ²⁺	4s 3S ₂ ^o -4p 3P ₃	68.78	200	—	—	0.56
(329.4)	{ Ar ⁺	4p 2P _{3/2} ^o -4d 2P _{3/2}	39.39	—	{0.81	{1.4	
	{ Ar ⁺	4p' 2F _{7/2} -5d 4F _{7/2}	40.66	—	—	—	
330.19	Ar ²⁺	4s 3S ₂ ^o -4p 3P ₂	68.76	200	—	—	0.38
330.73	Ar ⁺	4p 2P _{1/2} ^o -4d 2P _{1/2}	39.31	—	—	0.48	0.98
331.93	Ar ⁺	4s[3/2] ₂ ^o -7p[3/2] ₂	15.28	—	1.2	0.70	0.51
332.55	Ar ⁺	4s[3/2] ₂ ^o -7p[5/2] ₃	15.27	—	0.63	0.26	0.10
333.61	Ar ²⁺	4s' 3D ₃ ^o -4p' 3F ₃	71.49	200	—	—	0.79
334.47	Ar ²⁺	4s' 3D ₃ ^o -4p' 3F ₃	71.47	180	—	—	0.62
335.09	Ar ⁺	4p' 2F _{5/2} ^o -4d' 2F _{5/2}	40.58	—	—	1.9	1.2
335.85	Ar ²⁺	4s' 3D ₃ ^o -4p' 3F ₂	71.45	160	—	—	0.57
336.35	Ar ⁺	4s'[1/2] ₁ ^o -9p[1/2] ₀	15.51	—	1.5	1.2	0.96
337.35	Ar ⁺	4s[3/2] ₁ ^o -7p[1/2] ₀	15.30	—	3.2	2.7	2.3
337.64	Ar ⁺	4p' 2F _{7/2} ^o -4d' 2F _{7/2}	40.57	—	—	2.2	1.3
338.84	Ar ⁺	4s[3/2] ₁ ^o -7p[3/2] ₁	15.28	—	0.75	0.65	0.76
338.85	Ar ⁺	4p 2S _{1/2} ^o -4d 2P _{3/2}	39.39	—	—	0.24	0.59
(339.4)	{ Ar ⁺	4s[3/2] ₂ ^o -6p[3/2] ₂	15.20	—	{2.1	{0.92	{0.35
	{ Ar ⁺	4s'[1/2] ₁ ^o -7f[3/2] _{1,2}	15.48	—	—	—	—
340.62	Ar ⁺	4s'[1/2] ₁ ^o -7p[1/2] ₀	15.47	0.39	2.2	1.8	1.4
345.41	Ar ⁺	4p 4P _{5/2} ^o -4d 4D _{3/2}	38.57	31.4	—	0.64	0.42
346.11	Ar ⁺	4s[3/2] ₁ ^o -6p[3/2] ₂	15.20	0.067	1.3	0.75	0.55
346.41	Ar ⁺	4p 2D _{3/2} ^o -4d 2F _{5/2}	39.02	—	—	0.76	0.79
347.67	Ar ⁺	4p 4P _{5/2} ^o -4d 4D _{5/2}	38.55	125	—	3.4	2.3
348.06	Ar ²⁺	4s' 3D ₃ ^o -4p' 3D ₃	71.33	160	—	—	0.76
349.12	Ar ⁺	4p 4P _{3/2} ^o -4d 4D _{3/2}	38.57	179	—	3.8	2.2
349.15	Ar ⁺	4p 4P _{3/2} ^o -4d 4D _{7/2}	38.53	231	—	7.4	3.0
349.97	Ar ²⁺	4s' 3D ₃ ^o -4p' 3D ₁	71.30	130	—	—	0.47
350.36	Ar ²⁺	4s' 3D ₃ ^o -4p' 3D ₂	71.30	120	—	—	0.46
350.65	Ar ⁺	4s[3/2] ₂ ^o -4f[5/2] _{3,2}	15.08	—	0.13	0.09	0.05
350.98	Ar ⁺	4p 4P _{1/2} ^o -4d 4D _{1/2}	38.60	255	—	1.4	3.3
351.11	Ar ²⁺	4s 3S ₁ ^o -4p 3P ₂	69.32	—	—	—	1.4
351.44	Ar ⁺	4p 4P _{3/2} ^o -4d 4D _{5/2}	38.55	136	—	3.5	2.4
353.53	Ar ⁺	4p 4P _{1/2} ^o -4d 4D _{3/2}	38.57	57	—	1.3	0.77
(354.6)	{ Ar ⁺	4p 2D _{3/2} ^o -4d 2F _{5/2}	39.02	—	—	{14	{11
	{ Ar ⁺	4p 2F _{5/2} ^o -4d' 2G _{7/2}	40.38	—	—	—	—
355.43	Ar ⁺	4s[3/2] ₂ ^o -6p[3/2] ₂	15.03	0.27	2.9	1.9	1.3
355.95	Ar ⁺	4p 2D _{3/2} ^o -4d 2F _{7/2}	38.92	288	—	8.4	4.6
356.10	Ar ⁺	4p' 2F _{7/2} ^o -4d' 2G _{9/2}	40.38	—	—	11	6.7
356.77	Ar ⁺	4s[3/2] ₂ ^o -6p[5/2] ₃	15.02	0.11	1.6	0.7	0.3
357.23	Ar ⁺	4s'[1/2] ₁ ^o -7p[1/2] ₀	15.30	0.51	4.6	3.8	3.2
357.66	Ar ⁺	4p 4D _{3/2} ^o -4d 4F _{7/2}	38.77	275	—	7.4	3.7
358.84	Ar ⁺	4p 4D _{5/2} ^o -4d 4F _{9/2}	38.71	303	—	8.7	3.1

(continued on next page)

Figure A.1 – Table 1 taken from Boffard. et al. [see Boffard, et al., (2007)].

Table 1 (continued)

Wavelength (nm)	Levels	E_{th} (eV)	A_{ij} (10^6 s^{-1})	$Q^{opv}(E) (10^{-20} \text{ cm}^2)$			Notes	
				25 eV	50 eV	100 eV		
360.65	1s ₄ -4p ₅	4s[3/2] ^o ₁ -6p[1/2] ₀	15.06	0.76	6.0	5.5	4.8	
362.21	Ar ⁺	4p ⁴ P _{3/2} ^o -5s ⁴ P _{1/2}	38.44	—	—	1.4	0.95	
363.27	1s ₄ -4p ₆	4s[3/2] ^o ₁ -6p[3/2] ₂	15.03	0.066	0.7	0.5	0.33	$Q(E_p)/Q(25 \text{ eV}) = 1.6$
363.45	1s ₄ -4p ₇	4s[3/2] ^o ₁ -6p[3/2] ₁	15.03	0.13	1.2	1.3	1.4	
363.98	Ar ⁺	4p' ² P _{3/2} ^o -4d' ² D _{5/2}	40.52	—	—	1.8	1.3	
364.98	1s ₂ -4p ₁	4s'[1/2] ^o ₁ -6p'[1/2] ₀	15.22	0.80	3.4	2.7	2.5	
365.95	1s ₄ -4p ₁₀	4s[3/2] ^o ₁ -6p[1/2] ₁	15.01	0.044	0.42	0.18	0.12	$Q(E_p)/Q(25 \text{ eV}) = 2.0$
367.07	1s ₂ -4p ₃	4s'[1/2] ^o ₁ -6p'[3/2] ₂	15.20	0.031	1.1	0.57	0.40	
367.52	1s ₂ -4p ₂	4s'[1/2] ^o ₁ -6p'[1/2] ₁	15.20	0.049	0.27	0.12	0.08	
372.93	Ar ⁺	4s ⁴ P _{5/2} -4p ⁴ S _{3/2}	35.73	48.0	—	5.8	3.4	
373.79	Ar ⁺	4p' ² D _{5/2} ^o -4d' ² F _{7/2}	40.57	—	—	4.4	2.7	
378.08	Ar ⁺	4p ⁴ D _{7/2} ^o -4d ⁴ D _{7/2}	38.53	77	—	2.5	1.2	
378.64	Ar ⁺	3d ⁴ D _{7/2} -4p ² D _{5/2}	35.44	1.5	—	0.80	0.55	
379.54	Ar ²⁺	3d'' ³ P ₂ ^o -4p'' ³ D ₃	73.12	—	—	—	0.07	
379.66	Ar ⁺	4p' ² D _{3/2} ^o -4d' ² D _{5/2}	40.52	—	—	0.42	0.30	
380.32	Ar ⁺	4p' ² D _{5/2} ^o -4d' ² D _{5/2}	40.52	—	—	2.2	1.5	
383.47	1s ₂ -4p ₅	4s'[1/2] ^o ₁ -6p[1/2] ₀	15.06	0.75	6.2	5.8	5.6	
384.15	Ar ⁺	4p ⁴ D _{3/2} ^o -4d ⁴ D _{1/2}	38.60	26.9	—	0.19	0.43	
384.54	Ar ⁺	4s ⁴ P _{5/2} -4p ² P _{3/2}	35.63	1.6	—	0.83	0.96	
385.06	Ar ⁺	4s ⁴ P _{3/2} -4p ⁴ S _{3/2}	35.73	38.7	—	4.9	2.6	
386.85	Ar ⁺	4p ⁴ S _{3/2} -4d ⁴ P _{3/2}	38.93	140	—	3.6	1.6	
389.47	1s ₂ -4p ₁₀	4s'[1/2] ^o ₁ -6p[1/2] ₁	15.01	0.057	0.61	0.30	0.20	$Q(E_p)/Q(25 \text{ eV}) = 2.0$
392.57	Ar ⁺	4p' ² F _{5/2} ^o -5s' ² D _{3/2}	40.04	—	—	3.3	3.9	
392.86	Ar ⁺	4s ⁴ P _{1/2} -4p ⁴ S _{3/2}	35.73	24.4	—	3.1	1.9	
394.61	Ar ⁺	4p' ² F _{7/2} ^o -5s' ² D _{5/2}	40.04	—	—	5.6	6.9	
394.75	1s ₅ -3p ₃	4s[3/2] ^o ₂ -5p[3/2] ₂	14.69	0.056	1.5	0.95	0.69	
394.90	1s ₅ -3p ₂	4s[3/2] ^o ₂ -5p[1/2] ₁	14.69	0.455	3.4	1.8	1.3	
396.84	Ar ⁺	3d ⁴ D _{5/2} -4p ⁴ D _{5/2}	35.31	4.8	—	1.5	0.81	
397.45	Ar ⁺	4s ⁴ P _{3/2} -4p ² P _{3/2}	35.63	—	—	1.1	1.4	
401.39	Ar ⁺	3d ⁴ D _{7/2} -4p ⁴ D _{7/2}	35.25	10.5	—	3.1	0.96	
404.29	Ar ⁺	4s' ² D _{3/2} -4p' ² D _{3/2}	37.25	40.6	—	6.5	4.3	
404.44	1s ₄ -3p ₃	4s[3/2] ^o ₁ -5p[3/2] ₂	14.69	0.333	6.7	4.1	2.7	
404.60	1s ₄ -3p ₂	4s[3/2] ^o ₁ -5p[1/2] ₁	14.69	0.041	0.35	0.19	0.14	
405.29	Ar ⁺	4s ² S _{1/2} -4p' ² P _{3/2}	39.56	67	—	8.7	13	
405.45	1s ₄ -3p ₄	4s[3/2] ^o ₁ -5p[3/2] ₁	14.66	0.027	0.37	0.16	0.09	
407.20	Ar ⁺	4s' ² D _{5/2} -4p' ² D _{5/2}	37.26	58	—	18	14	
408.24	Ar ⁺	4s ⁴ P _{5/2} -4p ² D _{5/2}	35.44	2.9	—	1.8	1.4	
408.24	Ar ⁺	4s ⁴ P _{5/2} -4p ² D _{5/2}	35.44	2.9	—	1.8	1.4	
(410.39)	Ar ⁺	4p ⁴ D _{7/2} ^o -5s ⁴ P _{3/2}	38.27	—	—	{9.9	{5.1	
		4p ² D _{5/2} -5s ² P _{3/2}	38.46	—	—	—	—	
413.17	Ar ⁺	4s' ² D _{3/2} -4p' ² P _{3/2}	37.19	85	—	14	20	
415.86	1s ₅ -3p ₆	4s[3/2] ^o ₂ -5p[3/2] ₂	14.53	1.40	19	13	8.5	
416.42	1s ₅ -3p ₇	4s[3/2] ^o ₂ -5p[3/2] ₁	14.52	0.288	5.1	5.1	4.8	
418.19	1s ₃ -3p ₂	4s'[1/2] ^o ₀ -5p'[1/2] ₁	14.69	0.561	5.3	2.8	2.1	
419.07	1s ₅ -3p ₈	4s[3/2] ^o ₂ -5p[5/2] ₂	14.51	0.280	8.6	5.0	3.6	
419.10	1s ₃ -3p ₄	4s'[1/2] ^o ₀ -5p'[1/2] ₁	14.58	0.539	6.2	3.0	1.9	
419.83	1s ₄ -3p ₅	4s[3/2] ^o ₁ -5p[1/2] ₀	14.58	2.57	26	23	20	
420.07	1s ₅ -3p ₉	4s[3/2] ^o ₂ -5p[5/2] ₃	14.50	0.967	26	10	4.4	
422.26	Ar ⁺	4p ² P _{3/2} ^o -5s ² P _{1/2}	38.56	—	—	0.95	1.6	
422.82	Ar ⁺	4s ⁴ P _{3/2} -4p ² D _{3/2}	35.44	13.1	—	7.1	4.9	
423.72	Ar ⁺	4s' ² D _{3/2} -4p' ² P _{3/2}	37.11	11.2	—	3.7	5.4	
425.12	1s ₅ -3p ₁₀	4s[3/2] ^o ₂ -5p[1/2] ₁	14.46	0.111	2.1	0.91	0.55	
425.94	1s ₂ -3p ₁	4s'[1/2] ^o ₁ -5p'[1/2] ₀	14.74	3.98	29	23	21	
426.63	1s ₄ -3p ₆	4s[3/2] ^o ₁ -5p[3/2] ₂	14.53	0.312	4.3	2.9	1.9	
426.65	Ar ⁺	4s ⁴ P _{5/2} -4p ⁴ D _{5/2}	35.31	16.4	—	5.1	2.8	
427.22	1s ₄ -3p ₇	4s[3/2] ^o ₁ -5p[3/2] ₁	14.52	0.797	15	14	13	
427.75	Ar ⁺	4s' ² D _{5/2} -4p' ² P _{3/2}	37.11	80	—	25	36	
428.29	Ar ⁺	4s ⁴ P _{3/2} -4p ⁴ D _{3/2}	35.06	13.2	—	1.2	0.75	
430.01	1s ₄ -3p ₈	4s[3/2] ^o ₁ -5p[5/2] ₂	14.51	0.377	12	7.0	5.1	
433.12	Ar ⁺	4s ⁴ P _{3/2} -4p ⁴ D _{3/2}	35.37	57.4	—	10	4.4	
433.36	1s ₂ -3p ₃	4s'[1/2] ^o ₁ -5p'[3/2] ₂	14.69	0.568	11	6.5	4.5	
433.53	1s ₂ -3p ₂	4s'[1/2] ^o ₁ -5p'[1/2] ₁	14.69	0.387	3.2	1.7	1.2	
434.52	1s ₂ -3p ₄	4s'[1/2] ^o ₁ -5p'[3/2] ₁	14.66	0.297	3.6	1.7	1.1	
434.81	Ar ⁺	4s ⁴ P _{5/2} -4p ⁴ D _{7/2}	35.25	117	—	33	12	

Figure A.2 - Table 1 (cont.) taken from Boffard, et al. [see Boffard, et al., (2007)].

Table 1 (continued)

Wavelength (nm)	Levels	E_n (eV)	A_{ij} (10^6 s $^{-1}$)	$Q^{opt}(E)$ (10^{-20} cm 2)			Notes
				25 eV	50 eV	100 eV	
435.22	Ar $^+$ 3d $^4D_{1/2}$ -4p $^4P^{\circ}_{1/2}$	35.40	21.2	—	2.1	1.7	
436.21	Ar $^+$ 3d $^2D_{3/2}$ -4p $^2D^{\circ}_{5/2}$	37.26	5.5	—	1.6	1.2	
436.78	Ar $^+$ 4s $^2S_{1/2}$ -5p $^2P^{\circ}_{1/2}$	39.34	—	—	3.9	4.9	
437.59	Ar $^+$ 4s $^2P_{3/2}$ -4p $^2S_{1/2}$	35.73	20.5	—	3.3	2.5	
437.97	Ar $^+$ 4s $^4P_{1/2}$ -4p $^4D^{\circ}_{1/2}$	35.40	100.	—	9.3	5.6	
438.51	Ar $^+$ 4s $^2S_{1/2}$ -5p $^4D^{\circ}_{3/2}$	39.33	—	—	4.5	5.9	
440.10	Ar $^+$ 3d $^4D_{7/2}$ -4p $^4F^{\circ}_{5/2}$	34.98	30.4	—	9.7	3.6	
442.09	Ar $^+$ 3d $^4D_{1/2}$ -4p $^4P^{\circ}_{3/2}$	35.02	3.1	—	0.61	0.33	
442.60	Ar $^+$ 4s $^4P_{3/2}$ -4p $^4D^{\circ}_{5/2}$	35.31	81.7	—	24	13	
443.02	Ar $^+$ 4s $^4D_{1/2}$ -4p $^4D^{\circ}_{3/2}$	35.37	56.9	—	10.	4.3	
443.10	Ar $^+$ 3d $^4D_{5/2}$ -4p $^4P^{\circ}_{5/2}$	34.98	10.9	—	2.7	0.9	
444.89	Ar $^+$ 4p $^2D^{\circ}_{5/2}$ -5s $^2D_{5/2}$	40.04	—	—	2.9	3.4	
447.48	Ar $^+$ 3d $^2D_{3/2}$ -4p $^2P^{\circ}_{1/2}$	37.19	29	—	5.1	7.2	
448.18	Ar $^+$ 3d $^2D_{5/2}$ -4p $^2D^{\circ}_{5/2}$	37.26	45.5	—	12	7.5	
449.10	Ar $^+$ 3d $^2D_{5/2}$ -4p $^2D^{\circ}_{3/2}$	37.25	4.6	—	0.77	0.53	
451.07	Ar $^+$ 1s $_2$ -3p $_5$ 4s'[1/2] $_1^{\circ}$ -5p[1/2] $_0$	14.58	1.18	9.7	9.2	8.8	
452.23	Ar $^+$ 1s $_3$ -3p $_{10}$ 4s'[1/2] $_0^{\circ}$ -5p[1/2] $_1$	14.46	0.0898	1.8	0.87	0.55	
454.51	Ar $^+$ 4s $^2P_{3/2}$ -4p $^2P^{\circ}_{3/2}$	35.63	47.1	—	24	32	
457.93	Ar $^+$ 4s $^2P_{1/2}$ -4p $^2S^{\circ}_{1/2}$	35.73	80.	—	12	9.8	
458.99	Ar $^+$ 4s $^2D_{3/2}$ -4p $^2F^{\circ}_{5/2}$	36.89	66.4	—	22	19	
459.61	Ar $^+$ 1s $_2$ -3p $_7$ 4s'[1/2] $_1^{\circ}$ -5p[3/2] $_1$	14.52	0.0947	1.7	1.8	1.6	
459.88	Ar $^+$ 3d $^2D_{3/2}$ -4p $^2P^{\circ}_{3/2}$	37.11	6.7	—	2.2	3.2	
460.96	Ar $^+$ 4s $^2D_{5/2}$ -4p $^2F^{\circ}_{7/2}$	36.90	78.9	—	37	32	
462.84	Ar $^+$ 1s $_2$ -3p $_8$ 4s'[1/2] $_1^{\circ}$ -5p[5/2] $_2$	14.51	0.0383	1.2	0.81	0.52	
463.72	Ar $^+$ 4s $^2D_{3/2}$ -4p $^2F^{\circ}_{3/2}$	36.89	7.1	—	2.3	2.0	
465.79	Ar $^+$ 4s $^2P_{3/2}$ -4p $^2P^{\circ}_{1/2}$	35.56	89.2	—	20.	23	
470.23	Ar $^+$ 1s $_2$ -3p $_{10}$ 4s'[1/2] $_1^{\circ}$ -5p[1/2] $_1$	14.46	0.109	2.3	1.1	0.68	
472.69	Ar $^+$ 4s $^2P_{3/2}$ -4p $^2D^{\circ}_{5/2}$	35.52	58.8	—	19	18	
473.21	Ar $^+$ 3d $^2D_{5/2}$ -4p $^2P^{\circ}_{3/2}$	37.11	6.7	—	2.3	3.4	
473.59	Ar $^+$ 4s $^4P_{5/2}$ -4p $^4P^{\circ}_{3/2}$	35.02	58.0	—	11	5.9	
474.68	2p $_{10}$ -8d $_6$ 4p[1/2] $_1$ -8d[1/2] $_0^{\circ}$	15.52	0.744 a	1.4	0.50	0.20	
475.29	2p $_{10}$ -8d $_5$ 4p[1/2] $_1$ -8d[1/2] $_1^{\circ}$	15.51	0.753 a	2.3	1.5	0.99	Resonance level
476.49	Ar $^+$ 4s $^2P_{1/2}$ -4p $^2P^{\circ}_{3/2}$	35.63	64	—	32	45	
476.87	2p $_{10}$ -6s $_{1''}$ 4p[1/2] $_1$ -6d'[3/2] $_2^{\circ}$	15.51	0.740 a	4.5	1.9	0.84	
480.60	Ar $^+$ 4s $^4P_{5/2}$ -4p $^4P^{\circ}_{5/2}$	34.98	78	—	23	8.4	
483.67	2p $_{10}$ -6s $_5$ 4p[1/2] $_1$ -9s[3/2] $_2^{\circ}$	15.47	0.102	2.5	0.86	0.45	
484.78	Ar $^+$ 4s $^4P_{3/2}$ -4p $^4P^{\circ}_{1/2}$	35.06	84.9	—	7.7	5.9	
487.63	2p $_{10}$ -7d $_3$ 4p[1/2] $_1$ -7d[3/2] $_2^{\circ}$	15.45	0.746 a	4.5	1.9	0.71	
487.99	Ar $^+$ 4s $^2P_{3/2}$ -4p $^2D^{\circ}_{5/2}$	35.44	82.3	—	42	29	
488.79	2p $_{10}$ -7d $_5$ 4p[1/2] $_1$ -7d[1/2] $_1$	15.44	1.3	3.1	1.4	0.98	Resonance level
488.90	Ar $^+$ 4s $^2P_{1/2}$ -4p $^2P^{\circ}_{1/2}$	35.56	19	—	4.5	5.2	
489.47	2p $_{10}$ -7d $_6$ 4p[1/2] $_1$ -7d[1/2] $_0^{\circ}$	15.44	1.8	1.6	0.63	0.27	
490.48	Ar $^+$ 3d $^2F_{5/2}$ -4p $^2F^{\circ}_{7/2}$	36.90	3.7	—	1.5	1.4	
493.32	Ar $^+$ 4s $^4P_{3/2}$ -4p $^4P^{\circ}_{3/2}$	35.02	14.4	—	2.7	1.3	
495.68	2p $_9$ -9d $_4'$ 4p[5/2] $_3$ -9d[7/2] $_4^{\circ}$	15.58	0.483 a	4.3	1.4	0.54	
496.51	Ar $^+$ 4s $^2P_{1/2}$ -4p $^2D^{\circ}_{3/2}$	35.52	39.4	—	12	11	
498.99	2p $_8$ -9d $_4$ 4p[5/2] $_2$ -9d[7/2] $_3$	15.58	0.233 a	1.9	1.0	0.61	
500.93	Ar $^+$ 4s $^4P_{3/2}$ -4p $^4P^{\circ}_{5/2}$	34.98	15.1	—	3.8	1.3	
501.72	Ar $^+$ 3d $^2D_{3/2}$ -4p $^2F^{\circ}_{5/2}$	36.89	20.7	—	6.6	5.4	
503.20	2p $_9$ -7s $_5$ 4p[5/2] $_3$ -10s[3/2] $_2^{\circ}$	15.54	0.117 a	0.99	0.29	0.11	$Q(E_p)/Q(25 \text{ eV}) = 1.6$
504.88	2p $_{10}$ -5s $_5$ 4p[1/2] $_1$ -8s[3/2] $_2^{\circ}$	15.36	0.46	1.7	0.51	0.17	$Q(E_p)/Q(25 \text{ eV}) = 1.4$
505.42	2p $_{10}$ -4s $_2$ 4p[1/2] $_1$ -7s'[1/2] $_1^{\circ}$	15.36	0.45	0.42	0.26	0.21	Resonance level
506.01	2p $_9$ -8d $_4'$ 4p[5/2] $_3$ -8d[7/2] $_4^{\circ}$	15.52	0.629 a	5.6	1.7	0.57	
506.20	Ar $^+$ 4s $^4P_{1/2}$ -4p $^4P^{\circ}_{3/2}$	35.02	22.3	—	4.0	2.1	
507.31	2p $_{10}$ -6d $_3$ 4p[1/2] $_1$ -6d[3/2] $_2^{\circ}$	15.35	0.059	1.2	0.41	0.17	
508.71	2p $_8$ -8d $_4$ 4p[5/2] $_2$ -8d[7/2] $_3$	15.53	0.16	1.7	1.4	1.2	
509.05	Ar $^+$ 3d $^2D_{5/2}$ -4p $^2P^{\circ}_{3/2}$	39.56	—	—	1.6	2.5	
510.47	2p $_7$ -9d $_{1''}$ 4p[3/2] $_1$ -9d[5/2] $_2^{\circ}$	15.58	0.151 a	1.2	0.34	0.14	
511.82	2p $_8$ -6s $_{1'''}$ 4p[5/2] $_2$ -6d'[5/2] $_3^{\circ}$	15.52	0.467 a	2.2	1.0	0.54	
512.58	Ar $^+$ 3d $^2D_{3/2}$ -4p $^2P^{\circ}_{1/2}$	39.61	—	—	0.83	1.6	
514.18	Ar $^+$ 3d $^2D_{5/2}$ -4p $^2F^{\circ}_{7/2}$	36.90	8.1	—	3.5	3.1	
514.53	Ar $^+$ 4s $^2P_{3/2}$ -4p $^4D^{\circ}_{5/2}$	35.31	10.6	—	2.7	1.7	
515.14	2p $_{10}$ -6d $_6$ 4p[1/2] $_1$ -6d[1/2] $_0^{\circ}$	15.31	2.39	2.3	0.97	0.39	

(continued on next page)

Figure A.3 - Table 1 (cont.) taken from Boffard, et al. [see Boffard, et al., (2007)].

Table 1 (continued)

Wavelength (nm)	Levels	E_{th} (eV)	A_{ij} (10^6 s^{-1})	$Q^{opt}(E)$ (10^{-20} cm^2)			Notes
				25 eV	50 eV	100 eV	
515.23	2p ₁₀ -5s ₁ ^{***}	4p[1/2] ₁ -5d'[5/2] ₂ ^o	15.31	0.11	1.0	0.29	0.11
516.23	2p ₁₀ -6d ₅	4p[1/2] ₁ -6d[1/2] ₁ ^o	15.31	1.9	6.1	3.0	1.8
517.62	Ar ⁺	3d ² D _{5/2} -4p' ² F _{5/2}	36.89	1.7	—	0.45	0.37
517.75	2p ₉ -6s ₅	4p[5/2] ₃ -9s[3/2] ₂ ^o	15.47	0.24	1.2	0.35	0.17
518.77	2p ₁₀ -5s ₁ ["]	4p[1/2] ₁ -5d'[3/2] ₂ ^o	15.30	1.32 ^b	12	3.8	1.3
521.05	2p ₉ -7d ₄	4p[5/2] ₃ -7d[7/2] ₃ ^o	15.45	0.11	0.56	0.49	0.38
522.13	2p ₉ -7d ₄ '	4p[5/2] ₃ -7d[7/2] ₄ ^o	15.45	0.88	11	3.6	1.3
525.28	2p ₈ -7d ₄	4p[5/2] ₂ -7d[7/2] ₃ ^o	15.45	0.54	3.2	2.9	2.4
525.45	2p ₇ -6s ₁ ^{***}	4p[3/2] ₁ -6d'[5/2] ₂ ^o	15.51	0.36	2.4	0.71	0.32
530.81	Ar ⁺	3d ² D _{5/2} -5p ⁴ S _{5/2}	39.46	—	—	0.38	0.24
531.77	2p ₃ -7s ₁ ^{***}	4p'[3/2] ₂ -7d'[5/2] ₂ ^o	15.63	0.311 ^a	2.3	1.1	0.66
534.74	2p ₇ -6s ₄	4p[3/2] ₁ -9s[3/2] ₁ ^o	15.47	—	0.46	0.52	0.46
537.35	2p ₇ -7d ₁ ["]	4p[3/2] ₁ -7d[5/2] ₂ ^o	15.46	0.27	3.4	1.3	0.55
541.05	2p ₆ -7d ₁ ["]	4p[3/2] ₂ -7d[5/2] ₂ ^o	15.46	0.20	2.5	1.0	0.43
542.14	2p ₉ -5s ₅	4p[5/2] ₃ -8s[3/2] ₂ ^o	15.36	0.733 ^a	2.7	0.86	0.40
544.00	2p ₁₀ -4s ₄	4p[1/2] ₁ -7s[3/2] ₁ ^o	15.18	0.19	0.72	0.54	0.51
544.22	2p ₉ -6d ₁ '	4p[5/2] ₃ -6d[5/2] ₃ ^o	15.35	0.093	1.0	0.65	0.31
545.17	2p ₁₀ -4s ₅	4p[1/2] ₁ -7s[3/2] ₂ ^o	15.18	0.47	2.2	0.75	0.40
545.74	2p ₈ -5s ₄	4p[5/2] ₂ -8s[3/2] ₁ ^o	15.35	0.36	1.3	1.5	1.6
546.72	2p ₈ -5s ₅	4p[5/2] ₂ -8s[3/2] ₂ ^o	15.36	0.076	0.36	0.12	0.05
547.35	2p ₈ -4s ₂	4p[5/2] ₂ -7s'[1/2] ₁ ^o	15.36	0.20	0.57	0.36	0.28
549.59	2p ₉ -6d ₄ '	4p[5/2] ₃ -6d[7/2] ₄ ^o	15.33	1.69	23	7.0	2.6
550.61	2p ₈ -6d ₄	4p[5/2] ₂ -6d[7/2] ₃ ^o	15.35	0.36	4.7	5.2	4.0
552.50	2p ₉ -5s ₁ ^{***}	4p[5/2] ₃ -5d'[5/2] ₂ ^o	15.32	0.17	1.8	0.73	0.35
(555.9)	{ 2p ₁₀ -5d ₃	4p[1/2] ₁ -5d[3/2] ₂ ^o	15.14	1.42	{17	{6	{2.3
	{ 2p ₄ -6s ₁ ^{***}	4p'[3/2] ₁ -6d'[5/2] ₂ ^o	15.51	0.22	—	—	—
557.25	2p ₈ -5s ₁ ^{***}	4p[5/2] ₂ -5d'[5/2] ₃ ^o	15.32	0.66	7.9	3.3	1.5
558.18	2p ₉ -5s ₁ ["]	4p[5/2] ₃ -5d'[3/2] ₂ ^o	15.30	0.056	1.0	0.35	0.14
558.87	2p ₈ -5s ₁ ^{***}	4p[5/2] ₂ -5d'[5/2] ₂ ^o	15.31	0.15	1.6	0.41	0.13
559.75	2p ₃ -6s ₁ ^{***}	4p'[3/2] ₂ -6d'[5/2] ₃ ^o	15.52	0.42	4.9	2.0	1.4
560.11	2p ₇ -6d ₂	4p[3/2] ₁ -6d[3/2] ₁ ^o	15.35	—	0.68	0.70	0.66
560.67	2p ₁₀ -5d ₅	4p[1/2] ₁ -5d[1/2] ₁ ^o	15.12	2.2	8.6	5.3	3.5
564.87	2p ₆ -5s ₄	4p[3/2] ₂ -8s[3/2] ₁ ^o	15.37	0.12	0.81	0.93	0.92
565.07	2p ₁₀ -5d ₆	4p[1/2] ₁ -5d[1/2] ₁ ^o	15.10	3.20	6.4	2.0	0.52
565.91	2p ₆ -5s ₅	4p[3/2] ₂ -8s[3/2] ₂ ^o	15.36	0.26	1.1	0.36	0.17
568.19	2p ₆ -6d ₁ '	4p[3/2] ₂ -6d[5/2] ₃ ^o	15.35	0.20	2.6	1.4	0.62
(569.0)	{ 2p ₆ -5s ₁ '	4p[3/2] ₂ -5d'[3/2] ₁ ^o	15.35	—	{6.4	{1.9	{0.63
	{ 2p ₂ -6s ₁ ["]	4p'[1/2] ₁ -6d'[3/2] ₂ ^o	15.51	—	—	—	—
570.09	2p ₆ -6d ₄	4p[3/2] ₂ -6d[7/2] ₃ ^o	15.35	0.59	0.63	0.76	0.58
573.95	2p ₇ -5s ₁ ^{***}	4p[3/2] ₁ -5d'[5/2] ₂ ^o	15.31	0.87	8.1	2.3	0.84
577.21	2p ₆ -5s ₁ ^{***}	4p[3/2] ₂ -5d'[5/2] ₂ ^o	15.32	0.20	2.8	1.2	0.64
577.40	2p ₃ -7d ₃	4p'[3/2] ₂ -7d[3/2] ₂ ^o	15.45	0.11	0.81	0.35	0.14
578.35	2p ₇ -5s ₁ ["]	4p[3/2] ₁ -5d'[3/2] ₂ ^o	15.30	0.081	0.41	0.14	0.04
578.95	2p ₆ -5s ₁ ^{***}	4p[3/2] ₂ -5d'[5/2] ₂ ^o	15.31	0.046	0.44	0.12	0.05
580.21	2p ₆ -6d ₅	4p[3/2] ₂ -6d[1/2] ₁ ^o	15.31	0.42	1.4	0.68	0.37
583.42	2p ₆ -5s ₁ ["]	4p[3/2] ₂ -5d'[3/2] ₂ ^o	15.30	0.50 ^b	3.5	1.2	0.36
586.03	2p ₁₀ -3s ₂	4p[1/2] ₁ -6s'[1/2] ₁ ^o	15.02	0.27 ^b	1.3	1.8	1.9
588.26	2p ₁₀ -3s ₃	4p[1/2] ₁ -6s'[1/2] ₁ ^o	15.01	1.23	1.1	0.38	0.27
588.86	2p ₉ -4s ₅	4p[5/2] ₃ -7s[3/2] ₂ ^o	15.18	1.29	5.2	1.8	0.91
591.21	2p ₁₀ -4s ₁ '	4p[1/2] ₁ -4d'[3/2] ₁ ^o	15.00	—	9.3	11	12
591.66	2p ₈ -5d ₂	4p[5/2] ₂ -5d[3/2] ₁ ^o	15.19	0.059	1.1	1.7	2.0
592.88	2p ₈ -4s ₄	4p[5/2] ₂ -7s[3/2] ₁ ^o	15.18	1.1	4.7	3.6	3.3
594.27	2p ₈ -4s ₅	4p[5/2] ₂ -7s[3/2] ₂ ^o	15.18	0.18	1.2	0.38	0.20
597.16	2p ₄ -4s ₃	4p'[3/2] ₁ -7s'[1/2] ₁ ^o	15.36	1.1	0.96	0.32	0.16
598.73	2p ₉ -5d ₄	4p[5/2] ₃ -5d[7/2] ₃ ^o	15.15	0.12	3.3	1.9	1.1
599.90	2p ₈ -5d ₁ ["]	4p[5/2] ₂ -5d[5/2] ₂ ^o	15.16	0.14	2.8	1.1	0.49
600.57	2p ₃ -5s ₄	4p'[3/2] ₂ -8s[3/2] ₁ ^o	15.37	0.14	0.64	0.75	0.81
601.37	2p ₉ -5d ₃	4p[5/2] ₃ -5d[3/2] ₂ ^o	15.14	0.14	1.1	0.46	0.19
602.51	2p ₃ -4s ₂	4p'[3/2] ₂ -7s'[1/2] ₁ ^o	15.36	0.90	1.9	1.1	0.91
603.21	2p ₉ -5d ₄ '	4p[5/2] ₃ -5d[7/2] ₄ ^o	15.13	2.36 ^b	41	15	5.4
(604.3)	{ 2p ₈ -5d ₄	4p[5/2] ₂ -5d[7/2] ₃ ^o	15.15	1.47 ^b	{18	{11	{6.5
	{ 2p ₃ -6d ₁ '	4p'[3/2] ₂ -6d[5/2] ₃ ^o	15.15	—	—	—	—
605.27	2p ₁₀ -4s ₁ ^{***}	4p[1/2] ₁ -4d'[5/2] ₂ ^o	14.95	0.19	2.7	0.78	0.32
605.94	2p ₁₀ -4s ₁ ["]	4p[1/2] ₁ -4d'[3/2] ₂ ^o	14.95	—	6.6	2.3	0.98

Figure A.4 - Table 1 (cont.) taken from Boffard, et al. [see Boffard, et al., (2007)].

Table 1 (continued)

Wavelength (nm)	Levels	E_{th} (eV)	A_{ij} (10^6 s^{-1})	$Q^{opt}(E)$ (10^{-20} cm^2)			Notes	
				25 eV	50 eV	100 eV		
606.48	2p ₃ -6d ₄	4p'[3/2] ₂ -6d[7/2] ₃ ^o	15.35	0.058	0.88	1.2	0.96	
609.88	2p ₇ -4s ₄	4p[3/2] ₁ -7s[3/2] ₁ ^o	15.18	0.52	1.9	1.4	1.3	Resonance level
610.11	2p ₂ -4s ₂	4p'[1/2] ₁ -7s'[1/2] ₁ ^o	15.36	0.33	0.51	0.33	0.28	Resonance level
610.56	2p ₄ -5s _{1'''}	4p'[3/2] ₁ -5d'[5/2] ₂ ^o	15.31	1.21	11	2.8	0.98	
611.35	2p ₇ -4s ₅	4p[3/2] ₁ -7s[3/2] ₂ ^o	15.18	0.047	0.51	0.17	0.09	$Q(E_p)/Q(25 \text{ eV}) = 1.6$
611.49	Ar ⁺	3d ² G _{3/2} -4p' ² F _{7/2} ^o	36.90	—	—	8.7	7.2	
612.74	2p ₈ -5d ₅	4p[5/2] ₂ -5d[1/2] ₁ ^o	15.12	0.11	0.72	0.42	0.31	Resonance level
612.87	2p ₂ -6d ₃	4p'[1/2] ₁ -6d[3/2] ₂ ^o	15.35	0.086	2.4	0.81	0.36	
614.54	2p ₃ -5s _{1''}	4p'[3/2] ₂ -5d'[5/2] ₃ ^o	15.32	0.76	8.4	3.3	1.8	
(615.5)	{ 2p ₆ -4s ₄ 2p ₄ -5s _{1'} }	{ 4p[3/2] ₂ -7s[3/2] ₁ ^o 4p'[3/2] ₁ -5d'[3/2] ₂ ^o }	{ 15.18 15.30}	{ 0.51 —}	{ 1.5 —}	{ 1.1 —}	{ 0.96 —}	Resonance level
616.51	2p ₃ -5s _{1'''}	4p'[3/2] ₂ -5d'[5/2] ₂ ^o	15.31	0.0989	0.94	0.25	0.10	
617.02	2p ₆ -4s ₅	4p[3/2] ₂ -7s[3/2] ₂ ^o	15.18	0.50	2.1	0.71	0.38	$Q(E_p)/Q(25 \text{ eV}) = 1.6$
617.23	Ar ⁺	3d ² G _{7/2} -4p' ² F _{5/2} ^o	36.89	20.0	—	4.8	4.1	
617.31	2p ₇ -5d _{1''}	4p[3/2] ₁ -5d[5/2] ₂ ^o	15.16	0.67	11	4.7	2.1	
621.25	2p ₆ -5d _{1'}	4p[3/2] ₂ -5d[5/2] ₃ ^o	15.17	0.39	4.7	4.0	2.5	$Q(E_p)/Q(25 \text{ eV}) = 1.5$
621.59	2p ₃ -5s _{1''}	4p'[3/2] ₂ -5d'[3/2] ₂ ^o	15.30	0.57	4.6	1.6	0.52	
624.84	2p ₇ -5d ₃	4p[3/2] ₁ -5d[3/2] ₂ ^o	15.14	0.068	0.76	0.30	0.12	
627.87	2p ₆ -5d ₄	4p[3/2] ₂ -5d[7/2] ₃ ^o	15.15	0.020	0.39	0.23	0.14	
629.69	2p ₂ -5s _{1''}	4p'[1/2] ₁ -5d'[3/2] ₂ ^o	15.30	0.90	6.9	2.4	0.73	
630.77	2p ₆ -5d ₃	4p[3/2] ₂ -5d[3/2] ₂ ^o	15.14	0.60	5.9	2.4	0.94	
636.49	2p ₇ -5d ₆	4p[3/2] ₁ -5d[1/2] ₁ ^o	15.10	0.56	1.2	0.38	0.10	
636.96	2p ₆ -5d ₅	4p[3/2] ₂ -5d[1/2] ₁ ^o	15.12	0.42	2.1	1.2	0.89	Resonance level
638.47	2p ₁₀ -3s ₄	4p[1/2] ₁ -6s[3/2] ₁ ^o	14.85	0.421	1.8	2.2	2.6	Resonance level
639.92	Ar ⁺	3d ⁴ F _{3/2} -4p ² D _{5/2} ^o	35.44	—	—	0.43	0.30	
641.63	2p ₁₀ -3s ₅	4p[1/2] ₁ -6s[3/2] ₂ ^o	14.84	1.16	7.7	3.0	1.8	$Q(E_p)/Q(25 \text{ eV}) = 1.5$
643.16	2p ₈ -3s ₂	4p[5/2] ₂ -6s'[1/2] ₁ ^o	15.02	0.051	0.36	0.47	0.60	Resonance level
646.66	2p ₅ -5d ₂	4p[1/2] ₀ -5d[3/2] ₁ ^o	15.19	0.15	4.2	7.4	10.	Resonance level
648.11	2p ₅ -4s ₄	4p[1/2] ₀ -7s[3/2] ₁ ^o	15.18	0.094	0.39	0.27	0.25	Resonance level
648.31	Ar ⁺	3d ² P _{3/2} -4p ² S _{1/2} ^o	35.73	10.6	—	1.4	1.1	
649.91	2p ₄ -5d ₂	4p'[3/2] ₁ -5d[3/2] ₁ ^o	15.19	—	0.68	1.1	1.4	Resonance level
651.38	2p ₄ -4s ₄	4p'[3/2] ₁ -7s[3/2] ₁ ^o	15.18	0.054	0.20	0.15	0.14	Resonance level
653.81	2p ₉ -4s _{1'''}	4p[5/2] ₃ -4d'[5/2] ₃ ^o	14.97	0.11	2.5	1.5	1.0	
660.40	2p ₉ -4s _{1''}	4p[5/2] ₃ -4d'[5/2] ₂ ^o	14.95	0.28	6.1	2.5	1.3	
663.82	Ar ⁺	3d ⁴ F _{5/2} -4p ⁴ D _{5/2} ^o	35.37	13.7	—	2.3	1.0	
663.97	Ar ⁺	3d ⁴ F _{3/2} -4p ⁴ D _{1/2} ^o	35.40	16.9	—	1.6	1.1	
664.37	Ar ⁺	3d ⁴ F _{9/2} -4p ⁴ D _{7/2} ^o	35.25	14.7	—	4.5	1.5	
666.07	2p ₇ -3s ₃	4p[3/2] ₁ -6s'[1/2] ₁ ^o	15.01	0.78	0.68	0.24	0.14	$Q(E_p)/Q(25 \text{ eV}) = 1.45$
666.41	2p ₈ -4s _{1'''}	4p[5/2] ₂ -4d'[5/2] ₂ ^o	14.95	0.15	2.0	0.61	0.25	
666.64	Ar ⁺	3d ² P _{1/2} -4p ² P _{1/2} ^o	35.56	8.8	—	1.9	1.9	
667.73	1s ₄ -2p ₁	4s[3/2] ₁ -4p'[1/2] ₀	13.48	0.236	2.6	2.1	2.1	
668.43	Ar ⁺	3d ⁴ F _{7/2} -4p ⁴ D _{5/2} ^o	35.31	10.7	—	3.4	2.1	
669.89	2p ₆ -3s ₂	4p[3/2] ₂ -6s'[1/2] ₁ ^o	15.02	0.16	1.1	1.3	1.4	Resonance level
675.28	2p ₁₀ -4d ₃	4p[1/2] ₁ -4d[3/2] ₂ ^o	14.74	1.93	35	14	5.6	
675.61	2p ₃ -5d ₃	4p'[3/2] ₂ -5d[3/2] ₂ ^o	15.14	0.36	3.9	1.6	0.77	
676.66	2p ₆ -4s _{1'}	4p[3/2] ₂ -4d'[3/2] ₁ ^o	15.00	0.40	4.4	5.2	5.8	Resonance level
686.13	Ar ⁺	3d ² P _{3/2} -4p ² P _{3/2} ^o	35.63	—	—	1.6	2.1	
687.13	2p ₁₀ -4d ₅	4p[1/2] ₁ -4d[1/2] ₁ ^o	14.71	2.78	26	11	5.9	Resonance level
687.96	2p ₇ -4s _{1'''}	4p[3/2] ₁ -4d'[5/2] ₂ ^o	14.95	0.18	3.3	1.1	0.39	
693.77	2p ₁₀ -4d ₆	4p[1/2] ₁ -4d[1/2] ₀	14.69	3.08	13	4.8	2.0	
696.02	2p ₆ -4s _{1''}	4p[3/2] ₂ -4d'[3/2] ₂ ^o	14.95	0.24	4.1	1.5	0.63	
696.54	1s ₅ -2p ₂	4s[3/2] ₂ -4p'[1/2] ₁	13.33	6.39	54	45	41	
699.22	2p ₂ -5d ₆	4p'[1/2] ₁ -5d[1/2] ₀	15.10	0.75	3.0	0.95	0.28	
703.03	2p ₉ -3s ₅	4p[5/2] ₃ -6s[3/2] ₂ ^o	14.84	2.67	17	6.9	3.8	$Q(E_p)/Q(25 \text{ eV}) = 1.5$
706.72	1s ₅ -2p ₃	4s[3/2] ₂ -4p'[3/2] ₂	13.30	3.80	52	35	26	
706.87	2p ₈ -3s ₄	4p[5/2] ₂ -6s[3/2] ₁ ^o	14.85	2.0	7.5	8.3	9.0	Resonance level
710.74	2p ₈ -3s ₅	4p[5/2] ₂ -6s[3/2] ₂ ^o	14.84	0.45	3.3	1.4	0.81	$Q(E_p)/Q(25 \text{ eV}) = 1.5$
712.58	2p ₄ -3s ₂	4p'[3/2] ₁ -6s'[1/2] ₁ ^o	15.02	0.60	4.3	5.3	6.1	Resonance level
714.70	1s ₅ -2p ₄	4s[3/2] ₂ -4p'[3/2] ₁	13.28	0.625	6.5	4.2	3.5	$Q(E_p)/Q(25 \text{ eV}) = 1.5$
715.88	2p ₄ -3s ₃	4p'[3/2] ₁ -6s'[1/2] ₀	15.01	2.1	2.5	0.84	0.53	$Q(E_p)/Q(25 \text{ eV}) = 1.5$
720.70	2p ₃ -3s ₂	4p'[3/2] ₂ -6s'[1/2] ₁ ^o	15.02	2.48	16	19	21	Resonance level
726.52	2p ₇ -4d ₂	4p[3/2] ₁ -4d[3/2] ₁ ^o	14.86	0.17	5.8	9.1	11	Resonance level
727.29	1s ₄ -2p ₂	4s[3/2] ₁ -4p'[1/2] ₁	13.33	1.83	15	12	11	

(continued on next page)

Figure A.5 - Table 1 (cont.) taken from Boffard, et al. [see Boffard, et al., (2007)].

Table 1 (continued)

Wavelength (nm)	Levels	E_{th} (eV)	A_{ij} (10^6 s^{-1})	$Q^{pp}(E)$ (10^{-20} cm^2)			Notes	
				25 eV	50 eV	100 eV		
731.17	2p ₇ -3s ₄	4p[3/2] ₁ -6s[3/2] ₁ ^o	14.85	1.7	5.7	6.2	6.7	Resonance level
731.60	2p ₂ -3s ₂	4p'[1/2] ₁ -6s'[1/2] ₁ ^o	15.02	0.96	5.5	6.8	8.1	Resonance level
(735.3)	{ 2p ₈ -4d ₄ 2p ₇ -3s ₅	{ 4p[5/2] ₂ -4d[7/2] ₃ ^o 4p[3/2] ₁ -6s[3/2] ₂ ^o	{ 14.78 14.84	{ 0.96 0.20 ^b	{ 31	{ 14	{ 8.8	
737.21	2p ₉ -4d ₄ '	4p[5/2] ₃ -4d[7/2] ₂ ^o	14.76	1.9	82	26	9.9	
738.40	1s ₄ -2p ₃	4s[3/2] ₁ -4p'[3/2] ₂	13.30	8.47	120	78	56	$Q(E_p)/Q(25 \text{ eV}) = 1.45$
739.30	2p ₆ -3s ₄	4p[3/2] ₂ -6s[3/2] ₁ ^o	14.85	0.72	3.5	3.9	4.5	Resonance level
741.23	2p ₄ -4s ₁ ^m	4p'[3/2] ₁ -4d'[5/2] ₂ ^o	14.95	0.39	8.6	2.6	0.92	
742.53	2p ₃ -4s ₁ ^m	4p'[3/2] ₂ -4d'[5/2] ₃ ^o	14.97	0.31	7.0	3.9	2.7	
743.53	2p ₆ -3s ₅	4p[3/2] ₂ -6s[3/2] ₂ ^o	14.84	0.90	6.9	2.8	1.5	$Q(E_p)/Q(25 \text{ eV}) = 1.5$
748.42	2p ₇ -4d ₃ ^m	4p[3/2] ₁ -4d[5/2] ₂ ^o	14.81	0.34	7.9	3.5	2.0	
750.39	1s ₂ -2p ₁	4s'[1/2] ₁ -4p'[1/2] ₀	13.48	44.5	512	418	401	
751.04	2p ₃ -4s ₁ ^m	4p'[3/2] ₂ -4d'[3/2] ₂ ^o	14.95	0.45	8.6	3.4	1.5	
751.47	1s ₄ -2p ₅	4s[3/2] ₂ -4p[1/2] ₀	13.27	40.2	267	256	269	
758.93	Ar ⁺	3d ⁴ P _{3/2} -4p ⁴ S _{3/2}	35.73	10.7	—	1.1	0.78	
762.89	2p ₂ -4s ₁ ^m	4p'[1/2] ₁ -4d'[3/2] ₂ ^o	14.95	0.29	7.2	2.6	1.2	
763.51	1s ₅ -2p ₆	4s[3/2] ₂ -4p[3/2] ₂	13.17	24.5	411	265	192	
767.00	2p ₈ -4d ₅	4p[5/2] ₂ -4d[1/2] ₁ ^o	14.71	0.28	2.5	1.0	0.51	Resonance level
772.38	1s ₅ -2p ₇	4s[3/2] ₂ -4p[3/2] ₁	13.15	5.18	71	62	60	
772.42	1s ₃ -2p ₂	4s'[1/2] ₀ -4p'[1/2] ₁	13.33	11.7	110	91	83	
779.86	2p ₇ -4d ₃	4p[3/2] ₁ -4d[3/2] ₂ ^o	14.74	0.087	1.6	0.59	0.22	
781.43	2p ₅ -4d ₂	4p[1/2] ₀ -4d[3/2] ₁ ^o	14.86		1.5	2.4	3.1	Resonance level
786.19	2p ₄ -4d ₂	4p'[3/2] ₁ -4d[3/2] ₁ ^o	14.86		2.7	3.8	4.9	Resonance level
786.82	2p ₅ -3s ₄	4p[1/2] ₀ -6s[3/2] ₁ ^o	14.85	0.350	1.5	1.8	2.0	Resonance level
789.11	2p ₆ -4d ₃	4p[3/2] ₂ -4d[3/2] ₂ ^o	14.74	0.95	15	6.5	2.5	
791.02	3d ₄ '-8V	3d[7/2] ₄ -8f[9/2] _{4,5}	15.55		2.0	1.5	1.4	
794.82	1s ₃ -2p ₄	4s'[1/2] ₀ -4p'[3/2] ₁	13.28	18.6	182	125	107	$Q(E_p)/Q(25 \text{ eV}) = 1.5$
800.62	1s ₄ -2p ₆	4s[3/2] ₂ -4p[3/2] ₂	13.17	4.90	81	53	36	
801.48	1s ₅ -2p ₈	4s[3/2] ₂ -4p[5/2] ₂	13.09	9.28	207	143	112	
803.72	2p ₁ -3s ₂	4p'[1/2] ₀ -6s'[1/2] ₁ ^o	15.02	0.359	2.4	3.0	3.6	Resonance level
804.61	2p ₇ -4d ₆	4p[3/2] ₁ -4d[1/2] ₀ ^o	14.69	1.12	4.1	1.5	0.58	
805.33	2p ₆ -4d ₅	4p[3/2] ₂ -4d[1/2] ₁ ^o	14.71	0.86	8.3	3.4	1.7	Resonance level
809.41	2p ₂ -4d ₂	4p'[1/2] ₁ -4d[3/2] ₁ ^o	14.86		1.6	2.5	3.0	Resonance level
810.37	1s ₄ -2p ₇	4s[3/2] ₂ -4p[3/2] ₁	13.15	25.0	334	275	255	
811.53	1s ₅ -2p ₉	4s[3/2] ₂ -4p[5/2] ₃	13.08	33.1	932	332	162	$Q(E_p)/Q(25 \text{ eV}) = 1.5$
811.92	2p ₄ -4d ₁ ^m	4p'[3/2] ₁ -4d[5/2] ₂ ^o	14.81		7.8	3.4	1.9	
825.51	3d ₄ '-7V	3d[7/2] ₄ -7f[9/2] _{4,5}	15.48		3.8	1.9	1.3	
826.45	1s ₂ -2p ₂	4s'[1/2] ₀ -4p'[1/2] ₁	13.33	15.3	141	117	106	
833.22	3d ₃ -5Z	3d[3/2] ₂ -5f'[5/2] _{2,3}	15.39		1.4	0.56	0.42	
838.47	2p ₃ -4d ₄	4p'[3/2] ₂ -4d[7/2] ₃ ^o	14.78	0.24	6.5	3.6	2.1	
839.22	3d ₃ -6Y	3d[3/2] ₂ -6f[5/2] _{2,3}	15.38		4.1	2.2	1.7	
840.82	1s ₂ -2p ₃	4s'[1/2] ₁ -4p'[3/2] ₂	13.30	22.3	338	236	175	$Q(E_p)/Q(25 \text{ eV}) = 1.45$
842.46	1s ₄ -2p ₈	4s[3/2] ₁ -4p[5/2] ₂	13.09	21.5	499	345	275	
852.14	1s ₂ -2p ₄	4s'[1/2] ₀ -4p'[3/2] ₁	13.28	13.9	145	98	85	$Q(E_p)/Q(25 \text{ eV}) = 1.5$
860.58	2p ₃ -4d ₃	4p[3/2] ₂ -4d[3/2] ₂ ^o	14.74	1.04	18	7.3	2.8	
862.05	2p ₅ -4d ₅	4p[1/2] ₀ -4d[1/2] ₁ ^o	14.71	0.92	8.1	3.4	1.7	Resonance level
866.79	1s ₃ -2p ₇	4s'[1/2] ₀ -4p[3/2] ₁	13.15	2.43	33	28	26	
867.84	2p ₄ -4d ₅	4p'[3/2] ₁ -4d[1/2] ₀ ^o	14.71		3.3	1.3	0.7	Resonance level
876.17	2p ₂ -4d ₃	4p'[1/2] ₁ -4d[3/2] ₂ ^o	14.74	0.95	17	6.7	2.7	
879.91	2p ₃ -4d ₅	4p'[3/2] ₂ -4d[1/2] ₁ ^o	14.71		7.3	2.9	1.5	Resonance level
885.00	3d ₄ '-6V	3d[7/2] ₄ -6f[9/2] _{4,5}	15.38		8.6	3.5	2.3	
906.68	3d ₄ -6V	3d[7/2] ₃ -6f[9/2] ₄	15.38		11	5.0	3.2	
907.54	2p ₂ -4d ₆	4p'[1/2] ₁ -4d[1/2] ₀ ^o	14.69	1.2	6.6	2.7	1.1	
912.30	1s ₅ -2p ₁₀	4s[3/2] ₂ -4p[1/2] ₁	12.91	18.9	582	267	163	$Q(E_p)/Q(25 \text{ eV}) = 1.5$
919.46	2p ₁₀ -2s ₂	4p[1/2] ₁ -5s'[1/2] ₁ ^o	14.25	1.76	16	12	9.3	Resonance level
919.86	3d ₅ -5X'	3d[1/2] ₁ -5f[3/2] _{1,2}	15.21		9.4	5.4	4.2	
922.45	1s ₂ -2p ₆	4s'[1/2] ₀ -4p[3/2] ₂	13.17	5.03	90	57	42	
929.16	2p ₁₀ -2s ₃	4p[1/2] ₁ -5s'[1/2] ₀ ^o	14.24	3.26	7.0	2.5	1.2	
935.42	1s ₂ -2p ₇	4s'[1/2] ₀ -4p[3/2] ₁	13.15	1.06	16	13	12	
965.78	1s ₄ -2p ₁₀	4s[3/2] ₁ -4p[1/2] ₁	12.91	5.43	157	76	47	$Q(E_p)/Q(25 \text{ eV}) = 1.5$
978.45	1s ₂ -2p ₈	4s'[1/2] ₀ -4p[5/2] ₂	13.09	1.47	31	23	18	
1005.2	3d ₄ '-5V	3d[7/2] ₄ -5f[9/2] _{4,5}	15.21		11	7.1	6.5	
1033.3	3d ₄ -5V	3d[7/2] ₃ -5f[9/2] ₄	15.21		5.7	4.1	3.7	
1046.7	Ar ⁺	3d ² F _{7/2} -4p ² D _{5/2}	35.44		—	4.6	3.1	

Figure A.6 - Table 1 (cont.) taken from Boffard, et al. [see Boffard, et al., (2007)].

Vita Auctoris

I was born in Chatham, Ontario, Canada on August 22, 1984. I enrolled at the University of Windsor in 2002 in Physics and High Technology and was a graduate of the Outstanding Scholars program. In 2003, the Outstanding Scholars Program first brought me in contact with Dr. J. W. McConkey, who took me under his wing and mentored me throughout my undergraduate degree. During the years that followed until my graduation, my knowledge and experience with physics grew as I began work on the very electron gun that would be used for this experiment. I graduated with Honours in 2007 and applied for my Master's degree at the University of Windsor, continuing the work I had begun in my undergraduate program. It was under the supervision of Dr. McConkey and Dr. Kedzierski, that I completed the work presented here.